UNIVERSITY OF CALIFORNIA, SAN DIEGO

Novel Electron Transport Behaviors of Materials at Extreme Conditions

A dissertation submitted in partial satisfaction of the

requirements for the degree Doctor of Philosophy

in

Materials Science and Engineering

by

Yuankan Fang

Committee in charge:

Professor M. Brian Maple, Chair
Professor Richard D. Averitt
Professor Ivan K. Schuller
Professor Sunil K. Sinha
Professor Paul K. L. Yu

2018

The dissertation of Yuankan Fang is approved, and it is acceptable in quality and form for publication on microfilm and electronically:

_____

_____

_____

_____

_____

Chair

University of California San Diego

2018

DEDICATION

EPIGRAPH

The aim of the wise is not to secure pleasure, but to avoid pain.

– Aristotle

TABLE OF CONTENTS

LIST OF FIGURES

LIST OF TABLES

ACKNOWLEDGEMENTS

Over the past five years I have received support and encouragement from a great number of individuals. I would like to first express my special appreciation and thanks to my advisor Professor M. Brian Maple for the dedicated help, insightful advice, deep inspiration, and continuous support throughout my Ph.D study. His enthusiasm, integral view on science, and high-quality work have made my research a thoughtful and rewarding journey. I also gratefully acknowledge the other members of my Ph.D. committee, Professor Ivan K. Schuller, Professor Paul K. L. Yu, Professor Sunil K. Sinha, and Professor Richard D. Averitt, for your brilliant comments and helpful suggestions.

The thesis would not have come to a successful completion, without the help I received from my colleagues and the members of Maple group during my time as a Ph.D. student in University of California San Diego. I would like to thank Dr. Benjamin White for the generous help in experiments and high-standard scientific writing, Dr. Duygu Yazici for exceptional research technologies in experimental physics and attitude in scientific research, Dr. Sheng Ran for sharing creative ideas in both research and life, Dr. Christian Wolowiec and Dr. Colin McElroy for introduction of high pressure technologies. Special thanks also goes to Dr. Sooyoung Jang, Dr. Ihno Jeon, Dr. Noravee Kanchanavatee, Alexander Breindel, Naveen Pouse, Zackary Rehfuss, Kalyan Sasmal, Ivy Lum, and Veronica Burnett for the trustworthy friendship and collaboration in various tasks. I would also like to thank Prof. Pei-Chun Ho for her knowledge and continuous cooperation in running the dilution refrigerator, Christine Coffey for her timely help in ordering lab supplies and submitting research articles.

I owe my deepest gratitude towards my parents for their love, support, and sacrifices at the every stage of my life. They are the ultimate role models, teaching me every good things that really matter in life. Their infallible love and support has always been my strength and enables me to complete much of what I have done and become who I am.

Funding for the research was supported by National Nuclear Security Administration under the Stewardship Science Academic Alliance Program through the US Department of Energy (DOE) under Grant No. DE-NA0001841, the US Department of Energy, Office of Basic Energy Sciences, Division of Materials Sciences and Engineering under Grant No. DE-FG02-04-ER46105, and National Science Foundation under Grant No. DMR 1206553.

The text and data presented in Chapter 3 are reprints of material that appears in "Enhancement of superconductivity in $La_{1-x}Sm_xO_{0.5}F_{0.5}BiS_2$," Y. Fang, D. Yazici, B. D. White, and M. B. Maple, *Phys. Rev. B* **91**, 064510 (2015). The dissertation author is the primary investigator and author of this article.

The text and data presented in Chapter 4 are reprints of material that appears in "Pressure-induced phase transition in $La_{1-x}Sm_xO_{0.5}F_{0.5}BiS_2$," Y. Fang, D. Yazici, B. D. White, and M. B. Maple, *Phys. Rev. B* **92**, 094507 (2015). The dissertation author is the primary investigator and author of this article.

The text and data presented in Chapter 5 are reprints of material that appears

in "Upper critical magnetic field of $Ln\mathrm{O}_{0.5}\mathrm{F}_{0.5}\mathrm{BiS}_2$ (Ln = La, Nd) superconductors at ambient and high pressure," Y. Fang, C. T. Wolowiec, A. J. Breindel, D. Yazici, P-C. Ho, and M. B. Maple, *Supercond. Sci. and Tech.* **30**, 115004 (2017). The dissertation author is the primary investigator and author of this article.

The text and data presented in Chapter 6 are reprints of material that appears in "High-pressure effects on non-fluorinated BiS_2-based superconductors $\mathrm{La}_{1-x}M_x\mathrm{OBiS}_2$ (M = Ti and Th)," Y. Fang, D. Yazici, I. Jeon, and M. B. Maple, *Phys. Rev. B* **96**, 214505 (2017). The dissertation author is the primary investigator and author of this article.

The text and data presented in Chapter 7 are reprints of material that appears in "Chemical substitution and high pressure effects on superconductivity in the $Ln\mathrm{OBiS}_2$ (Ln= La-Nd) system," Y. Fang, C. T. Wolowiec, D. Yazici, and M. B. Maple, *Nov. Supercond. Mater.* **1**, 79 (2015). The dissertation author is the primary investigator and author of this article.

The text and data presented in Chapter 8 are reprints of material that appears in "Evidence for a conducting surface ground state in high-quality single crystalline FeSi," Y. Fang, S. Ran, W. Xie, S. Wang, Y. S. Meng, and M. B. Maple, PNAS, in publication. The dissertation author is the primary investigator and author of this article.

VITA

2010	Bachelor of Science in Engineering Mechanics Shijiazhuang Tiedao University, China
2013	Master of Science in Materials Science and Engineering Zhejiang University, China
2018	Doctor of Philosophy in Materials Science and Engineering University of California San Diego Advisor: M. Brian Maple

PUBLICATIONS

Y. Fang, S. Ran, W. Xie, S. Wang, Y. S. Meng, and M. B. Maple, "Anomalous electron transport behavior of high quality FeSi single crystals," *arXiv: 1804.02036*

Y. Fang, D. Yazici, I. Jeon, and M. B. Maple, "High-pressure effects on non-fluorinated BiS2-based superconductors $La_{1-x}M_xOBiS_2$ (M = Ti and Th)," *Phys. Rev. B* **96**, 214505 (2017)

Y. Fang, C. T. Wolowiec, A. J. Breindel, D. Yazici, P-C. Ho, and M. B. Maple, "Upper critical magnetic field of $LnO_{0.5}F_{0.5}BiS_2$ (Ln = La, Nd) superconductors at ambient and high pressure," *Supercond. Sci. and Tech.* **30**, 115004 (2017)

C. T. Wolowiec, Y. Fang, C. A. McElroy, J. R. Jeffries, R. L. Stillwell, E. Svanidze, J. M. Santiago, E. Morosan, S. T. Weir, Y. K. Vohra, and M. B. Maple, "Pressure effects in the itinerant antiferromagnetic metal TiAu," *Phys. Rev. B* **95**, 214403 (2017)

A. Ślebarski, J. Goraus, M. M. Maśka, P. Witas, M. Fijałkowski, C. T. Wolowiec, Y. Fang, and M. B. Maple, "Effect of atomic disorder and Ce doping on superconductivity of $Ca_3Rh_4Sn_{13}$: Electric transport properties under high pressure," *Phys. Rev. B* **93**, 245126 (2016)

Y. Fang, C. T. Wolowiec, D. Yazici, and M. B. Maple, "Chemical substitution and high pressure effects on superconductivity in the LnOBiS$_2$ (Ln = La-Nd) system," *Nov. Supercond. Mater.* **1**, 79 (2015)

Y. Fang, D. Yazici, B. D. White, and M. B. Maple, "Pressure-induced phase transition in $La_{1-x}Sm_xO_{0.5}F_{0.5}BiS_2$," *Phys. Rev. B* **92**, 094507 (2015)

B. D. White, D. Yazici, P-C. Ho, N. Kanchanavatee, N. Pouse, Y. Fang, A. J. Breindel, A. J. Friedman, and M. B. Maple, "Weak hybridization and isolated localized magnetic moments in the compounds CeT_2Cd$_{20}$ (T = Ni, Pd)," *J. Phys.: Condens. Matter*, **27**, 315602 (2015)

Y. Fang, D. Yazici, B. D. White, and M. B. Maple "Enhancement of superconductivity in $La_{1-x}Sm_xO_{0.5}F_{0.5}BiS_2$," *Phys. Rev. B* **91**, 064510 (2015)

Y. Fang, C. Meng, W Zhu, D. He, G. Du, and J. Jiang "Shock-induced phase transitions of α-Ce_3Al," *J. Appl. Phys.* **113**, 103507 (2013)

Y. Pang, Y. Fang, and J. Liu, "Band gaps of one-dimensional magneto-electro-elastic quasi-periodic structures," *Chin. J. Solid Mech.* **33**, 153 (2012)

H. B. Lou, Y. K. Fang, Q. S. Zeng, Y. H. Lu, X. D. Wang, Q. P. Cao, K. Yang, X. H. Yu, L. Zheng, Y. D. Zhao, W. S. Chu, T. D. Hu, Z. Y. Wu, R. Ahuja, and J. Z. Jiang, "Pressure-induced amorphous-to-amorphous configuration change in Ca-Al metallic glasses," *Sci. Rep.* **2**, 376 (2012)

Y. Fang, and J. Jiang, "High-pressure effects on Ti–Zr–Ni metallic glass and its corresponding quasicrystal," *J. Non-Cryst. Solids* **358**, 3212 (2012)

FIELDS OF STUDY

Major Field: Materials Science and Engineering

Electron transport behavior, magnetic order, and phase transitions of materials at extreme conditions

M. Brian Maple, Bernd T. Matthias Professor of Physics,
University of California San Diego

ABSTRACT OF THE DISSERTATION

Novel Electron Transport Behaviors of Materials at Extreme Conditions

by

Yuankan Fang

Doctor of Philosophy in Materials Science and Engineering

University of California San Diego, 2018

Professor M. Brian Maple, Chair

In condensed matter physics, the term ”extreme condition” mostly refers to a environment of extreme temperatures, high pressures, and/or high magnetic fields. With the extension of these dimensions, we are facing a new world with many more exotic states of matter than what has been explored at ambient conditions. The mechanical, chemical, and physical properties of matter may dramatically changes in such conditions.

The primary subject of this thesis is the study of electron-electron and electron-phonon interplay of d- and f-electron materials at extreme conditions. It is well known that these materials are rich reservoirs for exotic and intriguing physical phenomena; their competition and interplay between localized magnetic moments in partially filled d- or f-electron shells, and conduction electron states lead to novel quantum criticality,

magnetic ordered state, superconductivity, and other interesting states of matters. Part of this thesis covers the research on synthesis of BiS_2-based superconductors, which has a layered structure that is very similar to high-T_c cuprate and Fe pnictide superconductors. The lattice parameters, crystal structure, and superconductivity of these materials turn out to be very sensitive to external environments. Evidence of pressure and magnetic field induced changes in superconductivity and structure of BiS_2 compounds are also presented. The latter part is focused on novel metallic ground state in FeSi. For over 50 years, this compound was believed to be a intrinsic narrow gap semiconductor. The study shows strong evidence of surface electron conducting of FeSi at low temperatures. Possibility of FeSi as a 3D topological insulator, surface magnetic ordered state, and novel Hall effects are also emphasized.

Chapter I

Introduction

Human kind benefits from a multitude of resources that are supplied by the nature. Collectively, these benefits are essential in regulating the environments in which we live including mild temperatures $\sim$25 K and an atmospheric pressure that ensure water in liquid state and a series of biochemical reactions to happen. In addition, the Earth's magnetic field, generated by electric currents in the conductive material of its core, extends from its interior out into space and protects us from the charged particles of the solar wind and cosmic rays. As these conditions are not only vital for the existence of life but also can be easily accessed, great efforts have been performed in the study of condensed matter physics at such conditions.

However, the emergence and persistence of such life friendly conditions are essentially a marvel both in terms of natural history and the universe: over 90% of the detectable substance in the Universe are subject to pressures above 10 GPa, the average temperature of the universe today is approximately 2.73 kelvins and this value is believed

to be extremely high at the early stage of the Universe [1]. Though formidable to life, the combinations of extreme temperature, high pressure, and high magnetic field are the environments that substances in the Universe most likely locate. The truth that has been overlooked for a long time or we are unwilling to admit is we know little about the states of substances in such conductions, due to the difficulty in reconstruction of such conductions in a controllable lab environment and the limits of in-situ measurement technologies.

It should be emphasized that the response of materials to the broad range of extreme conditions signals the materials' underlying structure and dynamics, provides insight into new phenomena, exposes failure modes that limit technological possibility, and presents novel routes for making new materials. Recently, it has been found that exposing materials to those regimes induces new physical phenomena that do not occur under ordinary conditions. Those extreme phenomena are central to many of the most fascinating grand challenges of science. The following parts of this section introduce background knowledge and presents a brief review of a few exciting breakthroughs in the research of novel states of materials in different environments that are closely related to the dissertation.

I.A Correlated phenomena in d- and f- electron materials

In conventional simple metals, electrons barely interact with other electrons and can be well described by Fermi liquid theory, i.e., electrons are treated as isolated particles in a homogenous background. However, electron-electron interactions have

been found in many materials and play a central role in determining the electronic, magnetic, optical, and even mechanical properties, which has proven to be of immense technological relevance and deep physical import.

The complex interplay between electrons and electrons, lattice structure, kinetic energy, and magnetic degrees of freedom is incredibly rich in d- and f-electron materials, resulting in competition between distinct ground states which have different symmetries. It is believed that new phases, which have surprising and useful properties, may appear near quantum phase transitions by changing parameters such as electronic configurations and magnetic filed. In the research of condensed matter physics and promising industrial applications, strong correlations act as a sort of lever arm, through which small changes in controllable parameters can have dramatic consequences on material properties.

On the other hand, the strong electron correlations which result in rich electronic material properties as introduced above also make them difficult to study. Unlike the relatively weak electron-electron repulsion, whose electronic behavior have been very well understood based on well developed perturbative methods such as k·p expansion theory, the local density and Hartree-Fock approximations, Thomas-Fermi screening in metals, etc [2]. In the case when interactions become sizable in the d- and f-electron materials, the electronic properties can not be well described by these controlled theoretical methods. The concepts of Landau adiabaticity principle and renormalizability have been came up and provided foundations for how we understande the complex interacting electron systems with a combination of sophisticated computational techniques such as quantum Monte Carlo, functional renormalization and various quantum cluster methods [3].

With the help of fast developing experimental and material growth techniques, we are able to some extent understand, predict, engineer, and control materials with desired electronic properties and tunable transitions between various phases in the d- and f-electron systems. Recent progress includes discovery and understanding many novel many-body phenomena: superconductors which exhibit zero resistivity up to 135 Kelvin, multi-ferroic materials which allow a magnetic field to write electric domains and an electric field to write magnetic domains, colossal magnetoresistance materials which change their electrical conductivity by orders of magnitude upon application of a magnetic field, heavy fermion materials which host electrons which behave thousands of times heavier than their actual mass, whereas the electrons in graphene behave as if they were massless, topological insulators which may extend fractional charges seen in existing materials into three dimensions.

I.B BiS_2-based superconductors

Many layered compounds have been found to be superconducting with a transition temperature (T_c) that is significantly higher than the T_c value of most other superconducting compounds. Examples include the famous high T_c Cu oxides, which have alternating stack of CuO_2 superconducting layers and blocking (insulating) layers, MgB_2, a binary compound with T_c = 39 K, and Fe-based superconductors. It seems that synthesis of new layered superconductors is a promising approach for the realization of a T_c that is close to room temperature.

In 2012, superconductivity with a T_c value of 8.6 K was found in $Bi_4O_4S_3$ which

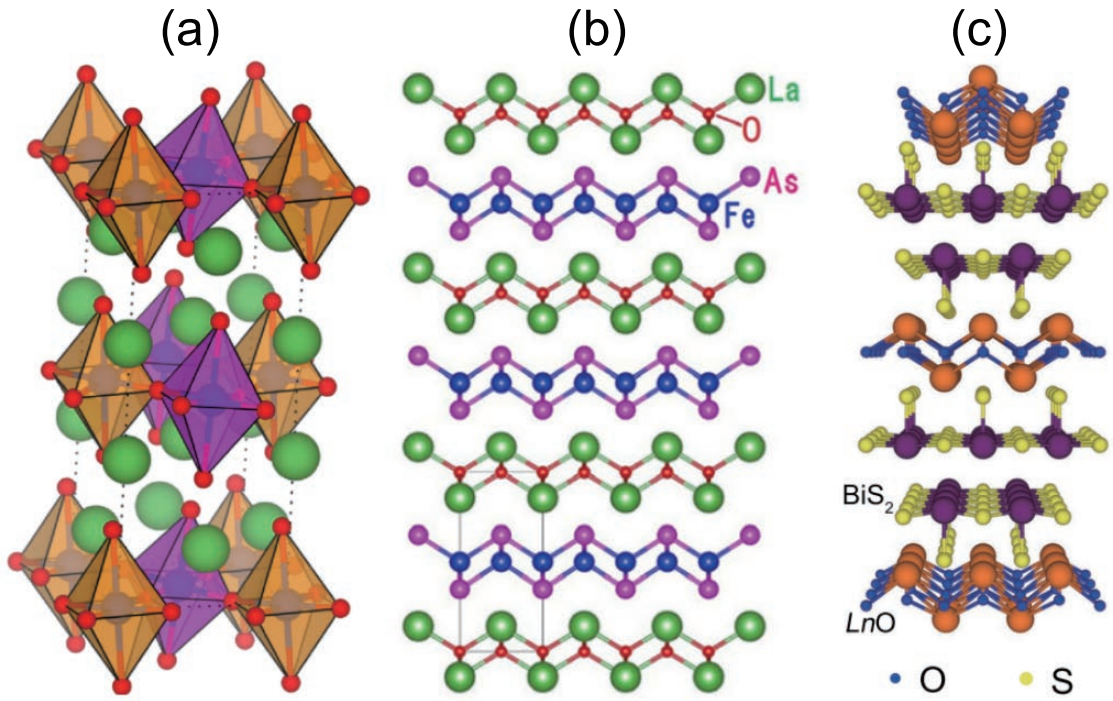

Figure I.1: Lattice structures of typical layered compounds (a) La_2CuO_4, (b) LaFeAsO, and (c) $LaOBiS_2$ which show superconductivity via electron doping [4–6].

has a layered crystal structure consisting of alternating superconducting BiS_2 layers and blocking layers [7]. Soon after this discovery, many superconducting compounds which contain BiS_2 have been found including $LnO_{0.5}F_{0.5}BiS_2$ (Ln = La, Ce, Nd, Pr, and Yb), $Bi_3O_2S_3$, $La_{1-x}M_xOBiS_2$ (M = Ti, Zr, Hf, and Th), $Sr_{1-x}La_xFBiS_2$, $EuBiS_2F$, and $Eu_3Bi_2S_4F_4$ [8–10]. The parent compounds in the BiS_2 family are band insulators. Similarly to cuprate and Fe-pnictide superconductors, it is believed that electron doping is essential for the emergence and enhancement of superconductivity [11–13]. For the $LnO_{0.5}F_{0.5}BiS_2$ (Ln = La, Ce, Nd, Pr, and Yb) system, the highest T_c values were found in the compounds with F substitution of $\sim$50%, which is close to the solubility limit of F in these compounds [6]. However, efforts of inducing superconductivity in BiS_2-based compounds through hole doping have not succeeded.

Lattice parameters are also essential for the superconductivity of BiS_2-based compounds. With heavier Ln elements, the lattice parameter a of the tetragonal phase $LnO_{0.5}F_{0.5}BiS_2$ decreases; however, the c-axis, which is perpendicular to the a-axis, increases with increasing atomic number of Ln elements, resulting in an overall effect of unit cell volume decreasing [6]. The typical values of superconducting transition temperature in the $LnO_{0.5}F_{0.5}BiS_2$ system increase from 3 K (Ln = La) to 4.5 K (Ln = Nd), indicating a clear lattice a dependence of superconductivity. Due to the incompatibility of heavier Ln elements to the lattice, attempts in preparing $LnO_{0.5}F_{0.5}BiS_2$ with Ln elements after Nd turned out to be unsuccessful. Instead, by partially replacing La with Sm, an enhancement of superconductivity is observed in the $La_{1-x}Sm_xO_{0.5}F_{0.5}BiS_2$ compound in which T_c increases from 2.8 K at x = 0.1 to 5.4 K at the solubility limit of x = 0.8 [10].

In addition to chemical substitution, the application of external pressure is another way to change the lattice parameters of the BiS_2-based superconductors. In the study of high pressure effects on a polycrystalline sample of $LaO_{0.5}F_{0.5}BiS_2$, a dramatic increase in T_c from 3 K to 10.7 K can be observed at the pressure of $\sim$0.5 GPa [14]. Similar sudden pressure-induced enhancement of T_c can also be found in $LnO_{0.5}F_{0.5}BiS_2$ (Ln = Ce, Pr, Nd) and $La_{1-x}Sm_xO_{0.5}F_{0.5}BiS_2$ [15, 16]. In-situ X-ray diffraction experiments on the high pressure state of these compounds suggest that the sudden enhancement of superconductivity is associated with structural phase transitions from an ambient pressure tetragonal phase to a high pressure monoclinic phase. Further increase of the pressure after the phase transition, however, results in a gradual suppression of superconductivity.

I.C The B20 crystals

The cubic B20 compounds with space group $P2_13$ have been investigated for over 50 years due to non-centrosymmetric crystallographic structure and fascinating physical properties. It has been predicted that the absence of the inversion center of the crystal structure produces the chiral spin-spin Dzyaloshinskii-Moriya (DM) interaction [17], resulting the emergence of spin helix whose chirality is closely related to the corresponding structural chirality. Examples of the B20 structure include many transition metal silicides and germanides. CrSi and CoSi appear to be simple paramagnetic (PM) metals [18]. FeSi was believed to be a narrow band gap semiconductor with unusual temperature dependence of magnetic susceptibility. MnSi has helimagnetic order below 30 K. Chemical substituted B20 materials, such as Mn and Co substituted FeSi, also display helimagnetism over wide regions as well as interesting behavior near the insulator-to-metal transitions [19, 20].

Due to the itinerant electron magnetism and complex spin order at low temperatures, great research interests have been focused on the B20 MnSi compound. MnSi orders helimagnetically along the [111] direction below 29.5 K with the helical modulation $\lambda = \sim$19 nm that is significantly larger than lattice constant. And hence, a strongly exchange enhanced spectrum of ferromagnetic spin fluctuation across the entire Brillouin zone in MnSi is expected [21]. On the other hand, the spin fluctuation theory was verified by experimental measurements of the spin fluctuations in MnSi [22]. Meanwhile, polarized neutron scattering studies performed in the 1980s suggest the helimagnetism

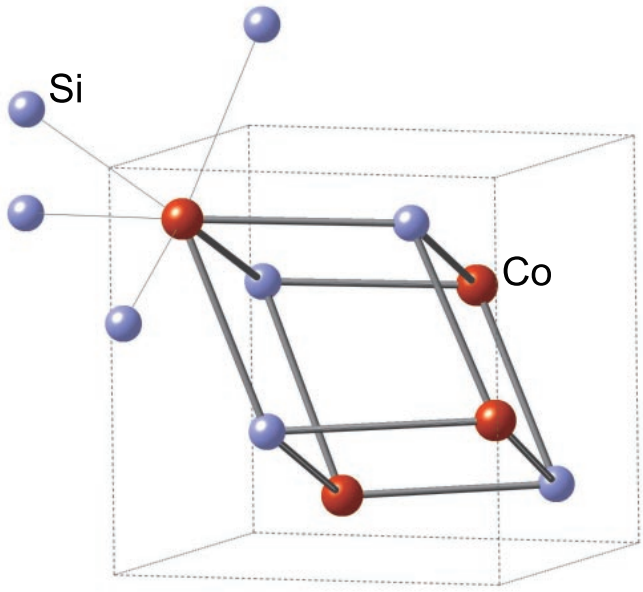

Figure I.2: The crystal structure of CoSi showing lack of inversion symmetry. The dashed lines indicate the unit cell.

in MnSi, which provides the first experimental evidence of a homochiral spin [23].The magnetism and the temperature of magnetic transition temperature for MnSi can be suppressed by applying external pressures. The magnetic order disappears at a critical pressure of about 1.5 GPa [24]. In addition, a crossover from the second-order to a first-order phase transition was observed at a pressure of $\sim$1.2 GPa [25].

Similar to MnSi, magnetic anomalies corresponding to skyrmion lattice ordering were also observed in FeGe. The competition of ferromagnetic exchange, Dzyaloshinskii–Moriya interaction, and magnetic anisotropy leads to a variety of complex magnetic behaviors in FeGe. At ambient condition, FeGe crystallize in B20 cubic structure. Above 893 K, the cubic B20 structure changes into the hexagonal B35 structure with CoSn type. Further increasing of the temperature to 1010 K results a monoclinic high-temperature phase, which has the same structure as CoGe [26]. Among the known cubic B20 chiral

magnets, FeGe has the highest critical magnetic transition temperature (278 K). Under a magnetic field of $\sim$300 Oe, the helical spin structure in FeGe turns into the conical phase with the propagation vector along the direction of external magnetic field [27]. The electron transport properties of FeGe exhibits anomalies under pressure: the magnetic order is strongly suppressed and metallic conducting can be observed up to 30 GPa which is contradict to the results of theoretical predictions based on the breakdown of magnetism [28].

Iron silicide, FeSi, is considered to be a strongly correlated semiconductor with a very narrow gap. At low temperatures, no evidence of intrinsic magnetic order was found in FeSi; however, paramagnetic susceptibility behavior can be observed at high temperatures, resulting a broad maximum around 500 K [29]. This phenomenon is initially reported to be related with the narrow semiconducting band gap in the material, which allows a change from semiconducting to metallic behaviour at moderate temperature [30]. However, the following theoretical calculations of the band structure do not confirm such a picture [31]. Recent photoemission experiments on FeSi also can not provide any evidence of the Kondo resonance near the Fermi level [32]. Currently, there are two completely different approaches for interpretation of the anomalies behavior observed in FeSi: the coupling with the lattice excitations is assumed to be dominant in the first approach, whereas the second one is focused on the renormalization of the electronic spectrum related to the electron–electron correlations [33, 34]. On the other hand, silicon has been considered as a important alloying element with iron in the Earth outer core, and thus, the mechanical and physical properties of FeSi attracts great research interest

to geologists.

I.D Materials Under High Pressure

Under application of external pressure, many solids undergo significant changes in their chemical, physical, and mechanical properties. As a fundamental thermodynamic variable, pressure is not only broadly used to describe the extreme conditions of materials, but it is also experimentally controlled to induce several important effects on interatomic interactions. Pressure provides a new research dimension in physical sciences, resulting emergence of intriguing high pressure physics and chemistry. Under high pressures, many new theories in chemistry and physics have been established; novel materials are synthesized and discovered, and various routes for recovery to ambient pressure are established and explored. Besides, studies of materials under high pressure are crucial for understanding the interior mineralogy, chemical composition, dynamics, and mineral formation inside the Earth and celestial bodies. The impact and importance of high pressure science has been widely emphasized especially during the last decade.

I.D.1 Pressure-induced structural phase transitions

Structural phase transitions originate from qualitative changes in the potential energy landscape. By altering interatomic distances and bonding patterns, high pressure can change the energetic stability of the various possible structures and thus generate new materials through structural phase transitions. The classic B1-B2 transition in NaCl, which requires the ratios of R(Na)/R(Cl) smaller than 0.73, is a very good example. This

transition can only be induced under pressure due to the fact that R(Cl) must decrease relative to R(Na) [35]. Similar pressure-induced structure phase transition can also be observed in all other alkali halides.

For silicate oxides, with increasing external pressure, the ionic radius of silicon and oxygen increases due to the high compressiblity of the oxygen anion compared to silicon, resulting a conversion of all silicon tetrahedra in the material into silicon octahedra at high pressure and high temperature conditions [36]. In the cases of many silicides and oxides, the application of pressure forces the atoms to occupy a smaller volume, leading to high pressure structures composed of the closely packed atoms. However, because of the complicated inner and outer electron structures, the phase diagrams for even single element can be very complex with pressure. Both Li and Na display unusual melt-down phenomena induced by quantum effects. When they eventually solidify at lower temperatures, the simple metals adopt a range of highly complex structures previously unobserved in any element. Na remains a liquid at room temperature at 110 GPa, while Li has a melting point of 190 K at 45 GPa, by far the lowest melting point among the elemental metals [37].

Through our knowledge of phase transitions and phase diagrams of materials under pressure is growing very fast, a accurate determination of phase equilibrium and phase diagram is still very difficult due to the complex phase transitions, limits of experimental methods, and possible metastabilities of materials. The determined phase boundaries of condensed matters may be effected by the experimental conditions such as hydrostatic environment, compression rates, and temperatures. Besides, it is

not unusual to have two or more phases coexist in a large pressure range. For example, pressure-induced amorphization has been widely reported in many materials; however, some of the amorphization effects which are believed to be related with the formation of nanocrystals or structural intermediates can be bypassed if the materials are in more hydrostatic pressure environment [38, 39].

I.D.2 Electronic phase transitions under pressure

In addition to structural phase transitions, pressure may dramatically alters electronic properties, such as electron delocalization, valence change, electron hybridization, spin-paring, etc, which has been widely investigated. For most materials, the interatomic distances are reduced while interatomic intercations can be significantly enhanced, resulting a broadening of the energy bands, band overlap, and insulator to metal transition. This effect provide possibility of creating novel electronic states including novel long-range spin or charge ordering states and superconductors.

At ambient pressure, 22 pure elements have been found superconductivity; however, there are 35 more elements turn into superconductors including rare gas elements under pressure. For high T_c cuprate superconductors, pressure has been used to achieve the record high T_c of 164 K [40]. In the case of Fe-based (K, Tl)$_{1-x}$Fe$_2$Se$_{2-y}$, T_c value reaches a maximum of 33 K with pressure and then vanishes at a quantum critical point; however, superconductivity reemerges as a second crest at 48 K [41]. This behavior provides evidence of comprehensive pressure induced changes in the magnetic superlattice, electronic charge, spin fluctuation, orbital/spin degrees of freedom, and quantum critical

Table I.1: Representative materials that is superconducting at high pressure condition.

Material	Pressure (GPa)	Year	T_c (K)
H (Metallic)	$\sim$300	1968	290 (predicted)
(Ba,Ca)-Hg–Cu–O	31	1994	164
S	190	1997	17
Li	48	2002	20
Ca	216	2006	29
Sm(O,F)FeAs	6	2008	55
Sc	107	2008	19.6
(Tl,K,Rb)-Fe-Se	12	2012	48
H-S	155	2015	203

point.

High pressure can be used to effectively tune the electronic correlations and tightly bond orbitals begin to mix with neighboring orbitals, resulting electron delocalization. Light rare rarth metals, such as Ce, Pr, and Gd, exhibit pressure-induced sudden volume changes. This behavior has been approached by various models including fully dynamical treatment of correlations in the lattice using dynamical mean-field theory, suggesting a strong connection between the 4f electronic structure and the volume-collapse [42]. The famous γ to α phase transition in Ce with a sudden volume collapse of $\sim$30% is a good example [43]. Kondo-like aspects in the $4f$ electron delocalization was also observed in Gd metal. Different with what been observed in Ce, a prolonged and continuous delocalization was found in Gd throughout the entire pressure range, indicating that the volume-collapse transition is only part of the electron delocalization. The following optical indicate no apparent change in the 4f moment across the collapse, suggesting that Kondo screening is responsible for the expected Pauli-like behavior in magnetic

susceptibility [44].

Many transition metals and rare earth compounds belong to correlated electron systems. The structure and magnetic properties of these materials are complicated due to the interactions of the charge, spin, lattice, and orbital moments. At ambient pressure, FeO and CoO are paramagnetic insulators with a rock salt crystal structure above the Neel temperature (T_N). Below T_N, both compounds transform into anti-ferromagnetic states accompanied with lattice distortions and structural phase transitions. The lattice distortions are generally believed to be related with magnetoelastic coupling. Under pressure, FeO and CoO undergo structural phase transition to a rhombohedral lattice at $\sim$15 GPa and $\sim$43 GPa, respectively [45], which was reported to be associated with a transition of magnetic ordering before the structural phase transition [46]. $LaCrO_3$ is another compound that shows coexistence of a structural and magnetic phase transition under pressure, which provides evidence that magnetic order, spin orientation, magnetic moment, and structural changes are correlated [47].

Bibliography

[1] A. Albrecht, P. J. Steinhardt, M. S. Turner, and F. Wilczek, Phys. Rev. Lett. **48**, 1437 (1982).

[2] A. D. Becke, J. Chem. Phys. **98**, 1372 (1993).

[3] P. E. Blöchl and M. Parrinello, Phys. Rev. B **45**, 9413 (1992).

[4] K. Deguchi, Y. Takano, and Y. Mizuguchi, Sci. Technol. Adv. Mater. **13**, 1878 (2012).

[5] J. W. Furness, Y. Zhang, C. Lane, I. G. Buda, B. Barbiellini, R. S. Markiewicz, A. Bansil, and J. Sun, Commun. Phys. **1** (2018).

[6] Y. Fang, C. T. Wolowiec, D. Yazici, and M. B. Maple, Nov. Supercond. Mater. **1** (2015).

[7] Y. Mizuguchi, H. Fujihisa, Y. Gotoh, K. Suzuki, H. Usui, K. Kuroki, S. Demura, Y. Takano, H. Izawa, and O. Miura, Phys. Rev. B **86**, 220510(R) (2012).

[8] D. Yazici, K. Huang, B. D. White, A. H. Chang, A. J. Friedman, and M. B. Maple, Phil. Mag. **93**, 673 (2013).

[9] Y. Mizuguchi, Physics Procedia **58**, 94 (2014).

[10] Y. Fang, D. Yazici, B. D. White, and M. B. Maple, Phys. Rev. B **91**, 064510 (2015).

[11] G. R. Stewart, Rev. Mod. Phys. **83**, 1589 (2011).

[12] J. Paglione and R. L. Greene, Nat. Phys. **6**, 645 (2010).

[13] D. C. Johnston, Adv. Phys. **59**, 803 (2010).

[14] C. T. Wolowiec, D. Yazici, B. D. White, K. Huang, and M. B. Maple, Phys. Rev. B **88**, 064503 (2013).

[15] C. T. Wolowiec, B. D. White, I. Jeon, D. Yazici, K. Huang, and M. B. Maple, J. Phys.: Condens. Matter **25**, 422201 (2013).

[16] Y. Fang, D. Yazici, B. D. White, and M. B. Maple, Phys. Rev. B **92**, 094507 (2015).

[17] T. Moriya, Phys. Rev. B **120**, 91 (1960).

[18] J. H. Wernick, G. K. Wertheim, and R. C. Sherwood, Phys. Rev. B **7**, 1431 (1972).

[19] N. Manyala, J. F. Ditusa, G. Aeppli, and A. P. Ramirez, Nature **454**, 976 (2008).

[20] N. Manyala, Y. Sidis, J. F. DiTusa, G. Aeppli, D. Young, and Z. Fisk, Nature **404**, 581 (2000).

[21] Y. Ishikawa, Y. Noda, Y. J. Uemura, C. F. Majkrzak, and G. Shirane, Phys. Rev. B **31**, 5884 (1985).

[22] G. G. Lonzarich and L. Taillefer, J. Phys. C: Solid State Phys. **18**, 4339 (1985).

[23] Y. Ishikawa and M. Arai, J. Phys. Soc. Jpn. **53**, 2726 (1984).

[24] C. Thessieu, J. Flouquet, G. Lapertot, A. NStepanov, and J. D., Solid State Communications **95**, 707 (1995).

[25] C. Pfleiderer, G. McMullan, and G. Lonzarich, Physica B **206**, 847 (1995).

[26] M. Richardson, Acta Chem. Scand. **21**, 2305 (1967).

[27] B. Lebech, J. Bernhard, and T. Freltoft, J. Phys.: Condens. Matter **1**, 6105 (1989).

[28] P. Pedrazzini, H. Wilhelm, D. Jaccard, T. Jarlborg, M. Schmidt, M. Hanfland, L. Akselrud, H. Q. Yuan, U. Schwarz, Y. Grin, and F. Steglich, Phys. Rev. Lett. **98**, 047204 (2007).

[29] V. Jaccarino, G. K. Wertheim, J. H. Wernick, L. R. Walker, and S. Arajs, Phys. Rev. **160**, 476 (1967).

[30] D. Mandrus, J. L. Sarrao, A. Migliori, J. D. Thompson, and Z. Fisk, Phys. Rev. B **51**, 4763 (1995).

[31] L. F. Mattheiss and D. R. Hamann, Phys. Rev. B **47**, 13114 (1993).

[32] M. Klein, D. Zur, D. Menzel, J. Schoenes, K. Doll, J. Röder, and F. Reinert, Phys. Rev. Lett. **101**, 046406 (2008).

[33] J. Kuneš and V. I. Anisimov, Phys. Rev. B **78**, 033109 (2008).

[34] V. V. Mazurenko, A. O. Shorikov, A. V. Lukoyanov, K. Kharlov, E. Gorelov, A. I. Lichtenstein, and V. I. Anisimov, Phys. Rev. B **81**, 125131 (2010).

[35] H. M. William A. Bassett, Taro Takahashi and J. S. Weaver, J. Appl. Phys. **39**, 319 (1968).

[36] L.-G. Liu, Nature **258**, 510 (1975).

[37] C. L. Guillaume, E. Gregoryanz, O. Degtyareva, M. I. McMahon, M. Hanfland, S. Evans, M. Guthrie, S. V. Sinogeikin, and H. K. Mao, Nature Physics **7**, 211 (2011).

[38] J. Haines, O. Cambon, R. L. Parc, and C. Levelut, Phase Transitions **80**, 1039 (2007).

[39] Q. Y. Hu, J. F. Shu, A. Cadien, Y. Meng, W. G. Yang, H. W. Sheng, and H. K. Mao, Nat. Commun. **6**, 211 (2015).

[40] L. Gao, Y. Y. Xue, F. Chen, Q. Xiong, R. L. Meng, D. Ramirez, C. W. Chu, J. H. Eggert, and H. K. Mao, Phys. Rev. B **50**, 4260 (1994).

[41] L. Sun, X.-J. Chen, J. Guo, P. Gao, Q.-Z. Huang, H. Wang, M. Fang, X. Chen, G. Chen, Q. Wu, C. Zhang, D. Gu, X. Dong, L. Wang, K. Yang, A. Li, X. Dai, H. K. Mao, and Z. Zhao, Nature **483**, 67 (2012).

[42] A. K. McMahan, R. T. Scalettar, and M. Jarrell, Phys. Rev. B **80** (2009).

[43] M. J. Lipp, A. P. Sorini, J. Bradley, B. Maddox, K. T. Moore, H. Cynn, T. P. Devereaux, Y. Xiao, P. Chow, and W. J. Evans, Phys. Rev. Lett. **109**, 195705 (2012).

[44] J. Akella, G. S. Smith, and A. P. Jephcoat, J. Phys. Chem. Solids **49**, 573 (1988).

[45] Y. Ding, Y. Ren, P. Chow, J. Zhang, S. C. Vogel, B. Winkler, J. Xu, Y. Zhao, and H. K. Mao, Phys. Rev. B **74**, 144101 (2006).

[46] Y. Ding, L. Yang, C.-C. Chen, H.-S. Kim, M. J. Han, W. Luo, Z. Feng, M. Upton, D. Casa, J. Kim, T. Gog, Z. Zeng, G. Cao, H. K. Mao, and M. van Veenendaal, Phys. Rev. Lett. **116**, 216402 (2016).

[47] J.-S. Zhou, J. A. Alonso, A. Muoñz, M. T. Fernández-Díaz, and J. B. Goodenough, Phys. Rev. Lett. **106**, 057201 (2011).

Chapter II

Experimental Details

II.A Sample Preparation

The synthesis of new materials has been recognized as the most essential element in advancing technology and a key step in investigating novel physical, mechanical and chemical properties of condensed matter system for the long term; however, it generally remains more of an art than a science in that the physics behind it is too complicated to be well described. As a compromise, much effect has been devoted in developing techniques for material synthesis. Due to the limited space, this dissertation will mainly focus on two techniques: the solid-state reaction in preparing bulk poly-crystalline materials and the flux method for making single crystals.

II.A.1 Solid State Reaction

Solid state reaction in general refers to all solventless processes leading from the mixture of solid reactants to a solid product. It has been studied for many years and

numerous principles that provide an understanding of the chemistry associated with this field have been proposed. The confined environment of the reactant crystal lattice can control the kinetic features of a reaction and hence the nature of products. Generally, solid state reactions have the advantages in: (1) limited formation of side products, (2) no solvents are needed in the reaction and hence no waste disposal issues, (3) the constrained environment may lead to novel chemical reactions, (4) cascade reactions can be carried out quite easily, and (5) kinetic trapping of highly reactive intermediates [1–4].

The starting materials are weighed and mixed in the calculated stoichiometric ratios, thoroughly grounded into fine powders, and pressed into pellets using a designed die-kit and isostatic press. The resulting pellets are then placed and sealed in a quartz tube. Pellet container may be used to prevent chemical reactions of the starting materials with the quartz. The mixture is heated to high temperatures below the melting points of the starting materials. With appropriate high temperature and atmosphere conditions, thermal energy overcomes the free energy constraints and induces chemical reactions among the starting materials resulting new crystal structures. The products of this process may be re-grounded, sealed, and annealed at high temperature for several times to promote homogeneity of the samples.

II.A.2 Flux Method

Growth of crystals via solidification from the melt has been a widely used technique: crystallization from high temperature solutions allows single crystal growth of a wide range of materials. By utilizing this technique, the raw elemental materials are

dissolved into a solvent called a flux, which allows an enhanced diffusion of reactants in contrast to a solid state reaction. In many cases, these melts act not only as solvents, but can also be reactants which provide species that can be incorporated into the final product.

A significant advantage of the flux method is that the elemental reactants can dissolve into the flux at a temperature that can be much lower than their melting temperature and thus crystals are grown at a relatively low temperature. This is critical if the starting material melts incongruently, or exhibits undesired phase transitions at high temperatures. On the other hand, thermal strain can also be minimized in flux growth due to the low growth temperatures and very slow cooling rates.

In this dissertation, the raw elemental reagents and the flux metals were weighed and placed in an alumina crucible, which was then sealed in a quartz tube after being flushed with argon and evacuated. The quartz tube was placed into a furnace and then gradually heated to the desired temperature. After dwelling, the tube was slowly cooled back to a temperature that is slightly above the melting temperature of the flux and centrifuged to separate the solid products and the liquid flux. Selected examples of single-crystalline samples of transition metal silicides are shown in the Fig. II.1.

II.B High Pressure Technologies

Pressure has long been regarded as a powerful thermodynamic parameter that is able to alter the structures and properties of materials. However, due to the difficulty in obtaining megabar hydrostatic pressure and in performing measurements inside pressure

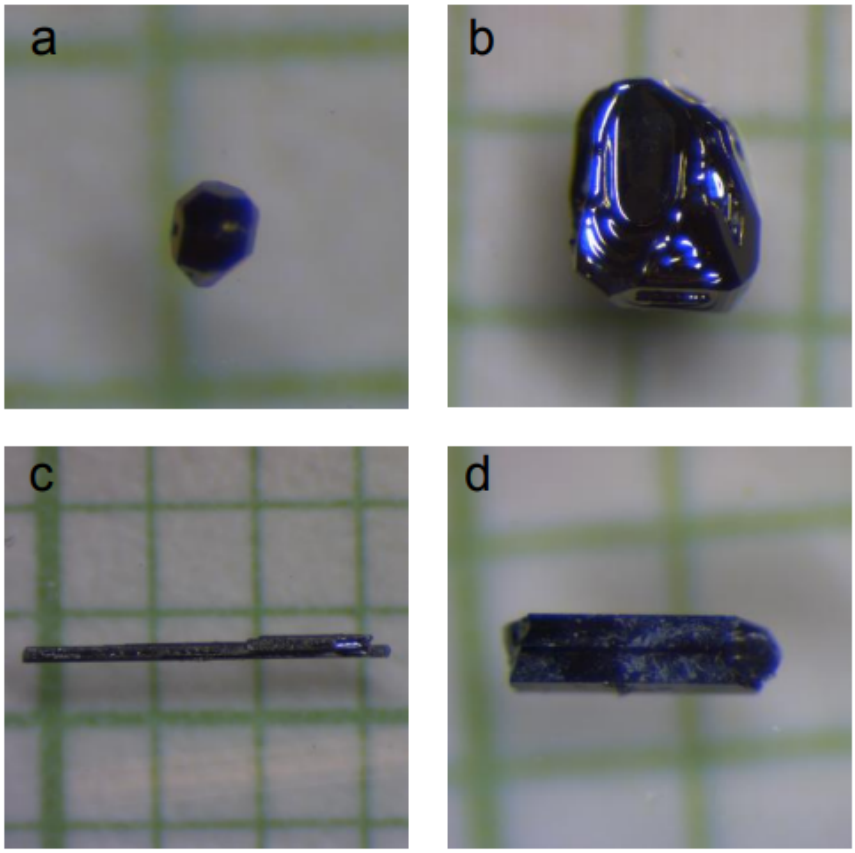

Figure II.1: Morphologies of single single-crystaline samples of CoSi (a), MnSi (b), NiSi (c), and OsSi (d), respectively

vessels, investigations of materials under pressure lag behind other environmental variables such as temperature and magnetic field [5]. Recent developments in micro probing technology and the emergence of various high pressure cells has made the research on materials at extreme condition with a combination of high pressure, high magnetic filed, and low temperature a new dimension of condensed matter physics. In this section, popular high pressure technologies are briefly introduced.

II.B.1 Piston-Cylinder High Pressure Cell

Due to the relatively large sample chamber and the usage of liquid pressure transmission media, the piston-cylinder cell (PCC) provides an excellent hydrostatic environment up to $\sim$3 GPa and is very suitable to investigate magnetic and transport properties of stress-sensitive materials.

Figure II.2 shows the core components of the PCC used in the experiments of this dissertation. The samples wired using the standard four-wire configuration is set on the Cu-Be sample holder. This setup is then pressed into a Teflon capsule which is filled with a mixture of n-pentane and isoamyl alcohol as a pressure medium. A MP35N nonmagnetic steel cylinder is used to constrain and protect the sample chamber. By squeezing the sample space, moderate hydrostatic high pressure environment can be achieved. The pressures applied to the samples were inferred from the Tc of a high-purity (above 99.99%) Sn disk inside the sample chamber of the cell using the well-established behavior of $T_c(P)$ in high-purity Sn [6].

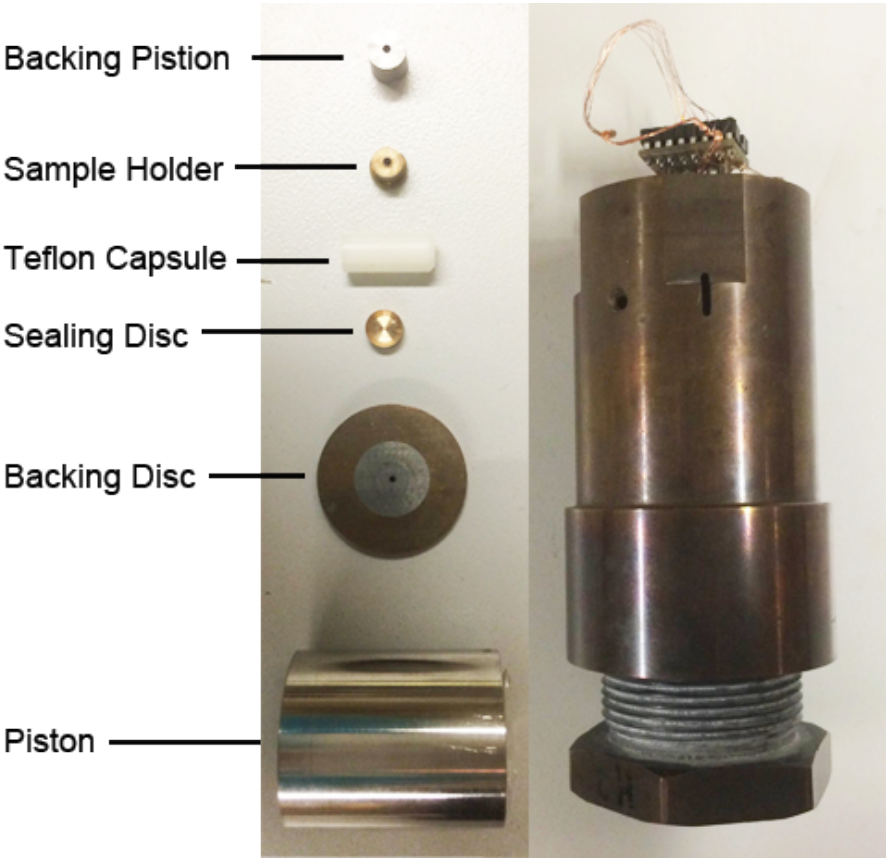

Figure II.2: (Left) Components of the hydrostatic piston-cylinder cell for measurements of electrical resistivity of samples. (Right) CuBe clamp for the piston-cylinder cell.

II.B.2 Bridgman anvil clamped Cell

The Bridgman anvil cell (BAC) is a typical large volume press cell that uses opposing tungsten carbide anvils to generate high pressure on the the samples in between the anvil. Due to the solid pressure transmission medium (fine steatite powder) used for the BAC, the samples inside the cell are usually in a non-hydrostatic environment; However, the pressure on the samples inside the Bridgman anvil cell can as high as 16 GPa, which is significantly higher than the pressure inside a PCC. Besides, BAC has been widely used for high pressure research mainly by offering the possibility to introduce a large number of wires into the pressure chamber.

The design of the pressure cell is based on the classic Bridgman setup[7]. The sample space is formed by a pyrophyllite gasket (machined to have a 3.5 mm outer diameter, 2 mm inner diameter, and 0.200 mm thickness), which is fixed on the lower tungsten carbide (WC) anvil and squeezed between the flat parts of the two opposed anvils. Pyrophyllite, an aluminum silicate hydroxide, is used for its high friction coefficient with respect to metals and its intermediate internal friction coefficient. The high frictional forces allow the pyrophyllite gasket to withstand the high pressure difference existing across its radius. On the other hand, the prophyllite gasket are still sufficiently compressible due to the intermediate internal friction. Since pyrophyllite is a porous material, a solid pressure transmitting medium is required.

A steatite disk is placed on top of the anvil (see Fig. II.3), inside the pyrophyllite ring, serving as the pressure transmission medium. The samples and pressure manometer are set on the disk and wired using pre-annealed fine Pt wires as shown in Fig. II.3(a).

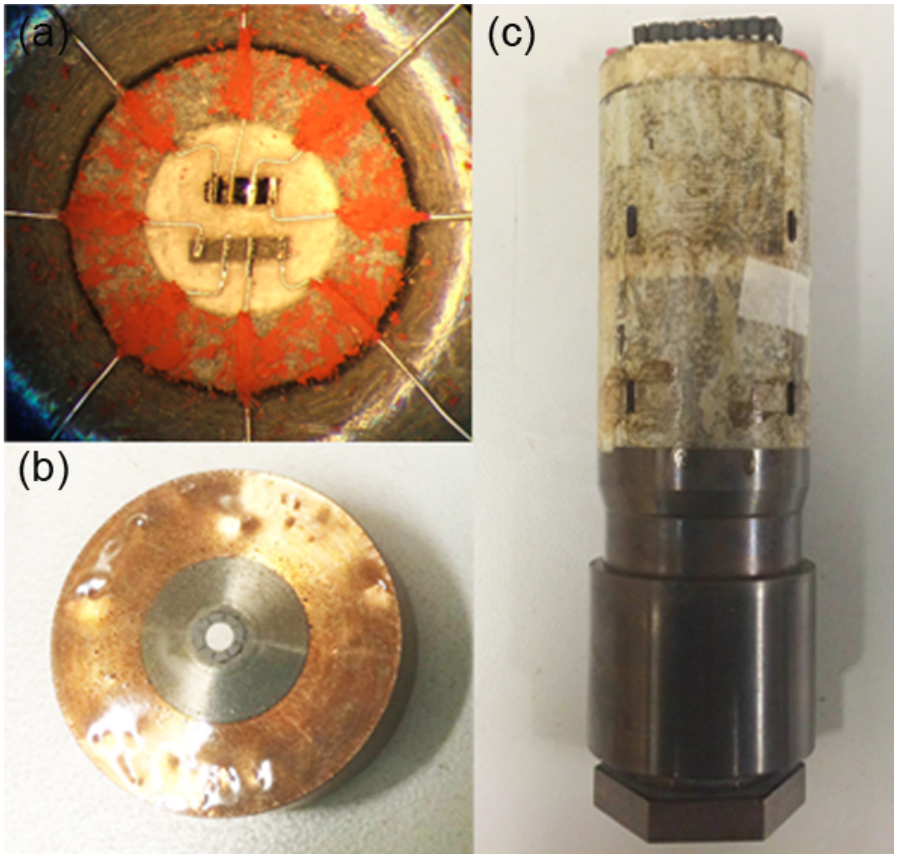

Figure II.3: (a) Top view of the Bridgman anvil with wired sample and a Pb manometer. (b) Top view of the set up of the sample chamber. (c) Side view of the Bridgman anvil cell clamp.

To fill the extra space of the sample space, another pressed steatite disk is placed over the top of the samples. The pressure is determined from the superconducting transition of a strip of lead foil placed adjacent to the sample and measured using a four-lead resistive method.

II.B.3 Diamond Anvil High Pressure Cell

The multiple-anvil devices are a powerful tool in the hands of the high-pressure researcher for the study of phase transitions and material synthesis, great efforts have

been conducted in developing novel high pressure devices. The invention of diamond anvil cell (DAC) was revolutionary to high pressure science, it led to studies of condensed matter under static high pressure conditions extending into the multi-megabar range. Besides, the combination of such high pressure techniques with optical absorption and reflection measurements has made the structure determination of solids under pressure possible [8, 9].

Similar to PCC and BAC, the basic principle of the DAC is very simple; a sample placed between the flat parallel faces of two opposed diamond anvils (see Fig. II.4) is subjected to pressure when a force pushes the two opposed anvils together. The sample space is formed by the opposed diamond anvils and the gasket (steel or Ru), which is prepared by drilling a hole (0.2 mm in diameter) at the center of the indentation made by the anvil face on a metal sheet.The gasket is seated on the lower diamond flat in the same orientation as it had when making the indentation. Then the sample and a pressure indicator are placed in the hole as shown in FIG. II.4(b). The extra sample space is filled by using either liquid or solid pressure transmission medium depending on the purpose of the measurements, and then sealed by placing the upper anvil on the upper side of the gasket.

For high-pressure electrical conductivity measurement, magnetic susceptibility experiments, or electrical heating experiments, a designer diamond anvil may be used. The diamond anvil has a unique pattern of microcircuits, usually made of tungsten, which are fabricated on the diamond tip and then encapsulated within a diamond film. In most cases, the pressure of the sample space is determined by using a small sphere ruby, which

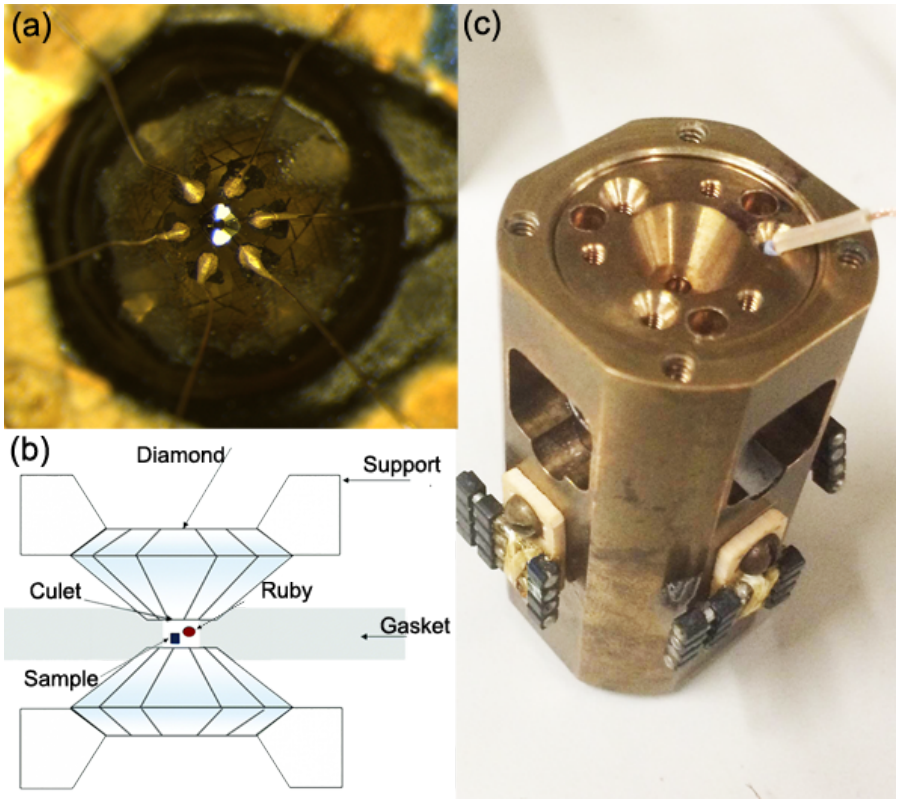

Figure II.4: (a) A photograph of the designed diamond with external wires. (b) A schematic view of the diamond anvil cell sample chamber in which a metalic gasket, anvil diamonds, and a ruby (pressure indicator) are shown. (c) A photograph of the diamond anvil Cell for low temperature resistance measurements.

is chemically inert, and has strong fluorescence activated by a green laser light.

Bibliography

[1] G. Kaupp, CrystEngComm **5**, 117 (2003).

[2] G. W. Cave, C. L. Raston, and J. L. Scott, Chem. Commun. **21**, 2159 (2001).

[3] M. Sakamoto, Chem. Eur. J. **5**, 684 (1997).

[4] F. Toda, Acc. Chem. Res. **28**, 480–486 (1995).

[5] H.-K. Mao, X.-J. Chen, Y. Ding, B. Li, and L. Wang, Reviews of Modern Physics **90** (2018).

[6] T. Smith, C. W. Chu, and M. B. Maple, Cryogenics **9**, 53 (1969).

[7] P. W. Bridgman, Proc. Am. Acad. Arts Sci. **81** (1952).

[8] Q. S. Zeng, H. W. Sheng, Y. Ding, L. Wang, W. G. Yang, J.-Z. Jiang, W. L. Mao, and H.-K. Mao, Science **332**, 1404 (2011).

[9] H. B. Lou, Y. K. Fang, Q. S. Zeng, H. Lu, Y, X. D. Wang, Q. P. Cao, K. Yang, X. H. Yu, L. Zheng, Y. D. Zhao, W. S. Chu, T. D. Hu, Z. Y. Wu, R. Ahuja, and J. Z. Jiang, Scientific Reports **2**, 376 (2012).

Chapter III

Enhancement of Superconductivity in $La_{1-x}Sm_xO_{0.5}F_{0.5}BiS_2$

III.A Introduction

Since the discovery of superconductivity in $Bi_4O_4S_3$,[1, 2] a tremendous amount of effort has been made to synthesize new superconducting materials with BiS_2-layers. Through fluorine substitution for oxygen, the compounds $LnO_{1-x}F_xBiS_2$ (*Ln* = La, Ce, Pr, Nd, Yb) were soon reported to have superconducting transition temperatures, T_c, ranging from 2 to 10 K.[3–10] Superconductivity can also be induced in $LaOBiS_2$ via substitution of tetravalent elements, such as Th^{4+}, Hf^{4+}, Zr^{4+}, and Ti^{4+}, for trivalent Ln^{3+}.[11] Very recently, bulk superconductivity was observed in La substituted $SrFBiS_2$.[12] These compounds form in a tetragonal structure with space group *P4/nmm*, composed of alternate stacking of double superconducting BiS_2 layers and blocking *Ln*O or SrF layers.[3–5, 7, 11, 12] Thus, there exists significant phase space to design and synthesize

analogous superconductors by changing the chemical environment of the blocking layers or modifying the superconducting layers.

The T_c values for samples of the superconducting compounds *Ln*$O_{1-x}F_xBiS_2$, prepared at ambient pressure, increase with increasing atomic number for *Ln* = La - Nd.[7, 8] Non-superconducting samples of *Ln*$BiOS_2$ (*Ln* = La, Ce, Pr, Nd, Sm, Gd, Dy, Yb) were successfully synthesized decades ago;[13] however, attempts to prepare fluorine-substituted samples of *Ln*$BiO_{1-x}F_xS_2$ for *Ln* = Sm - Tm, which could potentially exhibit superconductivity, have been unsuccessful. Since the highest T_c in as-grown samples of $LaO_{1-x}F_xBiS_2$ is ∼2.8 K for x = 0.5, we felt that it would be instructive to systematically substitute Sm for La in $LaO_{0.5}F_{0.5}BiS_2$ in order to determine the solubility limit and to address the question of whether $SmO_{0.5}F_{0.5}BiS_2$ might be a superconductor.

In this paper, we report the evolution of superconductivity and the normal-state properties of samples with *nominal* chemical composition $La_{1-x}Sm_xO_{0.5}F_{0.5}BiS_2$ from x = 0.1 to the Sm solubility limit near x = 0.8. Evidence for an enhancement with x of both T_c and the volume fraction is presented. The increasing volume fraction suggests that high-quality samples of $SmO_{0.5}F_{0.5}BiS_2$ might exhibit bulk superconductivity if the phase could be stabilized. Performing a linear extrapolation of T_c vs. x to x = 1 allowed us to estimate $T_c \sim 6.2$ K for $SmO_{0.5}F_{0.5}BiS_2$. The results are consistent with the trend of T_c vs. *Ln* for the reported *Ln*$O_{0.5}F_{0.5}BiS_2$ compounds. Until the heavy lanthanide variants can be synthesized, the results reported herein for *Ln* = Sm constitute a test case for a promising approach to make a preliminary assessment of superconductivity in *Ln*$O_{0.5}F_{0.5}BiS_2$ compounds.

III.B Experimental Details

Polycrystalline samples of $La_{1-x}Sm_xO_{0.5}F_{0.5}BiS_2$ were synthesized by means of solid state reaction as described elsewhere.[7] Powder X-ray diffraction experiments were performed at room temperature using a Bruker D8 Discover x-ray diffractometer with Cu-K_α radiation. All resulting patterns were analyzed by Rietveld refinement using the GSAS+EXPGUI software package.[14, 15] Electrical resistivity measurements were performed by means of a standard four-wire technique using a Linear Research LR700 ac impedance bridge and a home-built probe in a liquid ^{4}He Dewar from 300 K to $\sim$1.1 K. Alternating current (ac) magnetic susceptibility measurements were made down to $\sim$1.1 K in a liquid ^{4}He Dewar using home-built magnetic susceptibility coils and the Linear Research LR700 impedance bridge. Direct current (dc) magnetic susceptibility measurements were carried out using a Quantum Design Magnetic Properties Measurement System (MPMS). Specific heat measurements were performed in a Quantum Design Physical Property Measurement System (PPMS) Dynacool using a standard thermal relaxation technique.

III.C Results and Discussion

A representative XRD pattern for $La_{1-x}Sm_xO_{0.5}F_{0.5}BiS_2$ with x = 0.7 is shown in Fig. **??**, plotted with its refined pattern for comparison. For $x \leqslant 0.8$, the main diffraction peaks can be fitted well by the Rietveld refinement method to a $CeOBiS_2$-type tetragonal crystal structure with space group *P4/nmm*. The refinement analysis

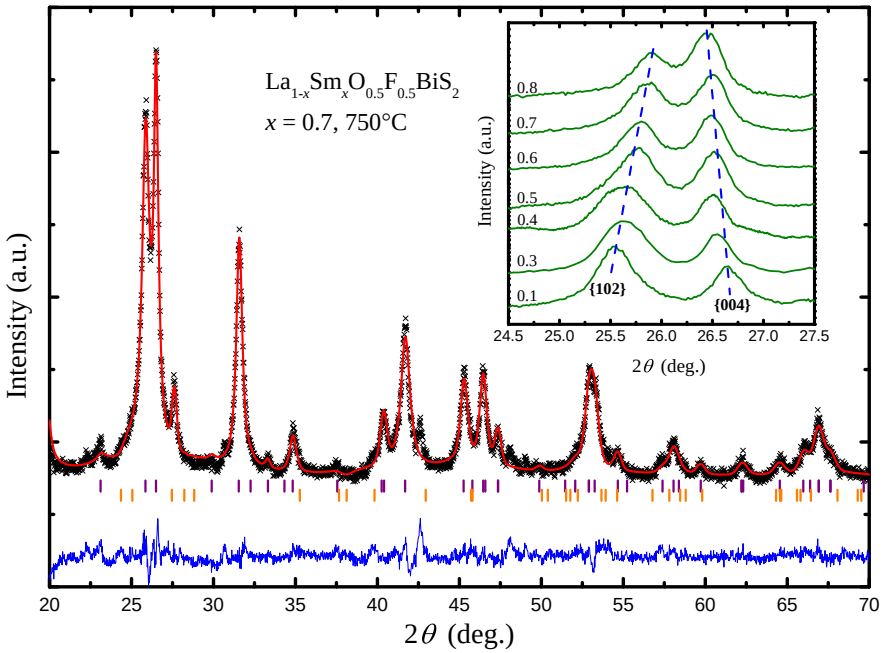

Figure III.1: X-ray diffraction pattern of $La_{0.3}Sm_{0.7}O_{0.5}F_{0.5}BiS_2$ as a representative example. Black crosses denote the experimental data. Red and blue lines are the calculated XRD pattern and the difference between the observed and calculated patterns, respectively. Tick marks represent calculated peak positions of the main phase (purple) and LaF_3 (orange). The reliability factors are wRp = 5.27% and Rp = 3.99%. (Inset) XRD profiles of the $\{102\}$ and $\{004\}$ peaks of $x = 0.1$ to 0.8. The dashed lines are guides to the eye.

demonstrates the presence of negligible secondary phases like La(Sm)O and Bi_2S_3, but the main impurity in the samples was found to be La(Sm)F_3, typically around 3-5 wt.% for x = 0.1 - 0.7 and around 8 wt.% for x = 0.8 samples. This situation results in a lower fluorine concentration in the main superconducting phase compared with the nominal chemical composition. This is consistent with a very recent study which shows that the actual electron doping level in $LaO_{1-x}F_xBiS_2$ could be much smaller than expected.[16] However, an exact evaluation of the actual chemical composition of the main phase is very difficult due to the multi-phase polycrystalline nature of the samples and the insensitiveness of energy dispersive spectroscopy (EDS) to light elements. To be consistent with previous studies on $LnO_{1-x}F_xBiS_2$, the nominal chemical compositions of the main phase, $La_{1-x}Sm_xO_{1-x}F_xBiS_2$, is used throughout this artical. For $x \geqslant$ 0.9, samples contain a considerable amount of impurities and the parent compound $SmO_{0.5}F_{0.5}BiS_2$ could not be synthesized, indicating a Sm solubility limit near 80%.[17] The main diffraction peaks, $\{102\}$ and $\{004\}$, shift with increasing x (see the inset of Fig. III.1), indicating a systematic change in the lattice parameters. The Sm concentration dependence of the lattice parameters *a*, *c*, and unit-cell volume *V* for x = 0.1 to 0.8 are summarized in Fig. III.1. Although superconductivity is observed in the nominal x = 0.9 sample, its lattice parameters are not plotted here because of the appreciable amount of impurities that make XRD analysis unreliable. As the Sm concentration increases from x = 0.1 to 0.8, the *a* axis decreases continuously, while the *c* axis increases, leading to a decrease in unit-cell volume of $\sim$3%. Extrapolation of the unit-cell volume linearly to x = 1 provides an estimated unit-cell volume V = 211.7 Å^3 for $SmO_{0.5}F_{0.5}BiS_2$

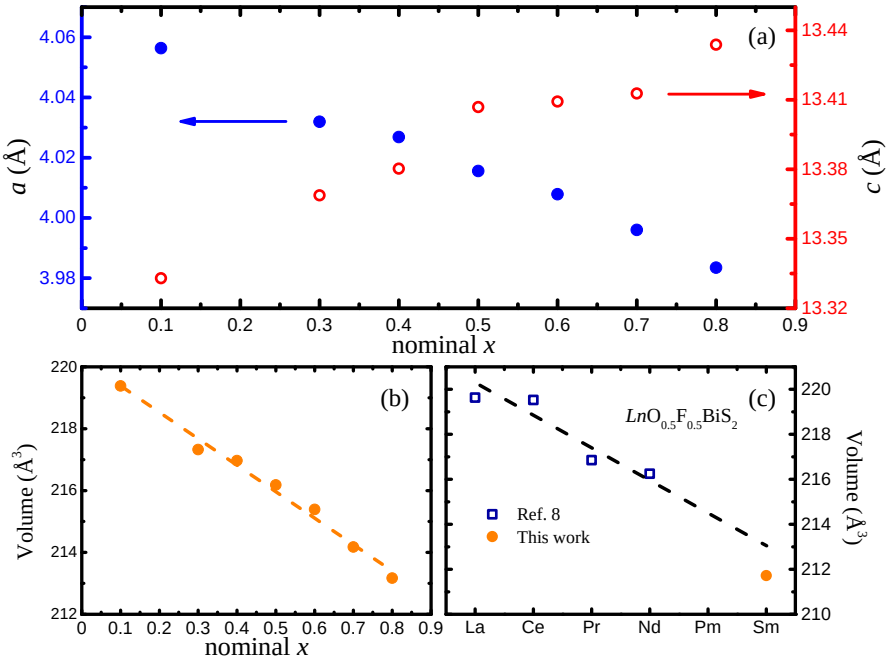

Figure III.2: Dependence of lattice parameters a (left axis) and c (right axis), and unit-cell volume V on nominal Sm concentration x. (c) V for $Ln\mathrm{O}_{0.5}\mathrm{F}_{0.5}\mathrm{BiS}_2$ (*Ln* = La, Ce, Pr, Nd) from Ref. 8 and estimated V for $\mathrm{SmO}_{0.5}\mathrm{F}_{0.5}\mathrm{BiS}_2$. Dashed lines are guides to the eye.

(see Fig. III.2(c)), which is slightly below an extrapolation of the measured unit-cell volumes for the reported $Ln\mathrm{O}_{0.5}\mathrm{F}_{0.5}\mathrm{BiS}_2$ compounds in which the *Ln* ion is believed to be trivalent.[7]

Electrical resistivity ρ vs. temperature T in zero magnetic field is depicted in Fig. III.3. Upon cooling, $\rho(T)$ increases until the onset of the superconducting transition for all samples, indicating semiconducting-like behavior. Previous studies on electrical transport behavior in single crystalline samples of $Ln\mathrm{O}_{1-x}\mathrm{F}_x\mathrm{BiS}_2$ (*Ln* = La, Ce, Nd) do not provide a cohesive or consistent picture of the intrinsic behavior; both metallic and semiconducting-like behavior were observed in these samples depending on the synthesis mothod and the chemical composition.[18, 19] Since single crystalline samples of $\mathrm{La}_{1-x}\mathrm{Sm}_x\mathrm{O}_{0.5}\mathrm{F}_{0.5}\mathrm{BiS}_2$ were not used in this study, it is difficult to determine whether

the observed semiconducting-like behavior might be related to poor intergain contact or not. However, if this is a bulk effect in single grains, the samples with higher Sm concentration would have smaller semiconducting energy gaps compared with those with lower Sm concentration since the semiconducting-like behavior is suppressed with Sm substitution.

With Sm substitution for La, the T_c of $La_{1-x}Sm_xO_{0.5}F_{0.5}BiS_2$ gradually increases and reaches a maximum value of $T_{c,\rho}$ = 5.4 K for x = 0.8 as is shown in Fig. III.4. The value of $T_{c,\rho}$ is defined by the temperature where the electrical resistivity falls to 50% of its normal-state value, and the width of the transition is characterized by identifying the temperatures where the electrical resistivity decreases to 90% and 10% of that value. For x = 0.9, due to the presence of an appreciable amount of impurities like LaF_3, the actual chemical composition of the sample is probably quite different from the nominal composition (i.e., less fluorine). This would be expected to cause a decrease in T_c,[5] which is consistent with our results. Extrapolating $T_{c,\rho}(x)$ for $x \leqslant 0.8$ linearly to x = 1 yields an estimate for the expected T_c of $SmO_{0.5}F_{0.5}BiS_2$ of ~6.2 K (see Fig. III.4), which is significantly higher than the T_c reported for other $LnO_{0.5}F_{0.5}BiS_2$ compounds synthesized at ambient pressure.[7, 8] We recently became aware of a report that the parent compound $SmO_{0.5}F_{0.5}BiS_2$ could be synthesized by solid state reaction and it does not exhibit superconductivity above 2 K.[20] However, both this work and a recent study on the system $Nd_{1-z}Sm_zO_{1-y}F_yBiS_2$ show solubility limits of Sm by using the same synthesis method.[17] The T_c of $La_{1-x}Sm_xO_{0.5}F_{0.5}BiS_2$ seems closely related to the lattice parameters shown in Fig. III.2(a), which is consistent with the study of the

chemical pressure effects on $Ce_{1-x}Nd_xO_{1-y}F_yBiS_2$ and $Nd_{1-z}Sm_zO_{1-y}F_yBiS_2$.[17, 21] Besides, the T_c values of $La_{1-x}Sm_xO_{0.5}F_{0.5}BiS_2$ are probably intermediate between those of the parent compounds $LaO_{0.5}F_{0.5}BiS_2$ and $SmO_{0.5}F_{0.5}BiS_2$, otherwise it would be difficult to explain why T_c increases as we substitute non-magnetic La ions by magnetic Sm ions.

The effect of annealing temperature on the resistivity and T_c were also investigated. An annealing temperature of 800°C is suitable to prepare $La_{1-x}Sm_xO_{0.5}F_{0.5}BiS_2$ samples for $x \leqslant 0.3$. However, for $x \geqslant 0.5$, annealing the samples at 800°C caused a significant increase in the amount of impurities, resulting in a large normal-state electrical resistivity and low T_c. To reduce the concentration of these impurities, different heat-treatment temperatures were used to synthesize the samples. By decreasing the annealing temperature, it was possible to significantly enhance T_c and reduce the normal-state electrical resistivity (see Fig. III.3(b)) for the samples with high Sm concentrations. On the other hand, when the x = 0.8 sample is annealed at 750°C, T_c is very similar but the electrical resistivity is slightly lower, compared with the T_c and resistivity values for samples annealed at 710°C. This suggests that the optimal annealing temperature for synthesizing $La_{1-x}Sm_xO_{0.5}F_{0.5}BiS_2$ samples with $x \geqslant 0.5$ is probably around 750°C.

Figure III.5(a) shows the temperature dependence of zero-field-cooled (ZFC) and field-cooled (FC) dc magnetic susceptibility under an applied magnetic field of 10 Oe. The samples exhibit reasonable diamagnetic signals associated with the induced supercurrent during ZFC measurements, suggesting that the samples are bulk superconductors. A paramagnetic contribution to the magnetic susceptibility around T_c, which is larger at

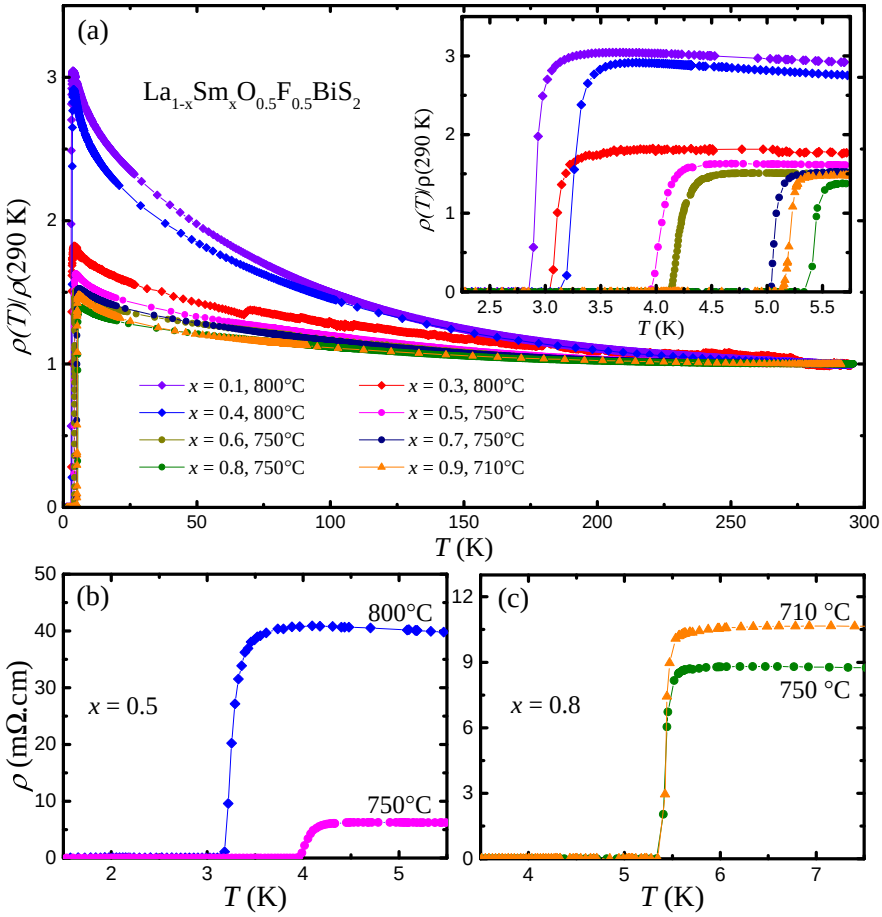

Figure III.3: (a) Temperature dependence of the electrical resistivity, $\rho(T)$, normalized by its value at 290 K, ρ(290 K), for $La_{1-x}Sm_xO_{0.5}F_{0.5}BiS_2$. The inset displays the data in panel (a) from 2 to 6 K, emphasizing the superconducting transitions. (b) and (c) Electrical resistivity $\rho(T)$ for two samples with $x = 0.5$ and $x = 0.8$, respectively. The annealing temperature used for each sample is denoted.

lower external magnetic fields and for higher Sm concentration samples, was observed during both FC and ZFC measurements as shown in Fig. III.5(b). Similar features have been reported in certain copper oxide superconductors, Nb disks, MgB_2, and Pb, and are generally referred to as a paramagnetic Meissner effect (PME).[22–27] However, further work needs to be done in order to determine whether the observed paramagnetic signal is associated with the PME or is related to movement of the samples in an inhomogeneous external magnetic field in the MPMS system.[28, 29] A jump from negative to positive magnetic susceptibility during ZFC measurements in the data for x = 0.7, 0.8 is an instrumental artifact resulting from a brief loss of the temperature control near the boiling point of ^{4}He, during which the temperature will suddenly increase above T_c and then slowly return to the set point. This induces extra irreversible magnetic flux penetration during ZFC measurements in the samples with $T_c > 4.4$ K. AC magnetic susceptibility data for selected samples with x = 0.1, 0.5, 0.7, and 0.9 are plotted in Figs. III.5(c) and (d). The smooth transitions in both ac and dc magnetic susceptibility data imply there is probably only one phase that contributes to the observed bulk shielding signal. No evidence of a structural phase transition induced by Sm substitution was observed.[30–32]

We defined T_c in dc and ac magnetic susceptibility measurements as the temperature at which the ZFC and FC data separate and the point where the imaginary part drops below zero, respectively. The $T_{c,\chi dc}$ values determined from χ_{dc} measurements increase monotonically from 2.65 K for x = 0.1 to 5.20 K for x = 0.8 as shown in Fig. III.4. Furthermore, dc and ac susceptibility measurements reveal enhanced volume and shielding fractions at 2 K with increasing Sm substitution (Fig. III.5(e)), respectively, indicating

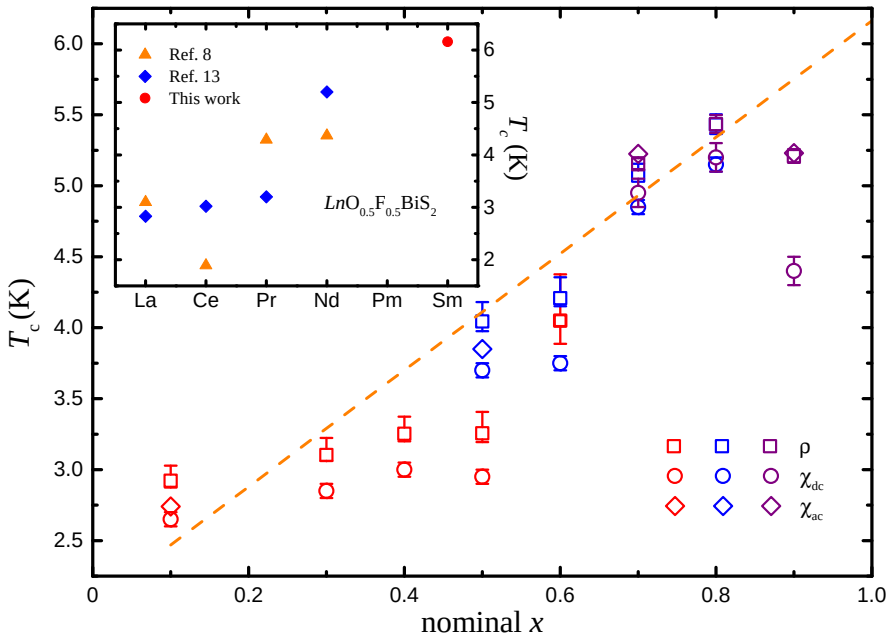

Figure III.4: Superconducting critical temperature T_c vs. nominal Sm concentration x of $La_{1-x}Sm_xO_{0.5}F_{0.5}BiS_2$. Red, blue, and purple symbols represent results for samples annealed at 800°C, 750°C, and 710°C, respectively. The dashed line is a linear fit of $T_{c,\rho}$ from $x = 0.1$ to $x = 0.8$. (Inset) $T_{c,\rho}$ of $LnO_{0.5}F_{0.5}BiS_2$ compounds reported in Refs. 8 and 13 together with the estimated $T_{c,\rho} = 6.2$ K of $SmO_{0.5}F_{0.5}BiS_2$.

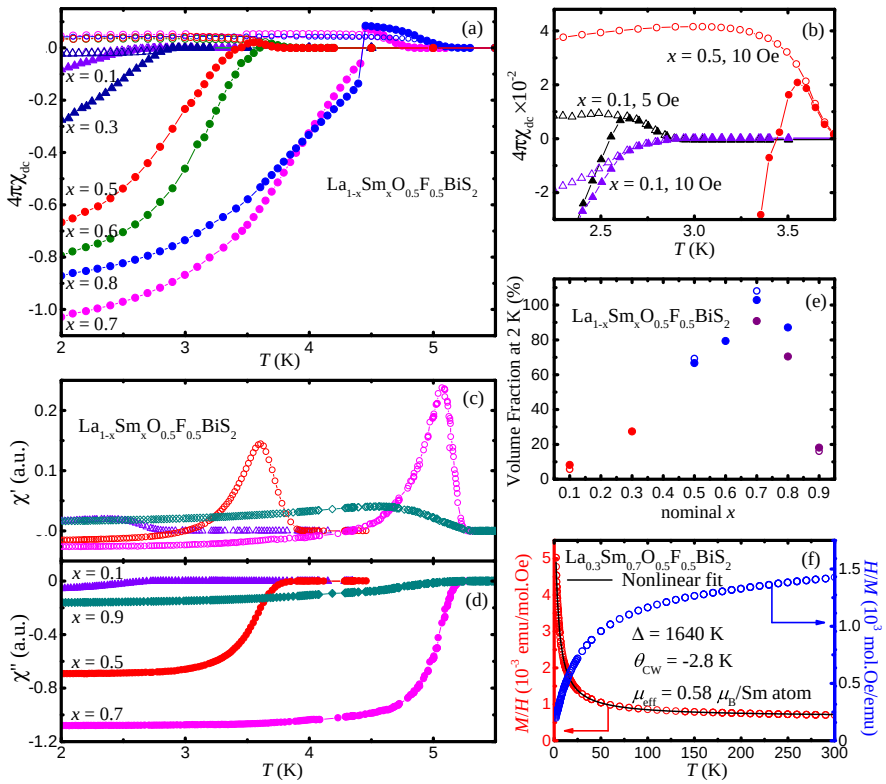

Figure III.5: (a) Zero-field-cooled (ZFC) (filled symbols) and field-cooled (FC) (open symbols) dc magnetic susceptibility data for $La_{1-x}Sm_xO_{0.5}F_{0.5}BiS_2$ in an applied magnetic field of 10 Oe. (b) Paramagnetic-like behavior of selected samples with x = 0.1 and 0.9 in applied magnetic fields of 5 Oe and 10 Oe, respectively. Magnetic susceptibility data for x = 0.1 in 10 Oe is also plotted for comparison. (c) Real and (d) imaginary part of the ac magnetic susceptibility for selected samples. (e) Evolution of shielding volume fraction with Sm substitution. Open and filled circles correspond to ac and dc susceptibility; red, blue, and purple colored data points represent measurements on samples annealed at 800°C, 750°C and 710°C, respectively. (f) M/H and H/M vs. T data in the normal state for $La_{0.3}Sm_{0.7}O_{0.5}F_{0.5}BiS_2$, measured from 2 to 300 K in an applied magnetic field of 5 kOe. The solid line is a nonlinear fit using Eq. (1).

improvements in the quality of the samples. The optimal volume fraction is obtained at x = 0.7. With further Sm substitution, however, the volume fraction rapidly decreases, coinciding with the appearance of an appreciable amount of non-superconducting secondary phases. The fact that the T_c of the sample with x = 0.8 is higher than that of the sample with x = 0.7, which shows the highest volume fraction, implies that superconductivity in $La_{1-x}Sm_xO_{0.5}F_{0.5}BiS_2$ could be further enhanced if samples could be prepared with a higher Sm concentration.

Magnetization *M*, divided by magnetic field *H*, *M*/*H*, for *H* = 5 kOe and *x* = 0.7 is displayed as a function of temperature in Fig. III.5(f) (left axis). In addition to distinct non-Curie Weiss behavior (see Fig. III.5(f), right axis), there is no evidence for magnetic order down to 2 K. Inverse of dc magnetic susceptibility χ^{-1} vs. *T* data doesn't change linearly with temperature. Unlike other heavy lanthanides, the energy between the *J* = 5/2 ground state and the *J* = 7/2 first excited state in Sm^{3+} is only 0.12 eV and the Van Vleck term should be considered when modeling the magnetic susceptibility of compounds containing Sm.[33, 34] Hence, the temperature dependence of the magnetization was fitted by a modified Curie-Weiss law:

$$\frac{M}{H} = \frac{N_A}{k_B}\left[\alpha_J \mu_B^2 + \frac{\mu_{eff}^2}{3(T-\theta_{CW})}\right], \tag{III.1}$$

in which N_A is Avogadro's number, k_B is Boltzmann's constant, μ_B is the Bohr magneton, μ_{eff} is the effective magnetic moment in Bohr magnetons, and θ_{CW} is the Curie-Weiss temperature. We define $\alpha_J = 20/7\Delta$, where Δ is the energy separation between the

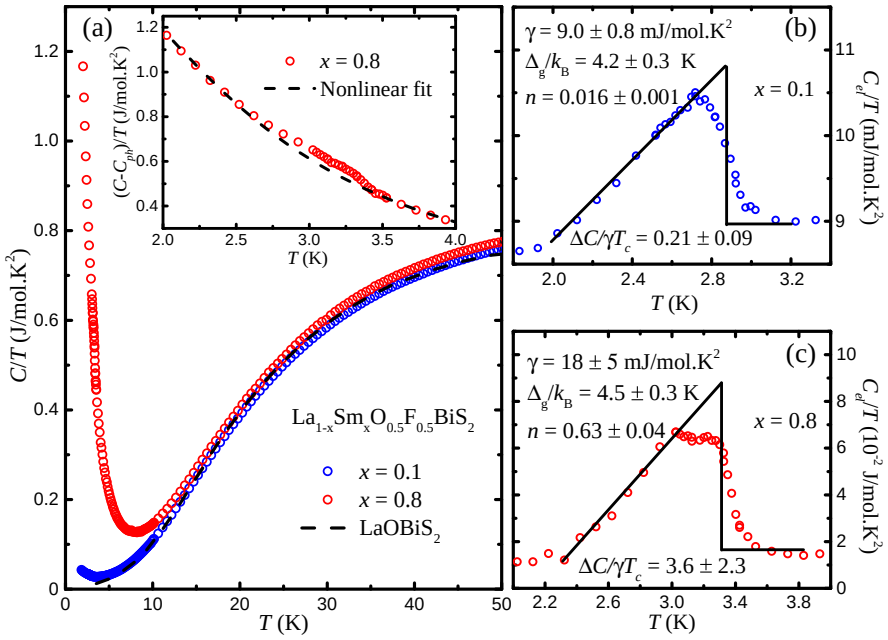

Figure III.6: Specific heat C divided by temperature, C/T, vs. T for $La_{1-x}Sm_xO_{0.5}F_{0.5}BiS_2$ with x = 0.1, 0.8 and for $LaOBiS_2$. (Inset) $(C\text{-}C_{ph})/T$ vs. T, where C_{ph} is the lattice contribution, and a fit of the Schottky anomaly contribution for $La_{0.2}Sm_{0.8}O_{0.5}F_{0.5}BiS_2$ (dashed line). (b) and (c) Electronic contribution C_{el}/T of $La_{1-x}Sm_xO_{0.5}F_{0.5}BiS_2$ with x = 0.1 and x = 0.8, respectively. An entropy conserving construction is shown, which is used to define T_c.

J = 5/2 ground state multiplet and the J = 7/2 first excited state multiplet for Sm.[35] From the best fit of the M/H data using Eq. (1), values for Δ, θ_{CW}, and μ_{eff} were found to be 1640 K, -2.8 K, and 0.58 μ_B/Sm atom, respectively. The experimental Δ value is close to the estimated value for free Sm^{3+} ($\sim$1500 K).[33] The effective magnetic moment of the samples are considerably smaller than the free Sm^{3+} ion value of 0.845 μ_B/Sm atom. Similar low values of μ_{eff} have been reported in other studies[36, 37] and are not necessarily evidence for an intermediate valence for Sm; an accurate theoretical description of experimental data in Sm systems is complicated by the combined effects of the crystalline electric field (CEF) effects and J-mixing.[38]

The results of specific heat *C* measurements for x = 0.1, 0.8, and a nonmagnetic reference compound $LaOBiS_2$ are displayed in Fig. III.6(a), plotted as *C*/*T* vs. *T*. Above 10 K, the specific heat of the compounds are almost the same, due to similar lattice contributions. The upturns in C/T vs. T below 3.7 K and 8.0 K for the samples with x = 0.1 and 0.8, respectively, which overlap with the superconducting transitions, are due to a Schottky contribution (C_{Sch}) caused by CEF splitting of the J = 5/2 Hund's rule ground state multiplet. Hence, the specific heat of the samples consists of electronic (C_{el}), phonon (C_{ph}), and Schottky (C_{Sch}) contributions. The best fit of the $LaOBiS_2$ data below 7 K using $C(T) = C_{el}(T) + C_{ph}(T) = \gamma T + A_3T^3 + A_5T^5$, yields the normal-state electronic specific heat coefficient γ = 3.32 mJ/mol K^2 and the coefficients of the phonon contribution A_3 = 0.655 mJ/mol K^4 and A_5 = 4.27 μJ/mol K^6. Representative (C-C_{ph})/*T* vs. *T* data for x = 0.8 are shown in the inset of Fig. III.6(a). The phonon contribution of the Sm-substituted samples was assumed to be the same as for $LaOBiS_2$ and was subtracted from the specific heat. The remaining specific heat data could be fitted with the following expression:

$$C(T)/T = \gamma + nC_{Sch}/T = \gamma + n\frac{R}{T}\frac{\left(\frac{\Delta_g}{k_BT}\right)^2 e^{\left(\frac{\Delta_g}{k_BT}\right)}}{\left[1+e^{\left(\frac{\Delta_g}{k_BT}\right)}\right]^2}. \qquad \text{(III.2)}$$

The second term in Eq. (2), nC_{Sch}/T, represents a Schottky anomaly in which n is the number of Sm atoms per formula unit that contribute to the Schottky anomaly, Δ_g is the splitting between the ground state and the first excited state doublet of the J = 5/2 Hund's rule ground state multiplet, k_B is Boltzmann's constant, and *R* is the ideal gas

constant. The best fits to the $C(T)/T$ data for the $La_{1-x}Sm_xO_{0.5}F_{0.5}BiS_2$ samples with x = 0.1 and 0.8 provide very similar Δ_g splitting values, but different γ values (listed in Figs. III.6(b) and (c)). Subtracting both $C_{ph}(T)$ and $C_{Sch}(T)$ from $C(T)$ data yields the electronic specific heat $C_{el}(T)$ contribution, revealing a clear feature around T_c, which provides evidence for bulk superconductivity.

The electronic contribution to the specific heat data for the x = 0.1 sample shows a jump at $\sim$2.8 K, which is consistent with the T_c obtained from the resistivity and magnetization measurements. However, for the sample with x = 0.8, the T_c values estimated from the entropy conserving-constructions are considerably lower than the $T_{c,\rho}$ values determined from $\rho(T)$ measurements, which may suggest an inhomogeneous distribution of Sm in the polycrystalline samples. Domains with high Sm concentration would result in relatively high T_c values in the electrical resistivity measurement. In contrast, a considerable amount of domains, which are associated with the bulk superconductivty of the sample, could contain a lower Sm concentration with lower T_c. Values of $\Delta C/\gamma T_c$ of 0.21 $\pm$ 0.09 and 3.6 $\pm$ 2.3 were extracted from the $C_{el}(T)$ data for x = 0.1 and 0.8, respectively. The uncertainties associated with values of γ, Δ_g, n, and $\Delta C/\gamma T_c$, which are shown in Fig. III.6(b) and (c), are appreciable for the following reasons. First, making a precise evaluation of the Schottky contribution to the specific heat is very difficult since the local environments of the Sm ions may be quite different due to sample inhomogeneity and the temperatures that have been measured are not low enough to observe the complete profile of the Schottky anomaly. Second, the Schottky contribution to the specific heat at low temperatures is much more significant than the electronic contribution; a slight

error in evaluating the Schottky anomaly may result in a considerable uncertainty of the γ value. Third, secondary impurity phases also contribute to the specific heat; however, quantitative analysis of their contributions is very difficult since the amount and exact chemical compositions of these phases are not known with high precision. Finally, there are many variable parameters that are involved in the specific heat analysis, which introduces additional uncertainty into each best-fit value. We estimated the uncertainties associated with the best-fit values for γ, Δ_g, and n by considering both the errors inherent to the specific heat measurements as well as the range of values for γ, Δ_g, and n that lead to optimized fits of the C/T data using Eq. (2). The magnitude of the specific heat jump ΔC at T_c depends sensitively on the values of Δ_g and n since they characterize the large Schottky anomaly contribution to specific heat that is subtracted from the measured C/T data to obtain the electronic contribution C_{el}/T. The uncertainties in the values of $\Delta C/\gamma T_c$ that are presented in Figs. III.6(b) and (c) take this into account and are quite large as a consequence. Given the uncertainties involved in the procedure for extracting the $\Delta C/\gamma T_c$ values, these estimates are consistent with bulk superconductivity; however, the question of whether or not the $\Delta C/\gamma T_c$ values of the samples are consistent with the BCS value of 1.43 remains open. To perform a more precise quantitative analysis, homogenous single phase samples of $La_{1-x}Sm_xO_{0.5}F_{0.5}BiS_2$ need to be prepared and the specific heat below 1.8 K should be investigated.

III.D Summary

In summary, the T_c and superconducting volume fraction were found to increase with x in the $La_{1-x}Sm_xO_{0.5}F_{0.5}BiS_2$ samples investigated in the experiments reported herein. The solubility limit of Sm has a large value of $x \sim 0.8$ in $La_{1-x}Sm_xO_{0.5}F_{0.5}BiS_2$, and a continuous decrease in the a axis and increase in the c axis is observed with increasing x. Bulk superconductivity was observed in the samples according to magnetic susceptibility and specific heat measurements. No evidence for a structural phase transition was found in this study. The results demonstrate that the superconducting critical temperature T_c of tetragonal BiS_2-based compounds is correlated with the lattice parameters and can be significantly enhanced by Sm substitution. This gives a promising way to further increase the T_c of BiS_2-based superconductors by modifying the blocking layers through the substitution of heavier *Ln* lanthanides (*Ln* = Eu - Tm) or synthesizing the parent $LnO_{1-x}F_xBiS_2$ compounds.

The text and data presented in this chapter are reprints of material that appears in "Enhancement of Superconductivity in $La_{1-x}Sm_xO_{0.5}F_{0.5}BiS_2$," Y. Fang, D. Yazici, B. D. White, and M. B. Maple, *Phys. Rev. B* **91**, 064510 (2015). The dissertation author is the primary investigator and author of this article.

Bibliography

[1] Y. Mizuguchi, H. Fujihisa, Y. Gotoh, K. Suzuki, H. Usui, K. Kuroki, S. Demura, Y. Takano, H. Izawa, and O. Miura, Phys. Rev. B **86**, 220510 (2012).

[2] S. K. Singh, A. Kumar, B. Gahtori, G. Sharma, S. Patnaik, and V. P. S. Awana, J. Am. Chem. Soc. **134**, 16504 (2012).

[3] V. P. S. Awana, A. Kumar, R. Jha, S. Kumar Singh, A. Pal, J. Saha, and S. Patnaik, Solid State Commun. **157**, 21 (2013).

[4] S. Demura, Y. Mizuguchi, K. Deguchi, H. Okazaki, H. Hara, T. Watanabe, S. James Denholme, M. Fujioka, T. Ozaki, H. Fujihisa, G. Yoshito, M. Osuke, Y. Takahide, T. Hiroyuki, and T. Yoshihiko, J. Phys. Soc. Jpn. **82**, 033708 (2013).

[5] Y. Mizuguchi, S. Demura, K. Deguchi, Y. Takano, H. Fujihisa, Y. Gotoh, H. Izawa, and O. Miura, J. Phys. Soc. Jpn. **81**, 114725 (2012).

[6] J. Xing, S. Li, X. Ding, H. Yang, and H.-H. Wen, Phys. Rev. B **86**, 214518 (2012).

[7] D. Yazici, K. Huang, B. D. White, A. H. Chang, A. J. Friedman, and M. B. Maple, Phil. Mag. **93**, 673 (2013).

[8] Y. Mizuguchi, Physics Procedia **58**, 94 (2014).

[9] K. Deguchi, Y. Mizuguchi, S. Demura, H. Hara, T. Watanabe, S. J. Denholme, M. Fujioka, H. Okazaki, T. Ozaki, H. Takeya, T. Yamaguchi, O. Miura, and Y. Takano, Europhys. Lett. **101**, 17004 (2013).

[10] R. Jha, A. Kumar, S. K. Singh, and V. P. S. Awana, Journal of superconductivity and novel magnetism **26**, 499 (2013).

[11] D. Yazici, K. Huang, B. D. White, I. Jeon, V. W. Burnett, A. J. Friedman, I. K. Lum, M. Nallaiyan, S. Spagna, and M. B. Maple, Phys. Rev. B **87**, 174512 (2013).

[12] X. Lin, X. Ni, B. Chen, X. Xu, X. Yang, J. Dai, Y. Li, X. Yang, Y. Luo, Q. Tao, G. Cao, and Z. Xu, Phy. Rev. B **87**, 020504 (2013).

[13] V. S. Tanryverdiew, O. M. Aliew, and I. I. Aliev, Inorg. Mater. **31**, 1361 (1995).

[14] A. C. Larson and R. B. Von Dreele, Los Alamos National Laboratory Report (1994).

[15] B. H. Toby, J. Appl. Crystallogr. **34**, 210 (2001).

[16] Z. R. Ye, H. F. Yang, D. W. Shen, J. Jiang, X. H. Niu, D. L. Feng, Y. P. Du, X. G. Wan, J. Z. Liu, X. Y. Zhu, H. H. Wen, and M. H. Jiang, Phys. Rev. B **90**, 045116 (2014).

[17] J. Kajitani, T. Hiroi, A. Omachi, O. Miura, and Y. Mizuguchi, arXiv preprint arXiv:1408.2625 (2014).

[18] M. Nagao, A. Miura, S. Demura, K. Deguchi, S. Watauchi, T. Takei, Y. Takano, N. Kumada, and I. Tanaka, Solid State Commun. **178**, 33 (2014).

[19] X. B. Wang, S. M. Nie, H. P. Wang, P. Zheng, P. Wang, T. Dong, H. M. Weng, and N. L. Wang, Phys. Rev. B **90**, 054507 (2014).

[20] G. S. Thakur, G. K. Selvan, Z. Haque, L. C. Gupta, S. L. Samal, S. Arumugam, and A. K. Ganguli, arXiv preprint arXiv:1410.0751 (2014).

[21] J. Kajitani, A. Omachi, T. Hiroi, O. Miura, and Y. Mizuguchi, Physica C **504**, 33 (2014).

[22] I. A. Chaban, J. Supercond. **13**, 1011 (2000).

[23] D. J. Thompson, M. S. M. Minhaj, L. E. Wenger, and J. T. Chen, Phys. Rev. Lett. **75**, 529 (1995).

[24] W. Braunisch, N. Knauf, V. Kataev, S. Neuhausen, A. Grütz, A. Kock, B. Roden, D. Khomskii, and D. Wohlleben, Phys. Rev. Lett. **68**, 1908 (1992).

[25] H. Sözeri, L. Dorosinskii, U. Topal, and I. Ercan, Physica C **408**, 109 (2004).

[26] S. Yuan, L. Ren, and F. Li, Phys. Rev. B **69**, 092509 (2004).

[27] E. L. Papadopoulou, P. Nordblad, P. Svedlindh, R. Schöneberger, and R. Gross, Phys. Rev. Lett. **82**, 173 (1999).

[28] T. P. Papageorgiou, H. F. Braun, and T. Herrmannsdörfer, Phys. Rev. B **66**, 104509 (2002).

[29] M. McElfresh, S. Li, and R. Sager, Quantum Design (San Diego) technical report (1996).

[30] Y. Mizuguchi, T. Hiroi, J. Kajitani, H. Takatsu, H. Kadowaki, and O. Miura, J. Phys. Soc. Jpn. **83**, 053704 (2014).

[31] H. Kotegawa, Y. Tomita, H. Tou, H. Izawa, Y. Mizuguchi, O. Miura, S. Demura, K. Deguchi, and Y. Takano, J. Phys. Soc. Jpn. **81**, 103702 (2012).

[32] C. T. Wolowiec, B. D. White, I. Jeon, D. Yazici, K. Huang, and M. B. Maple, J. Phys.: Condens. Matter **25**, 422201 (2013).

[33] J. H. Van Vleck, *The theory of electric and magnetic susceptibilities*, vol. 72 (Oxford University Press London, 1965).

[34] M. B. Maple, in *High-Pressure and Low-Temperature Physics* (Springer, 1978).

[35] D. Wagner, *Introduction to the Theory of Magnetism*, vol. 48 (Pergamon, 1972).

[36] M. B. Maple and D. Wohlleben, Phys. Rev. Lett. **27**, 511 (1971).

[37] K. Ahn, V. K. Pecharsky, and K. A. Gschneidner, Phys. Rev. B **76**, 014415 (2007).

[38] K. A. Gschneidner, L. Eyring, and G. H. Lander, *Handbook on the physics and chemistry of rare earths*, vol. 32 (Elsevier, 2001).

Chapter IV

Pressure-Induced Phase Transition in $La_{1-x}Sm_xO_{0.5}F_{0.5}BiS_2$

IV.A Introduction

The application of external pressure to materials has led to the discovery of many new superconductors and has apparently raised the record of the highest superconducting transition temperature, T_c, to 190 K in H_2S.[1] Due to its substantial impact on the crystalline and electronic structure of solids, applied pressure is recognized as a powerful tool to tune the T_c, critical fields, and other physical properties of superconductors.[2, 3] Recently, superconductivity with T_c values ranging from 2.7 to 10.6 K at ambient pressure has been reported for BiS_2-based compounds including $Bi_4O_4S_3$, $LnO_{1-x}F_xBiS_2$ (*Ln* = La, Ce, Pr, Nd, Yb), $La_{1-x}M_xOBiS_2$ (*M* = Ti, Zr, Hf, Th), $Sr_{1-x}La_xFBiS_2$, $EuBiS_2F$, and $Eu_3Bi_2S_4F_4$.[4–16] Similar to the cuprate and Fe-based superconductors, the structure of these compounds is characterized by alternate stacking of superconducting BiS_2

layers and charge-reservoir blocking layers, both of which are tunable by using chemical substitution or applying external pressure.[4, 5, 11, 14, 17, 18] Therefore, there is plenty of phase space to search for the optimal conditions for superconductivity in this family of compounds.

The compound $LaO_{0.5}F_{0.5}BiS_2$, synthesized under high pressure, was reported to have the highest T_c of $\sim$10.6 K in contrast to the $T_c \sim 3$ K of the same compound when it is synthesized at ambient pressure.[12, 19] Although the crystal structure of both the sample annealed at ambient pressure (AP) and the one synthesized under applied high pressure (HP) have the same space group *P4/nmm*, the strongly reduced lattice parameters a and c are considered to be related to the enhancement in T_c of HP samples.[12, 19, 20] On the other hand, $LaO_{0.5}F_{0.5}BiS_2$ (AP), which has a low T_c, undergoes a structural phase transition from tetragonal to monoclinic at a pressure of 0.7 GPa, and T_c is enhanced to 10.7 K.[21] Similar abrupt increases in T_c were also observed in the compounds $LnO_{0.5}F_{0.5}BiS_2$ (*Ln* = Ce, Pr, Nd), $LaO_{0.5}F_{0.5}BiSe_2$, $EuBiS_2F$ and $Eu_3Bi_2S_4F_4$ under pressure.[22–26] A gradual increase in T_c up to 5.4 K was observed at ambient pressure in $La_{1-x}Sm_xO_{0.5}F_{0.5}BiS_2$ with increasing Sm concentration until the solubility limit near x = 0.8.[27] The lattice parameter a in $La_{0.2}Sm_{0.8}O_{0.5}F_{0.5}BiS_2$ is significantly smaller compared with other BiS_2 based compounds; however, further optimization of superconductivity in this system is prevented by the presence of a solubility limit.[27] Hence, it would be interesting to explore the electrical transport properties of the system $La_{1-x}Sm_xO_{0.5}F_{0.5}BiS_2$ under pressure. Such an experiment will not only provide a broad picture of how T_c evolves at extreme conditions, but will also help to determine which

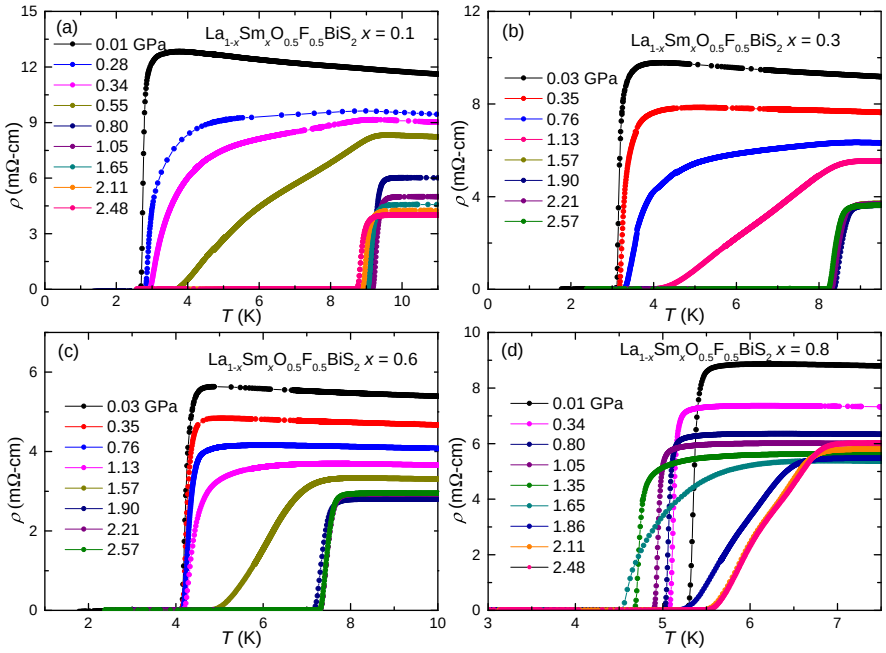

Figure IV.1: (a), (b), (c), (d) Temperature dependence of the electrical resistivity at various applied pressures near T_c for $La_{1-x}Sm_xO_{0.5}F_{0.5}BiS_2$ with x = 0.1, 0.3, 0.6, and 0.8, respectively. Lines are guides to the eye.

parameters are essential to promote superconductivity in the BiS_2-based compounds. Additionally, pressure may be particularly well suited to induce certain types of phase transitions in $La_{0.2}Sm_{0.8}O_{0.5}F_{0.5}BiS_2$ due to its extraordinarily small lattice parameters in ambient conditions.

IV.B Experimental Details

The synthesis and crystal structure analysis of $La_{1-x}Sm_xO_{0.5}F_{0.5}BiS_2$ are described elsewhere.[10, 27] The chemical composition of each sample presented in this paper is nominal; impurity phases, including La(Sm)F_3, La(Sm)O, and Bi_2S_3, typically $\sim$4 wt.% for x = 0.1, 0.3, 0.6 and $\sim$8 wt.% for x = 0.8, were found in these samples, which may cause slight differences between the nominal and actual chemical compo-

sitions of the samples.[27] Geometric factors for each sample were measured before applying pressure and used to calculate the electrical resistivity from measurements of resistance. Electrical resistance measurements from ambient pressure to $\sim$2.6 GPa were performed on samples with nominal Sm concentrations x = 0.1, 0.3, 0.6, 0.8 between 2 and 280 K using a standard four-probe method in a pumped ^{4}He dewar. External pressures were generated by a clamped piston-cylinder cell using a Teflon capsule filled with a 1:1 by volume mixture of n-pentane and isoamyl alcohol, which is known to be a good hydrostatic pressure medium.[28, 29] The pressures applied to the samples were inferred from the T_c of a high purity ($>$99.99 %) Sn disk inside the sample chamber of the cell using the well-established behavior of $T_c(P)$ in high purity Sn.[30] The width of the superconducting transition of Sn, indicated by an ac magnetic susceptibility measurement, is $\sim$0.1 K at ambient pressure and remains the same until $\sim$2.6 GPa. This result strongly suggests a good hydrostatic environment at low temperature and high pressure.

IV.C Results and Discussion

Measurements of the low-temperature resistivity $\rho(T)$ for $La_{1-x}Sm_xO_{0.5}F_{0.5}BiS_2$ (x = 0.1, 0.3, 0.6, 0.8) samples in zero magnetic field under applied pressures are depicted in Fig. IV.1. Superconducting (SC) transitions in which ρ abruptly drops from a finite value to zero were observed in each sample from ambient pressure to the highest pressure ($\sim$2.6 GPa) applied in this study. We defined T_c as the temperature where the electrical resistivity (ρ) falls to 50% of its normal-state value, and the width of the transition is characterized by identifying the temperatures where the electrical resistivity decreases to

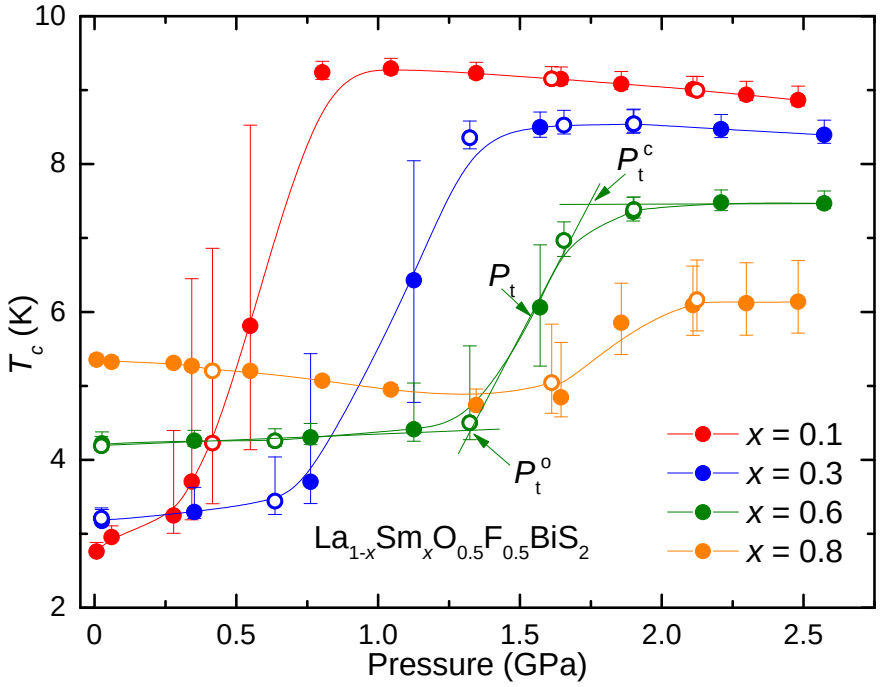

Figure IV.2: Superconducting critical temperature T_c vs pressure for $La_{1-x}Sm_xO_{0.5}F_{0.5}BiS_2$ (x = 0.1, 0.3, 0.6, 0.8). Filled and open circles with the same color represent T_c measured with increasing and decreasing pressure, respectively. The width of the superconducting transition is denoted by the vertical bars. $P_t{}^o$ and $P_t{}^c$ are defined as the pressure of the low-T_c to high-T_c phase transition onsets and completions, respectively; P_t is the midpoint between $P_t{}^o$ and $P_t{}^c$.

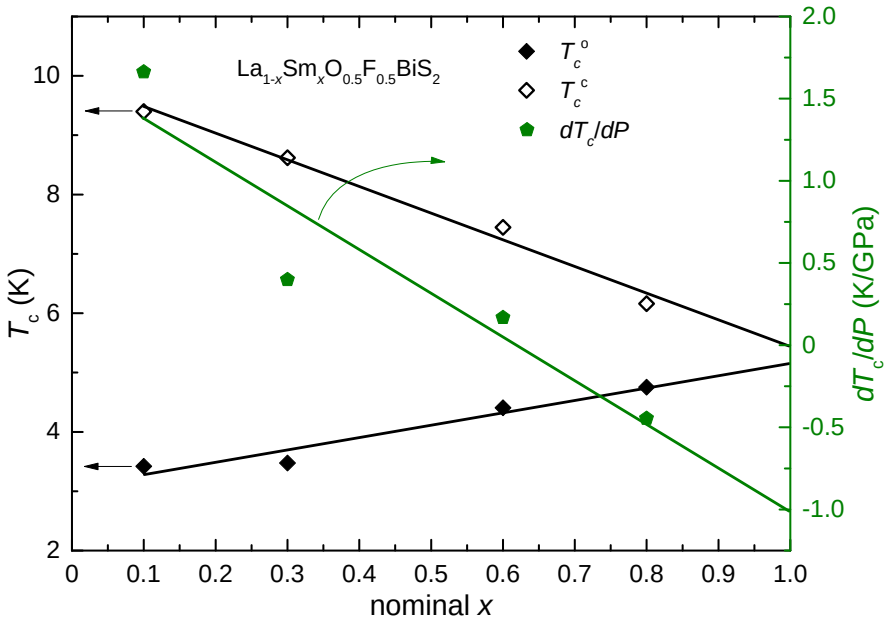

Figure IV.3: Sm concentration dependence of T_c at $P_t{}^o$ ($T_c{}^o$) and at $P_t{}^c$ ($T_c{}^c$) together with the initial rate of change in T_c with pressure (dT_c/dP) for $P < P_t{}^o$.

90% and 10% of its normal state value. Superconducting transitions are very sharp at low pressures for all of the samples. However, as can be seen in Fig. IV.1, the width of the SC transition is quite broad within a narrow range of pressures ($\sim$0.5 GPa), after which, T_c is remarkably enhanced and the transitions become sharp again for the samples with nominal x = 0.1, 0.3, 0.6. In the case of the x = 0.8 sample, however, the width of the SC transition remains broad at high pressures after the enhancement in T_c; this might be related to the x = 0.8 sample being so close to the solubility limit and possible chemical inhomogeneity of the sample.[27] This behavior reveals pressure-induced transitions from a low-T_c superconducting phase (SC1) to a high-T_c superconducting phase (SC2) in each sample.

The abrupt change in T_c under pressure is particularly apparent in the temperature-pressure phase diagram (see Fig. IV.2), in which $P_t{}^o$ is the onset of the phase transition,

$P_t{}^c$ is the pressure where the phase transition is complete, and P_t is the midpoint between $P_t{}^o$ and $P_t{}^c$. The broad superconducting transitions between $P_t{}^o$ and $P_t{}^c$ indicate the emergence of the SC2 phase; the sample in this pressure range is presumably in a mixture of the SC1 and SC2 phases. The values of T_c obtained in measurements with decreasing pressure (open symbols) are consistent with those measured with increasing pressure (filled symbols), revealing that the pressure-induced phase transitions are fully reversible. Tomita *et al.* recently reported a similar enhancement of T_c at ~0.7 GPa in polycrystalline samples of $LaO_{0.5}F_{0.5}BiS_2$, which was attributed to a structural phase transition from tetragonal to monoclinic due to sliding between two neighboring BiS_2-layers along the a-axis.[21] Since both $LaO_{0.5}F_{0.5}BiS_2$ and $La_{1-x}Sm_xO_{0.5}F_{0.5}BiS_2$ are characterized by the same crystal structure with space group group *P4/nmm* at ambient pressure and have similar chemical compositions, it seems likely that the pressure-induced enhancement of T_c for $La_{1-x}Sm_xO_{0.5}F_{0.5}BiS_2$ is also associated with a structural phase transition, i.e., the SC1 phase is tetragonal in structure as has been demonstrated by Ref. 27 and SC2 phase is probably monoclinic.

The T_c values of $La_{1-x}Sm_xO_{0.5}F_{0.5}BiS_2$ superconductors at ambient pressure gradually increase from ~2.7 K for x = 0.1 to ~5.4 K for x = 0.8 with increasing Sm substitution up to the solubility limit near x = 0.8.[27] However, the pressure dependence of T_c for all of the samples at $P < P_t{}^o$ differ significantly from each other. For the x = 0.1, 0.3, 0.6 samples, T_c is initially enhanced with increasing pressure almost linearly and dT_c/dP decreases with increasing Sm concentration as is shown in Fig. IV.3 (right axis). Although the value of T_c for x = 0.8 is the highest among the four compositions at

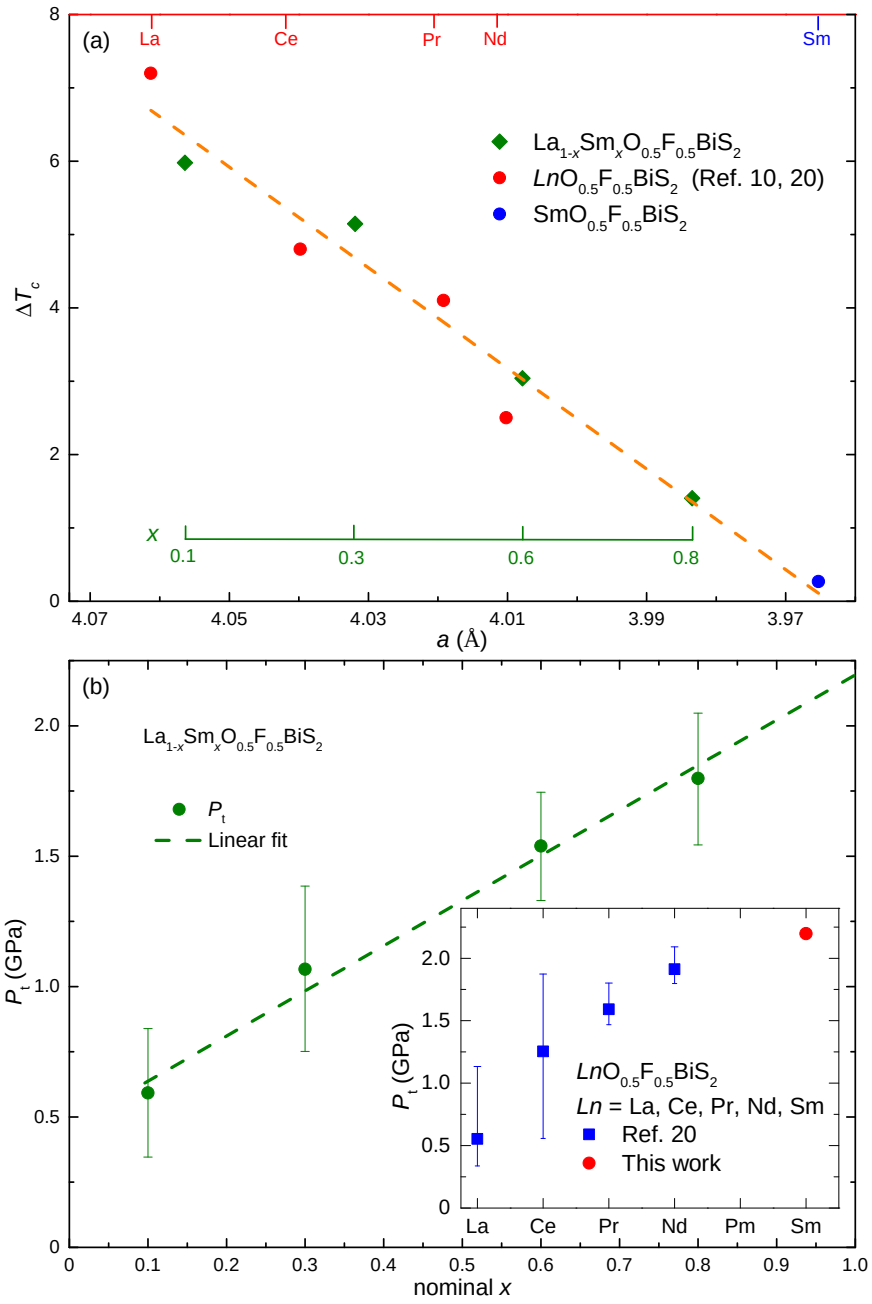

Figure IV.4: Dependence of (a) ΔT_c on lattice parameter a and (b) dependence of P_t on nominal Sm concentration. The inset in panel (b) displays the evolution of P_t as a function of *Ln*. Dashed lines are guides to the eye.

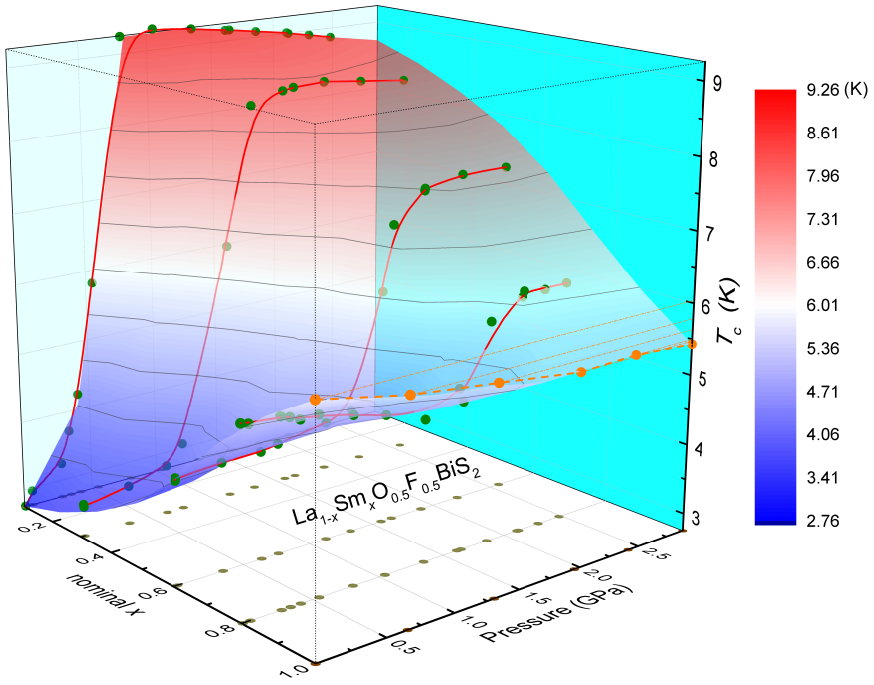

Figure IV.5: T_c plotted as a function of pressure and nominal Sm concentration x. The T_c of $SmO_{0.5}F_{0.5}BiS_2$ is estimated by linearly extrapolating the T_c of $La_{1-x}Sm_xO_{0.5}F_{0.5}BiS_2$ (x = 0.1, 0.3, 0.6, 0.8) below and above the phase transition near P_t. Filled circles in the x-y plane are projections of T_c.

ambient pressure, dT_c/dP is negative with a value of roughly -0.45 K/GPa, which results in a decreasing T_c with pressure down to $P_t{}^o$. These results suggest that reduction of the lattice parameter a, which is regarded to be essential to the enhancement of T_c for BiS_2-based compounds at ambient pressure,[11, 27, 31, 32] does not always result in an increase of T_c.

The T_c values at pressures just below and above the transition at P_t from SC1 to SC2 are plotted in Fig. IV.3 (left axis) and are denoted $T_c{}^o$ and $T_c{}^c$, respectively. Although $T_c{}^o$ increases with Sm substitution, $T_c{}^c$ is suppressed almost linearly from 9.4 K for x = 0.1 to 6.2 K for x = 0.8, resulting in a reduction of the size of the jump in T_c below and above the phase transition (ΔT_c) with increasing Sm concentration. This phenomenon

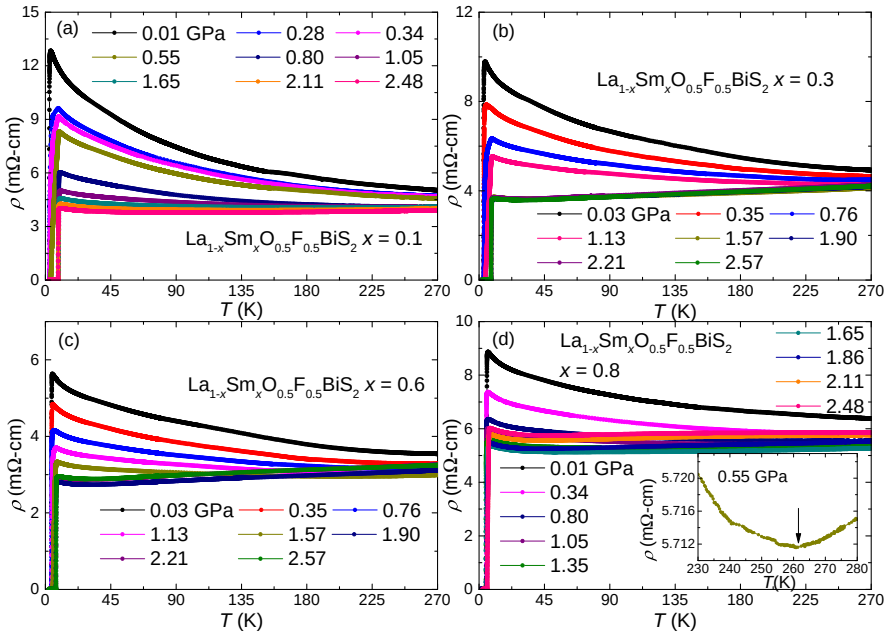

Figure IV.6: (a), (b), (c), (d) Electrical resistivity of $La_{1-x}Sm_xO_{0.5}F_{0.5}BiS_2$ with x = 0.1, 0.3, 0.6, and 0.8 under applied pressure from 270 K to ∼1.2 K, respectively. The inset of panel (d) is a representative $\rho(T)$ curve in which a minimum (indicated by the arrow) is observed in the normal state upon cooling.

is very similar to that which was observed for the compounds $LnO_{0.5}F_{0.5}BiS_2$ (*Ln* = La, Ce, Pr, Nd), in which the T_c values above the phase transition decrease with increasing *Ln* atomic number.[22] By linearly extrapolating both $T_c^{\rm o}$ and $T_c^{\rm c}$ of $La_{1-x}Sm_xO_{0.5}F_{0.5}BiS_2$ to x = 1, the estimated ΔT_c of $SmO_{0.5}F_{0.5}BiS_2$ is only ∼0.27 K, which is within the uncertainty of our estimate. If we plot ΔT_c for $LnO_{0.5}F_{0.5}BiS_2$, $La_{1-x}Sm_xO_{0.5}F_{0.5}BiS_2$, and the estimated ΔT_c for $SmO_{0.5}F_{0.5}BiS_2$ as a function of lattice parameter a, they are located almost on the same line despite the differences in their chemical composition (see Fig. IV.4(a)).

With Sm substitution for La, $P_{\rm t}$ increases from 0.59 GPa for x = 0.1 to 1.80 GPa for x = 0.8. The nearly linear evolution of $P_{\rm t}$ with Sm concentration (see Fig. IV.4(b)) enables one to estimate a $P_{\rm t}$ of ∼2.2 GPa for $SmO_{0.5}F_{0.5}BiS_2$, which is consistent with

the $P_{\rm t}$ values of other known LnO$_{0.5}$F$_{0.5}$BiS$_2$ compounds as is shown in the inset of Fig. 4(b).[22, 23] Figure IV.5 shows the T_c of La$_{1-x}$Sm$_x$O$_{0.5}$F$_{0.5}$BiS$_2$ at different pressures and Sm concentrations together with the estimated T_c of SmO$_{0.5}$F$_{0.5}$BiS$_2$ under pressure. The T_c at pressures below and above 2.2 GPa of SmO$_{0.5}$F$_{0.5}$BiS$_2$ is estimated from a linear extrapolation of the T_c values of the four samples below and above the phase transition, respectively. It can be seen that higher T_c values for the SC1 phase are found at higher Sm concentrations and lower pressures; however, higher T_c values for the SC2 phase are located in the region with lower Sm concentration just above the phase transition. In fact, by further reducing the Sm concentration to x = 0, a higher T_c value of $\sim$10.7 K could be obtained under pressure in LaO$_{0.5}$F$_{0.5}$BiS$_2$, which has the largest a lattice parameter among the LnO$_{0.5}$F$_{0.5}$BiS$_2$ compounds at ambient pressure.[21] On the other hand, reducing a enhances T_c at ambient pressure; however, it also reduces ΔT_c as discussed above. The pressure dependence of T_c below and above 2.2 GPa for SmO$_{0.5}$F$_{0.5}$BiS$_2$ has a similar trend and is almost indistinguishable as is shown in Fig. 5. Thus, the possibility that SmO$_{0.5}$F$_{0.5}$BiS$_2$ has the same phase at low and high pressures cannot be ruled out. Although it was reported that SmO$_{0.5}$F$_{0.5}$BiS$_2$ can be synthesized by solid state reaction,[33] this result might be helpful in explaining why this parent compound could not be synthesized in other studies using the same method.[27, 31]

As is shown in Fig. IV.6, $\rho(T)$ of La$_{1-x}$Sm$_x$O$_{0.5}$F$_{0.5}$BiS$_2$ increases with decreasing temperature at low pressures in their normal state, indicating semiconducting-like behavior, which is suppressed by applied pressure. However, as the representative $\rho(T)$ data in the inset of Fig. IV.6(d) show, a minimum near 262 K ($T_{\rm min}$) emerges at

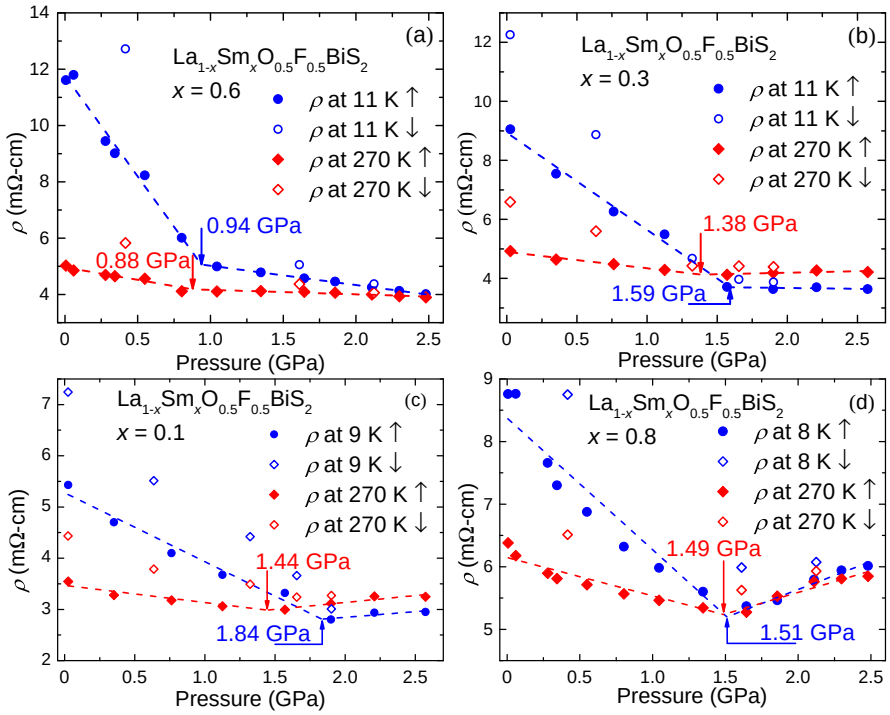

Figure IV.7: (a), (b), (c), (d) Electrical resistivity of $La_{1-x}Sm_xO_{0.5}F_{0.5}BiS_2$ with x = 0.1, 0.3, 0.6, and 0.8, respectively, at a temperature just above T_c in the normal state and at 270 K. The filled circles represent data collected with increasing pressure and the open circles are the data taken upon releasing the pressure. The dashed lines, which are guides to the eye, reflect the slopes of the pressure dependence of the electrical resistivity. Arrows indicate the pressure at which the slope changes.

pressures above 0.4 GPa. Semiconducting-like behavior is observed in $\rho(T)$ for $T < T_{\rm min}$. $T_{\rm min}$ decreases with increasing pressure and then saturates at $\sim$1.8 GPa, reaching a value of roughly 40 K. Except for the x = 0.1 sample, in which $T_{\rm min}$ does not saturate until $\sim$2.5 GPa, similar behavior is observed in the other samples under high pressures. However, the relationship between $T_{\rm min}$ and Sm concentration is still unclear. The appearance of a metallic-like to semiconducting-like cross over was also found in $Eu_3Bi_2S_4F_4$, $Sr_{1-x}La_xFBiS_2$ ($x \geqslant 0.45$), $LaOBiS_2$, and $ThOBiS_2$ at ambient pressure. In the first example, this behavior was attributed to a self-doping effect arising from Eu intermediate valence, while in the second example, it was ascribed to Anderson localization.[13, 16, 34] However, further work is required to identify the origin of the minimum in $La_{1-x}Sm_xO_{0.5}F_{0.5}BiS_2$ since the valence of Sm ions might change and sample defects might develop at high pressures.

Figure IV.7 shows ρ values at 270 K ($\rho_{270\rm K}$) and at certain low temperatures ($\rho_{\rm low}$), explicitly indicated in the figure, just higher than T_c for each sample. Both $\rho_{270\rm K}$ and $\rho_{\rm low}$ first decrease with increasing pressure almost linearly. However, the slope of the $\rho(P)$ curve changes at the pressure indicated by the arrows in Fig. IV.7, resulting in a kink for each $\rho(P)$ curve. For the x = 0.6 and 0.8 samples, a positive pressure coefficient of resistivity is observed at the pressures above the kink. Although the kink is located at pressures near $P_{\rm t}$, it should be noted that the kink does not necessarily coincide with the appearance of the SC2 phase, since both the phase transition between SC1 to SC2 and the appearance of metallic-like behavior may contribute to the normal-state electrical resistivity of the samples.

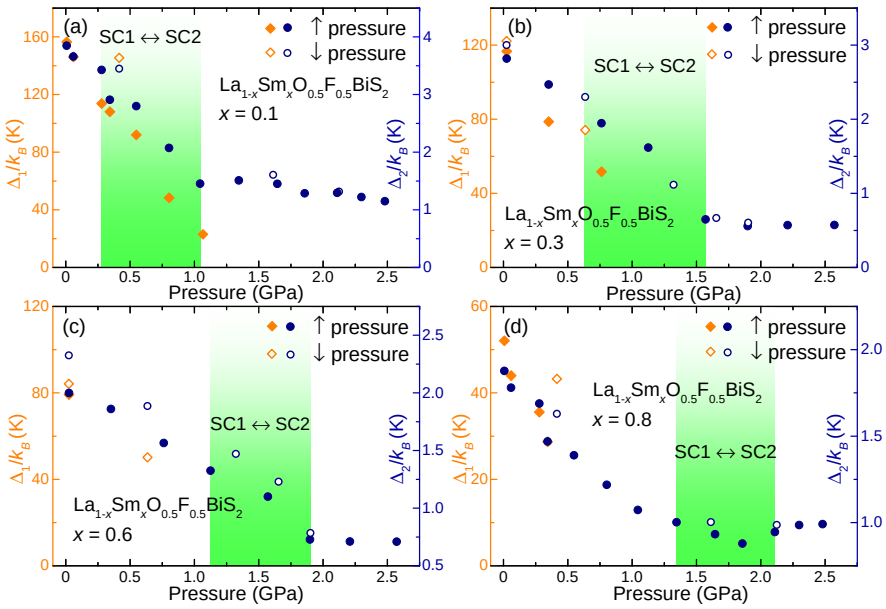

Figure IV.8: (a), (b), (c), (d) Evolution of the energy gaps Δ_1/k_B and Δ_2/k_B plotted as a function of pressure for x = 0.1, 0.3, 0.6, and 0.8, respectively. Filled and open symbols represent values that were obtained with increasing and decreasing pressure, respectively. Pressure ranges in which the low-T_c to high-T_c phase transition is observed and in which the normal-state electrical resistivity shows metallic-like behavior above 40 K are also indicated.

Since the electrical transport behavior of single crystals of $La_{1-x}Sm_xO_{0.5}F_{0.5}BiS_2$ has not yet been reported, it is still difficult to determine whether the observed semiconducting like behavior is related to poor intergain contact or whether it is an intrinsic property. If we assume that the semiconducting-like behavior is intrinsic, the energy gap can be estimated by using the simple activation-type relation:

$$\rho(T) = \rho_0 e^{\Delta/2k_B T}, \tag{IV.1}$$

where ρ_0 is a constant, k_B is the Boltzmann constant, and Δ is the energy gap.[35, 36] Because the relationship between $1/T$ and $\ln\rho$ is not linear for the whole temperature range in the normal state, the $\rho(T)$ data were fitted using Eq. (1) in two different temperature ranges, 270-160 K and 22-10 K, similar to the analysis in Refs. 22, 23, 35, 36. The energy gaps Δ_1/k_B and Δ_2/k_B, which are extracted from the high temperature and low temperature ranges, respectively, are plotted in Fig. IV.8. The gap Δ_1/k_B is not shown above the pressure at which metallic-like conduction is observed. It can be seen that both Δ_1/k_B and Δ_2/k_B are suppressed rapidly with increasing pressure; however, the value of Δ_1/k_B does not change significantly above $P_t{}^c$ with increasing pressure for all of the samples. Hence, the SC2 phase probably has a different band structure which is less sensitive to pressure.

Although T_c is reversible (i.e., there is no difference in values measured for increasing and decreasing pressure), values of Δ_1/k_B and Δ_2/k_B are higher for decreasing pressure than increasing pressure, indicating an enhancement of semiconducting-like be-

havior for all of the samples. A similar phenomenon was also observed in $LaO_{0.5}F_{0.5}BiS_2$ and $CeO_{0.5}F_{0.5}BiS_2$.[23] This behavior is associated with the pressure dependence of the electrical resistivity in which values of ρ obtained at similar pressures in measurements in which the pressure cell was being unloaded are significantly higher than those measured upon loading as the representative data show in Fig. IV.7. However, irreversible defects and disorder as well as a reduction of the geometric factors might develop in the samples under high pressures, which could contribute to a reduction in the conductivity of the samples. Since the energy gap Δ_1/k_B and Δ_2/k_B are derived from the electronic structure, there is no obvious reason why these fundamental quantities should show hysteretic behavior as a function of pressure.

IV.D Summary

Electrical resistivity measurements on polycrystalline samples of the BiS_2-based superconductors $La_{1-x}Sm_xO_{0.5}F_{0.5}BiS_2$ (x = 0.1, 0.3, 0.6, 0.8) were performed from 2 K to room temperature under applied pressures. In the normal state, semiconducting-like behavior is suppressed with increasing pressure. A reversible low-T_c to high-T_c superconductor phase transition was observed in all of the samples at a pressure that is proportional to the Sm concentration. With increasing Sm concentration, ΔT_c is suppressed and a larger pressure is necessary to induce the transition from the SC1 to the SC2 phase. It is also found that an optimal T_c could be tuned by decreasing the a lattice parameter in the SC1 phase at ambient pressure or by increasing a in the SC2 phase under pressure. These results indicate that the high-pressure behavior of Sm-substituted

$LaO_{0.5}F_{0.5}BiS_2$ is largely determined by Sm concentration or the lattice parameter a at ambient pressure. Therefore, the evolution of T_c under pressure for the parent compound $SmO_{0.5}F_{0.5}BiS_2$ can be estimated, and we find that the SC1 and SC2 phases exhibit almost indistinguishable T_c values; this result suggests that applied pressure may not induce a phase transition in $SmO_{0.5}F_{0.5}BiS_2$.

The text and data presented in this chapter are reprints of material that appears in "Pressure-Induced Phase Transition in $La_{1-x}Sm_xO_{0.5}F_{0.5}BiS_2$," Y. Fang, D. Yazici, B. D. White, and M. B. Maple, *Phys. Rev. B* **92**, 094507 (2015). The dissertation author is the primary investigator and author of this article.

Bibliography

[1] A. P. Drozdov, M. I. Eremets, and I. A. Troyan, arXiv preprint arXiv:1412.0460 (2014).

[2] K. Shimizu, K. Amaya, and N. Suzuki, J. Phys. Soc. Jpn **74**, 1345 (2005).

[3] A. S. Sefat, Rep. Prog. Phys. **74**, 124502 (2011).

[4] Y. Mizuguchi, H. Fujihisa, Y. Gotoh, K. Suzuki, H. Usui, K. Kuroki, S. Demura, Y. Takano, H. Izawa, and O. Miura, Phys. Rev. B **86**, 220510 (2012).

[5] S. K. Singh, A. Kumar, B. Gahtori, G. Sharma, S. Patnaik, and V. P. S. Awana, J. Am. Chem. Soc. **134**, 16504 (2012).

[6] V. P. S. Awana, A. Kumar, R. Jha, S. Kumar Singh, A. Pal, J. Saha, and S. Patnaik, Solid State Commun. **157**, 21 (2013).

[7] S. Demura, Y. Mizuguchi, K. Deguchi, H. Okazaki, H. Hara, T. Watanabe, S. James Denholme, M. Fujioka, T. Ozaki, H. Fujihisa, G. Yoshito, M. Osuke, Y. Takahide, T. Hiroyuki, and T. Yoshihiko, J. Phys. Soc. Jpn. **82**, 033708 (2013).

[8] Y. Mizuguchi, S. Demura, K. Deguchi, Y. Takano, H. Fujihisa, Y. Gotoh, H. Izawa, and O. Miura, J. Phys. Soc. Jpn. **81**, 114725 (2012).

[9] J. Xing, S. Li, X. Ding, H. Yang, and H.-H. Wen, Phys. Rev. B **86**, 214518 (2012).

[10] D. Yazici, K. Huang, B. D. White, A. H. Chang, A. J. Friedman, and M. B. Maple, Phil. Mag. **93**, 673 (2013).

[11] Y. Mizuguchi, Physics Procedia **58**, 94 (2014).

[12] K. Deguchi, Y. Mizuguchi, S. Demura, H. Hara, T. Watanabe, S. Denholme, M. Fujioka, H. Okazaki, T. Ozaki, H. Takeya, T. Yamaguchi, O. Miura, and Y. Takano, Europhys. Lett. **101**, 17004 (2013).

[13] D. Yazici, K. Huang, B. D. White, I. Jeon, V. W. Burnett, A. J. Friedman, I. K. Lum, M. Nallaiyan, S. Spagna, and M. B. Maple, Phys. Rev. B **87**, 174512 (2013).

[14] X. Lin, X. X. Ni, B. Chen, X. F. Xu, X. X. Yang, J. H. Dai, Y. K. Li, X. J. Yang, Y. K. Luo, Q. Tao, G. H. Cao, and Z. Xu, Phy. Rev. B **87**, 020504 (2013).

[15] H. F. Zhai, Z. T. Tang, H. Jiang, K. Xu, K. Zhang, P. Zhang, J. K. Bao, Y. L. Sun, W. H. Jiao, I. Nowik, I. Felner, Y. K. Li, X. F. Xu, Q. Tao, C. M. Feng, Z. A. Xu, and G. H. Cao, Phys. Rev. B **90**, 064518 (2014).

[16] H. F. Zhai, P. Zhang, S. Q. Wu, C. Y. He, Z. T. Tang, H. Jiang, Y. L. Sun, J. K. Bao, I. Nowik, I. Felner, Y. W. Zeng, Y. K. Li, X. F. Xu, Q. Tao, Z. A. Xu, and G. H. Cao, J. Am. Chem. Soc. **136**, 15386 (2014).

[17] D. Yazici, I. Jeon, B. D. White, and M. B. Maple, Physica C **514**, 218 (2015).

[18] Y. Mizuguchi, J. Phys. Chem. Solids **84**, 34 (2015).

[19] Y. Mizuguchi, T. Hiroi, J. Kajitani, H. Takatsu, H. Kadowaki, and O. Miura, J. Phys. Soc. Jpn. **83**, 053704 (2014).

[20] I. Pallecchi, G. Lamura, M. Putti, J. Kajitani, Y. Mizuguchi, O. Miura, S. Demura, K. Deguchi, and Y. Takano, Phys. Rev. B **89**, 214513 (2014).

[21] T. Tomita, M. Ebata, H. Soeda, H. Takahashi, H. Fujihisa, Y. Gotoh, Y. Mizuguchi, H. Izawa, O. Miura, S. Demura, K. Deguchi, and Y. Takano, J. Phys. Soc. Jpn. **83**, 063704 (2014).

[22] C. T. Wolowiec, B. D. White, I. Jeon, D. Yazici, K. Huang, and M. B. Maple, J. Phys.: Condens. Matter **25**, 422201 (2013).

[23] C. T. Wolowiec, D. Yazici, B. D. White, K. Huang, and M. B. Maple, Phys. Rev. B **88**, 064503 (2013).

[24] Y. K. Luo, H. F. Zhai, P. Zhang, Z. A. Xu, G. H. Cao, and J. D. Thompson, Phys. Rev. B **90**, 220510 (2014).

[25] J. Z. Liu, S. Li, Y. F. Li, X. Y. Zhu, and H.-H. Wen, Phys. Rev. B **90**, 094507 (2014).

[26] C. Y. Guo, Y. Chen, M. Smidman, S. A. Chen, W. B. Jiang, H. F. Zhai, Y. F. Wang, G. H. Cao, J. M. Chen, X. Lu, and H. Q. Yuan, Phys. Rev. B **91**, 214512 (2015).

[27] Y. Fang, D. Yazici, B. D. White, and M. B. Maple, Phys. Rev. B **91**, 064510 (2015).

[28] T. F. Smith, C. W. Chu, and M. B. Maple, Cryogenics **9**, 53 (1969).

[29] A. Jayaraman, A. R. Hutson, J. H. McFee, A. S. Coriell, and R. G. Maines, Rev. Sci. Instrum. **38**, 44 (1967).

[30] T. Smith, C. W. Chu, and M. B. Maple, Cryogenics **9**, 53 (1969).

[31] J. Kajitani, T. Hiroi, A. Omachi, O. Miura, and Y. Mizuguchi, J. Phys. Soc. Jpn. **84**, 044712 (2015).

[32] J. Kajitani, A. Omachi, T. Hiroi, O. Miura, and Y. Mizuguchi, Physica C **504**, 33 (2014).

[33] G. S. Thakur, G. K. Selvan, Z. Haque, L. C. Gupta, S. L. Samal, S. Arumugam, and A. K. Ganguli, Inorg. Chem. **54**, 1076 (2015).

[34] H. Sakai, D. Kotajima, K. Saito, H. Wadati, Y. Wakisaka, M. Mizumaki, K. Nitta, Y. Tokura, and S. Ishiwata, J. Phys. Soc. Jpn. **83**, 014709 (2014).

[35] H. Kotegawa, Y. Tomita, H. Tou, H. Izawa, Y. Mizuguchi, O. Miura, S. Demura, K. Deguchi, and Y. Takano, J. Phys. Soc. Jpn. **81**, 103702 (2012).

[36] I. Jeon, D. Yazici, B. D. White, A. J. Friedman, and M. B. Maple, Phys. Rev. B **90**, 054510 (2014).

Chapter V

Upper critical magnetic field of *Ln*$O_{0.5}F_{0.5}BiS_2$ (*Ln* = La, Nd) superconductors at ambient and high pressure

V.A INTRODUCTION

Measurements of the upper critical field, H_{c2}, can provide insight into the pair-breaking mechanisms present in superconducting materials and also aid in estimating other characteristics of superconductors such as coherence length and anisotropy. Since the discovery of the cuprates, a large number of high-T_c superconductors have been studied, thus fundamentally challenging the validity of the existing Bardeen-Cooper-

Schreiffer (BCS) theory of conventional superconductivity. The recently discovered BiS_2-based superconducting materials, which exhibit a layered crystal structure similar to the high-T_c cuprates and iron-based superconductors, provide another opportunity to investigate and develop a better understanding of superconductivity in these materials.[1–6] However, current studies on the BiS_2-based compounds are only at an early stage and some important questions remain regarding crystal structure, superconductivity, and their interrelation.[7–10]

One of the more striking phenomena displayed by many BiS_2-based superconductors, such as $LnO_{1-x}F_xBiS_2$ (*Ln* = La, Ce, Pr, Nd, Yb), $La_{1-x}Sm_xO_{0.5}F_{0.5}BiS_2$, $Eu_3Bi_2S_4F_4$, $EuBiS_2F$, $SrFBiS_2$, $LaO_{0.5}F_{0.5}BiSe_2$, and $Sr_{0.5}La_{0.5}FBiS_2$, is the rather abrupt enhancement of superconductivity from a low-T_c phase to a high-T_c phase with the application of a moderate amount of pressure on the order of a few GPa.[11–18] X-ray diffraction experiments reveal that $LaO_{0.5}F_{0.5}BiS_2$ and $EuBiS_2F$ undergo a structural phase transition from tetragonal ($P4/nmm$) to monoclinic ($P2_1/m$),[15, 19] which is believed to be related to the sudden increase in T_c. In addition to the remarkable difference in T_c, there are other essential differences in normal state properties between the low-T_c (SC1) and high-T_c (SC2) phases. In particular, the normal state electrical resistivity of $LaO_{0.5}F_{0.5}BiS_2$ in the SC2 phase is significantly smaller than that in the SC1 phase and $NdO_{0.5}F_{0.5}BiS_2$ shows metallic-like behavior in the SC2 phase instead of semiconducting-like behavior as in the SC1 phase.[12, 13]

In this paper, we report the evolution of superconductivity under external magnetic fields up to 8.5 T for polycrystalline samples of $LnO_{0.5}F_{0.5}BiS_2$ (Ln = La, Nd) in both

the SC1 and SC2 phases. For all samples, the temperature dependence of H_{c2} shows a concave upward curvature with decreasing temperature, which cannot be described by the one-band Ginzburg-Landau theory. The effects of external pressure and chemical composition on superconductivity with increasing external magnetic field for the four samples studied are presented. The anomalous behavior of the temperature dependence of H_{c2}, which was observed in the high pressure superconducting phase of $LaO_{0.5}F_{0.5}BiS_2$ and $NdO_{0.5}F_{0.5}BiS_2$ at $\sim$5 T and $\sim$3 T, respectively, will be described, and a comparison of the superconductivity observed in samples of $LaO_{0.5}F_{0.5}BiS_2$ in the high pressure phase (SC2) and the superconductivity observed in the high-pressure synthesized samples of $LaO_{0.5}F_{0.5}BiS_2$ which are measured at ambient pressure, will be discussed. We believe the results will be useful in understanding (1) whether the BiS_2-based superconductors are conventional or unconventional and (2) how the difference in crystal structure and local atomic environment of the BiS_2-based compounds affects superconductivity. This study also provides a plausible explanation for why the pressure-induced enhancements of T_c for $Ln O_{0.5}F_{0.5}BiS_2$ (Ln = La-Nd) decrease with heavier Ln. For convenience in the following discussion, as-grown samples measured at ambient pressure and under high pressure will be abbreviated as AG and HPAG, respectively. In addition, samples that were synthesized and studied by Mizuguchi *et al.* (Ref. 20), which were grown under high-pressure and high-temperature conditions, shall be abbreviated as HPT.

V.B EXPERIMENTAL DETAILS

As-grown polycrystalline samples of *Ln*$O_{0.5}F_{0.5}BiS_2$ (*Ln* = La, Nd) were synthesized and annealed at ∼800 °C in sealed quartz tubes as described elsewhere.[4, 6] The AG and HPAG samples of the same chemical composition came from the same pellet to ensure both samples have the same physical properties at ambient pressure. Hydrostatic pressure was generated by using a clamped piston-cylinder cell (PCC) in which a 1:1 by volume mixture of n-pentane and isoamyl alcohol was used as the pressure-transmitting medium. The pressures applied to the samples were estimated by measuring the T_c of a high purity (>99.99%) Sn disk inside the sample chamber of the cell and comparing the measured values with the well-determined $T_c(P)$ of high purity Sn.[21] The resistivity measurements of the AG $LaO_{0.5}F_{0.5}BiS_2$ sample at magnetic fields up to 1 T were performed by using a Quantum Design Physical Property Measurement System (PPMS) Dynacool using a standard four-wire technique from 5 to 1.8 K. Electrical resistivity measurements at temperatures down to 60 mK on the HPAG $LaO_{0.5}F_{0.5}BiS_2$ sample and the AG and HPAG $NdO_{0.5}F_{0.5}BiS_2$ samples were performed with an Oxford Instruments Kelvinox ^{3}He-^{4}He dilution refrigerator in magnetic fields ranging from 0 to 8.5 T. Previous studies have shown that the pressure-induced phase transition for $LaO_{0.5}F_{0.5}BiS_2$ and $NdO_{0.5}F_{0.5}BiS_2$ occurs at around 0.8 and 1.9 GPa, respectively, followed by a gradual decrease in T_c in both compounds with additional pressure.[12, 13, 19] The HPAG samples were measured under an applied pressure of ∼2.3 GPa to ensure that the SC2 phase was fully realized in the HPAG samples.

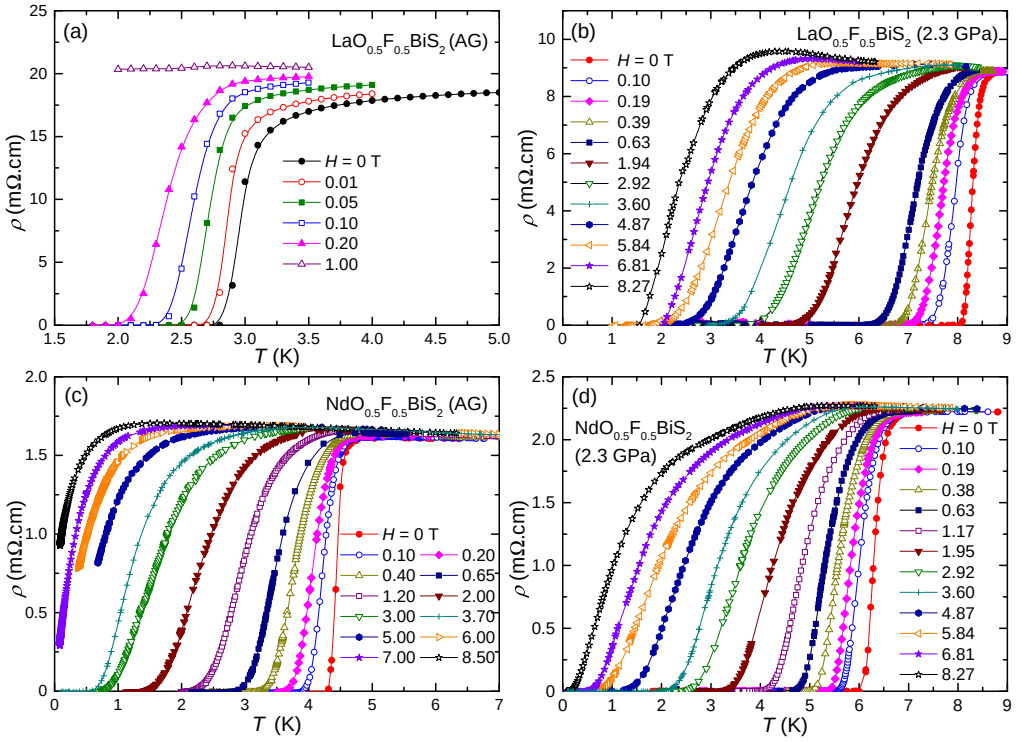

Figure V.1: (a), (b) Temperature T dependence of the electrical resistivity ρ for AG and HPAG samples of $LaO_{0.5}F_{0.5}BiS_2$, respectively. (c), (d) Electrical resistivity ρ vs. temperature for AG and HPAG samples of $NdO_{0.5}F_{0.5}BiS_2$, respectively. The external magnetic field for each $\rho(T)$ curve is also denoted in the figure.

V.C RESULTS AND DISCUSSION

Electrical resistivity ρ vs. temperature T superconducting transition curves at various magnetic fields up to 8.5 T in temperature ranges extending down to 60 mK for $LaO_{0.5}F_{0.5}BiS_2$ (AG and HPAG) and $NdO_{0.5}F_{0.5}BiS_2$ (AG and HPAG) are displayed in Fig. V.1(a)-(d), respectively. The normal state ρ increases slightly with increasing magnetic field for all four samples, revealing a positive magnetoresistivity. Superconductivity for all the samples is suppressed by the external magnetic field, as evinced by the shift of the superconducting transition curves to lower temperature with increasing magnetic field. If we define T_c as the temperature at which ρ falls to 50% of its normal state value,

the T_c values for $LaO_{0.5}F_{0.5}BiS_2$ and $NdO_{0.5}F_{0.5}BiS_2$ at 2.3 GPa are 8.28 K and 6.31 K, respectively, and the T_c values for the corresponding AG samples are 2.92 K and 4.54 K in zero magnetic field. The large difference in T_c between the AG and HPAG samples of the same compound and the sharp superconducting transition at zero magnetic field reveals that the AG samples are in the SC1 phase and the HPAG samples are in the SC2 phase.

As shown in Fig. V.1, superconducting transitions for all the samples are quite broad in high magnetic fields. It has been reported that anisotropy in single-crystalline samples of BiS_2-based superconductors is quite large.[22–24] For example, the upper critical field parallel to the ab-plane (${H_{c2}}^{ab}$) for single-crystalline samples of $\sim$30% substituted Nd(O,F)BiS_2 is estimated to be $\sim$42 T, whereas the upper critical field parallel to the c-axis (${H_{c2}}^{c}$) for the same compound is only about 1.3 T.[22] In other words, the superconducting state of grains whose c-axis is parallel to the applied magnetic field is more rapidly suppressed by applying high magnetic fields than the state of grains whose ab-plane is parallel to the applied magnetic field.[20] In Fig. V.2, we plotted the T dependence of the upper critical field in terms of the characteristic fields $H_{10\%\rho}$ and $H_{90\%\rho}$, evaluated at 10% and 90% of the normal state ρ at the onset of the superconducting transition. It should be noted that modeling of the $H_{10\%\rho}(T)$ curves is very difficult duo to the contributions of superconductivity from different directions. However, the significant difference between $H_{90\%\rho}(T)$ and $H_{10\%\rho}(T)$ is expected to be related to the large anisotropy of the upper critical field; $H_{90\%\rho}$ is expected to be close to the upper critical field for grains whose ab-plane is parallel to H.[20]

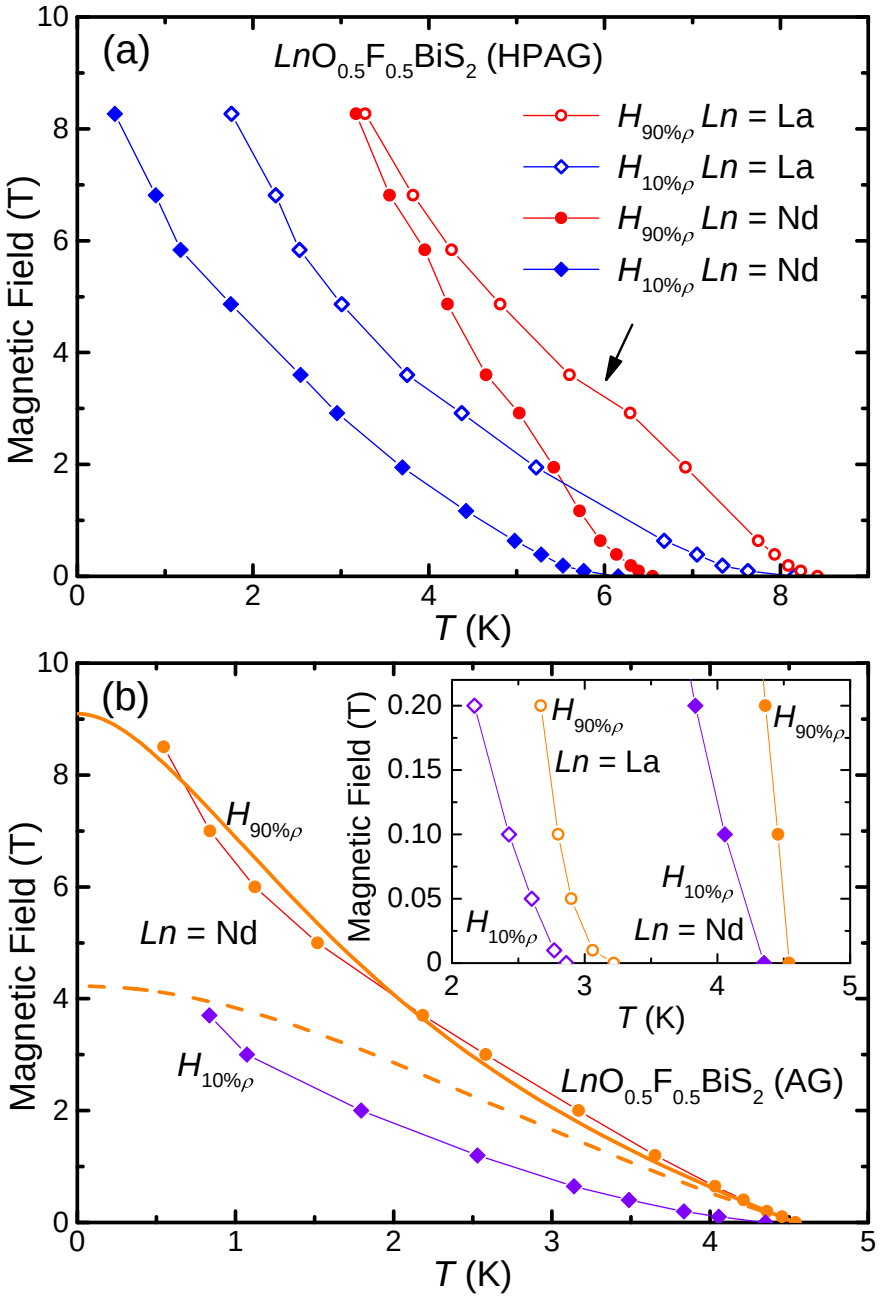

Figure V.2: (a) $H_{90\%\rho}$ and $H_{10\%\rho}$ for the samples in the SC2 phase plotted as a function of T. The open and filled symbols represent data obtained from $LaO_{0.5}F_{0.5}BiS_2$ and $NdO_{0.5}F_{0.5}BiS_2$, respectively. (b) T dependence of $H_{90\%\rho}$ and $H_{10\%\rho}$ for AG $NdO_{0.5}F_{0.5}BiS_2$. The dashed and solid lines are fits to the $H_{90\%\rho}(T)$ of the one-band WHH equation and the two band model, respectively. The inset shows $H_{90\%\rho}$ and $H_{10\%\rho}$ values (circular and rhombic symbols, respectively) for the AG $LaO_{0.5}F_{0.5}BiS_2$ (open symbols) and $NdO_{0.5}F_{0.5}BiS_2$ (filled symbols) from 0 to 0.20 T.

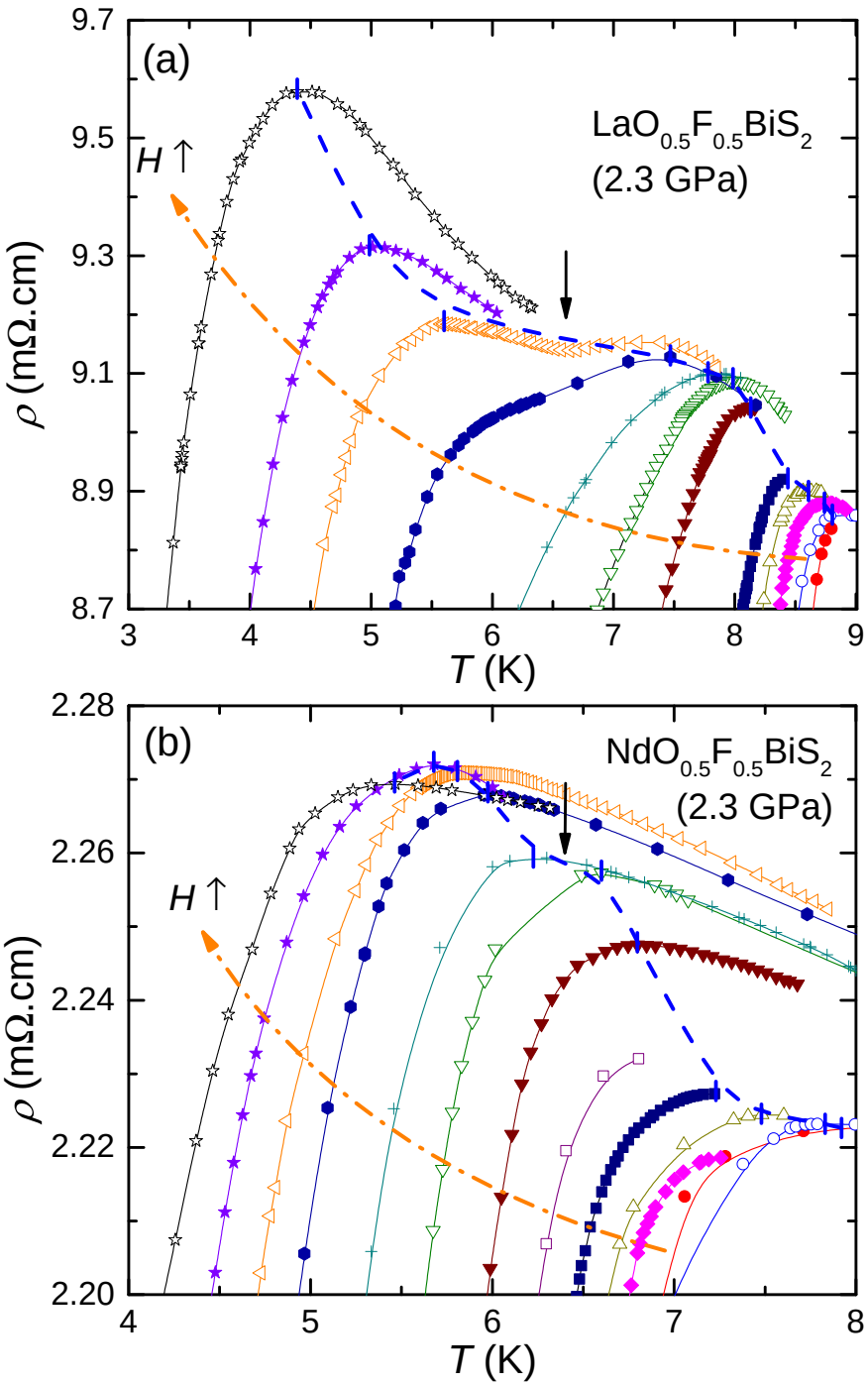

Figure V.3: Enlargement of T dependence of ρ for (a) HPAG $LaO_{0.5}F_{0.5}BiS_2$ and (b) HPAG $NdO_{0.5}F_{0.5}BiS_2$ near the onset of the superconducting transition. Black arrows indicate the anomalous behavior of $H_{onset}(T)$. The vertical ticks represent the onset of superconducting transition (T_c^{onset}) and the dashed lines are guides to the eye. The orange curves indicate the directions of field increasing and the magnetic field applied for each curve can be found in Fig. V.1 with the same symbol.

Application of an external magnetic field may destroy the Cooper pairs via the pair breaking interaction between the magnetic field and/or the momenta of the electrons (electromagnetic interaction) and the spins of the electrons (Zeeman interaction). With increasing H, superconductivity is suppressed more rapidly for the AG samples compared to the corresponding HPAG samples with the same chemical composition. Superconductivity in AG $LaO_{0.5}F_{0.5}BiS_2$ cannot be observed above 1.9 K when H reaches 1 T (shown in Fig. V.1(a)). As can be seen in Fig. V.2(a), despite the difference in T_c in zero magnetic field, the $H_{90\%\rho}$ increases more rapidly for HPAG $NdO_{0.5}F_{0.5}BiS_2$ with decreasing temperature compared to the $H_{90\%\rho}$ for HPAG $LaO_{0.5}F_{0.5}BiS_2$. However, $H_{90\%\rho}(T)$ curves are very similar for the two AG sample shown in the inset of Fig. V.2(b).

In the conventional one-band Ginzburg-Landau picture, the upper critical field increases linearly with decreasing T near T_c and then saturates to a finite value in the 0 K limit. A linear-like temperature dependence of H_{c2} has been observed down to 2 K in the AG $NdO_{0.5}F_{0.5}BiS_2$.[25] However, in this study, the T dependence of $H_{90\%\rho}$ and $H_{10\%\rho}$ for AG $NdO_{0.5}F_{0.5}BiS_2$ shows an uncharacteristic upward curvature with decreasing T below 2 K, which is remarkably different from the one band Werthamer-Helfand-Hohenberg (WHH) model (shown in Fig. V.2(b)). Similar behavior was also reported for AG samples of $LaO_{1-x}F_xBiS_2$ (x = 0.1-0.3) and $Bi_4O_4S_3$.[26, 27] In the present work, we also adopted the dirty two band model introduced in Ref. 28 (Eq. 19), which treats both interband scattering and paramagnetic effects as negligible. The corresponding estimated value of $H_{90\%\rho}(0)$ for AG $NdO_{0.5}F_{0.5}BiS_2$ is 9.1 T, which is significantly higher than the $H_{c2}(0)$ reported earlier (2.3 T) by using the WHH equation.[25] It should be

mentioned that although the two band model provides a better overall fit compared with the one-band WHH model, the difference between the experimental data and the fitting is still significant at low temperatures as shown in Fig. V.2(b). On the other hand, previous experimental and theoretical studies have not reached an agreement of whether the newly discovered BiS_2-based superconductors are conventional or unconventional. The poor description of the $H_{c2}(T)$ data is possibly a result of unconventional superconductivity.

For the HPAG $LaO_{0.5}F_{0.5}BiS_2$ sample, the increase of $H_{90\%\rho}$ with decreasing T slows down somewhat when the external magnetic field reaches $\sim$3 T (indicated by the black arrow in Fig. V.2(a)). This anomalous behavior is more remarkable in the evolution of ${T_c}^{onset}$, which is defined as the T at which ρ attains its maximum value, in various external magnetic fields. As shown in Fig. V.3(a), ${T_c}^{onset}$ is significantly suppressed with a slight increase in H at around 5 T. The temperature dependence of H_{onset} for HPAG $LaO_{0.5}F_{0.5}BiS_2$ (shown in Fig. V.4) is remarkably similar to that observed in the HPT sample of $LaO_{0.5}F_{0.5}BiS_2$ which was synthesized at a pressure of 2 GPa and temperature of 700 °C .[20] Possible anisotropy of the superconducting state within the BiS_2 plane, which may be induced by lattice distortion or residual strain along the superconducting layers in the high pressure and high temperature condition, is considered to be the origin of the anomalous behavior observed in $H_{onset}(T)$ for the HPT $LaO_{0.5}F_{0.5}BiS_2$.[20] In other words, the upper critical field for HPT $LaO_{0.5}F_{0.5}BiS_2$ synthesized at 2 GPa is different along the a- and b- axes. In this study, anisotropy of the upper critical field along the a- and b-axes can be induced due to the pressure-induced phase transition from the tetragonal phase (space group $P4/nmm$) to the monoclinic phase (space group $P2_1/m$).

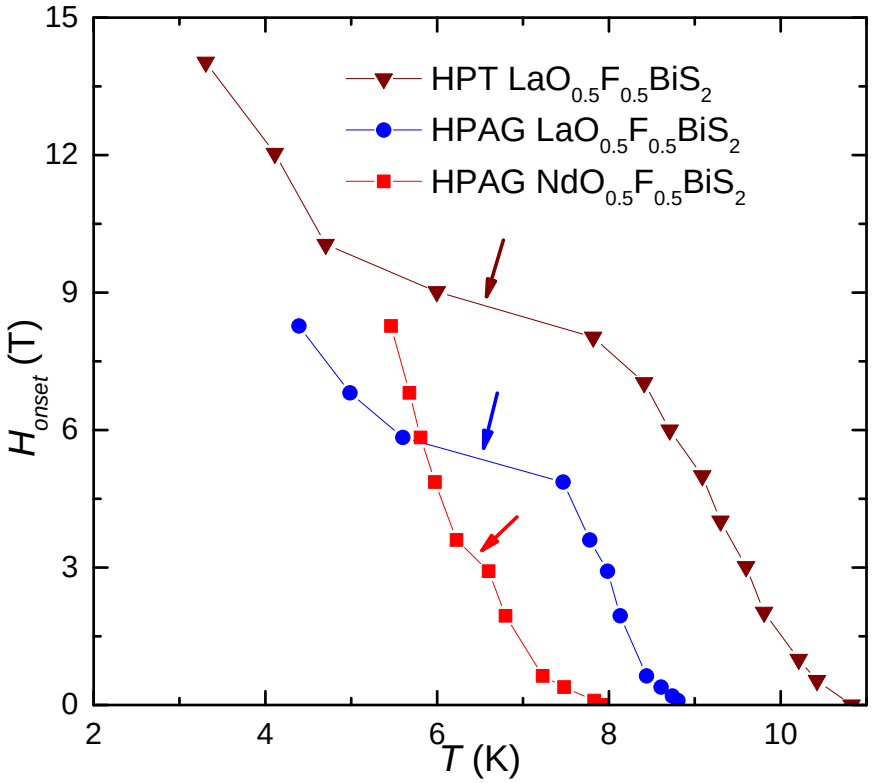

Figure V.4: (a) The H_{onset}-T phase diagrams for HPAG and HPT $LaO_{0.5}F_{0.5}BiS_2$ as well as HPAG $NdO_{0.5}F_{0.5}BiS_2$. The data for HPT $LaO_{0.5}F_{0.5}BiS_2$ are taken from Ref. 20. The anomalous behavior for each curve is indicated by the corresponding arrow.

Similar behavior can also be observed in the HPAG $NdO_{0.5}F_{0.5}BiS_2$. As displayed in Fig. V.3(b) and Fig. V.4, the T dependence of H_{onset} for HPAG $NdO_{0.5}F_{0.5}BiS_2$ shows a very subtle discontinuity in a narrow T range $\sim$0.5 K at around 3 T. It should be mentioned that a variety of theoretical and experimental studies have suggested that the band structure and superconductivity of the BiS_2-based compounds can be largely affected by a change in the crystal structures.[5, 7, 29–33] Anisotropic superconducting states within the ab-plane could be induced when the degeneracy of Bi-6p_x and Bi-6p_y orbital is lifted.[20] Our results indicate that the anisotropy of the upper critical field in the ab-plane of HPAG $NdO_{0.5}F_{0.5}BiS_2$ is not as large as that of HPAG $LaO_{0.5}F_{0.5}BiS_2$, and hence, based on the discussion above, suggests that the pressure-induced lattice deformation at 2.3 GPa in $NdO_{0.5}F_{0.5}BiS_2$ is not as significant compared with that in $LaO_{0.5}F_{0.5}BiS_2$. This also explains why the pressure-induced enhancement of the superconducting critical temperature ΔT_c in $NdO_{0.5}F_{0.5}BiS_2$ is only $\sim$2.5 K, which is much lower than the ΔT_c value of $LaO_{0.5}F_{0.5}BiS_2$ ($\sim$7.2 K).

Previous studies have revealed that it is possible to significantly increase T_c in the Ln(O,F)BiS_2 (Ln = La-Nd) superconductors by applying high pressure or by annealing/synthesizing the samples under high pressure.[12, 13, 18, 19, 34] Although the crystal structure of HPT samples is reported to be the same as the structure of AG samples at low pressure and is different from the monoclinic structure of the same compounds under high pressure,[34–36] T_c values of HPT samples and the corresponding (same chemical composition) HPAG samples in SC2 phase are very close. The enhancement of T_c for these compounds under pressure is considered to be related to the structural phase

transition;[19] however, there is no conclusive agreement regarding the enhancement of superconductivity in samples that are annealed or synthesized under pressure.[7, 35–38] The T_c value of HPAG $LaO_{0.5}F_{0.5}BiS_2$ plotted in Fig. V.3 is lower than the reported T_c value of the HPT $LaO_{0.5}F_{0.5}BiS_2$. This discrepancy can be attributed to the fact that the measurement of electrical resistivity on the HPAG sample of $LaO_{0.5}F_{0.5}BiS_2$ was performed at 2.3 GPa, well into the SC2 phase, where a gradual suppression of T_c occurs with increasing pressure. Nevertheless, the values of dH_{onset}/dT are nearly the same at each of the three different stages in the evolution of $H_{onset}(T)$ as shown in Fig. V.4. Our results raise the question of why superconductivity for the same compounds in this system, enhanced by the two different methods, is so similar. A thorough investigation of this problem may yield information that will help identify the essential parameters that determine T_c in the BiS_2-based superconductors.

One possible explanation for the enhanced superconductivity observed in the HPT samples of $LnO_{0.5}F_{0.5}BiS_2$ (Ln = La - Nd) is the presence of trace amounts of the monoclinic structure at ambient pressure; however, it has been observed that the pressure dependence of T_c for the HPAG samples is completely reversible, suggesting that it is unlikely for the monoclinic phase to survive in returning from high pressure to atmospheric pressure.[12, 13, 18] In addition, no additional curvatures in the T dependence of the resistivity, magnetic susceptibility, or specific heat due to the appearance of superconductivity from an additional superconducting phase have been reported yet. It has also been suggested that the enhanced superconductivity in the HPT samples may result from additional effects that high pressure annealing may have on the local

crystal structure including the shorter in plane Bi-S distances and higher symmetry in the ab-plane reported for the Ce(O,F)BiS_2 compound as well as the uniaxial strain along the c-axis that was observed in HPT samples of $LaO_{0.5}F_{0.5}BiS_2$ and $PrO_{0.5}F_{0.5}BiS_2$.[35–38]

The pressure-induced phase transition observed in $LaO_{0.5}F_{0.5}BiS_2$ was reported to involve sliding between the two neighboring BiS_2 layers along the a-axis, resulting in a slight increase of the angle between the ab and bc planes (β) from 90° at ambient pressure to 94° at ∼1 GPa.[19] The in-plane structure of the BiS_2 layers, which is considered to be essential for the superconductivity, as well as the in-plane structure of the La(O,F) blocking layers, are nearly the same after the phase transition. Considering the results obtained in this study, it seems that local distortions or changes in the local atomic environment, as caused by the application of pressure but also quenched via high pressure annealing, are probably critical in affecting superconductivity, perhaps even more than the structural phase transition itself. However, further investigations of the crystal structure of the AG, HPAG, and HPT are still needed for direct evidence of changes in local structure. Very recently, it was reported that "in-plane chemical pressure" is closely related to T_c in the BiS_2-based superconductors.[32] The in-plane chemical pressure is defined as the ratio of the expected bond distance between a Bi ion and its in-plane neighboring ions of S (or Se) to the experimental bond distance estimated by Rietveld refinements. The expected bond distance can be determined by using the ionic radii of Bi and S (or Se). Although the validity of such a relationship needs to be further confirmed, the results also emphasize the importance of local structure to superconductivity in BiS_2-based compounds.

V.D SUMMARY

To summarize, we performed electrical resistivity measurements on polycrystalline samples of *Ln*$O_{0.5}F_{0.5}BiS_2$ (*Ln* = La, Nd) in both the SC1 and SC2 phases under external magnetic fields up to 8.5 T and at temperatures down to 60 mK. Significant concave upward curvatures in the $H_{c2}(T)$ curves were observed and cannot be described by conventional one-band WHH theory. In addition, the T dependence of H_{onset} for HPAG $LaO_{0.5}F_{0.5}BiS_2$ shows anomalous behavior at around 5 T, revealing remarkable similarity to the superconductivity observed the HPT samples of $LaO_{0.5}F_{0.5}BiS_2$. If no high-pressure monoclinic phase exists in HPT $LaO_{0.5}F_{0.5}BiS_2$, the importance of the monoclinic phase would be diminished, suggesting the possibility of a greater importance in the role that local atomic environment plays in affecting superconductivity in the BiS_2-based compounds, though further investigations of atomic positions are still needed. In the case of HPAG $NdO_{0.5}F_{0.5}BiS_2$, the anomalous behavior in $H_{onset}(T)$ is very subtle, probably due to a mild pressure-induced deformation in crystal structure, which is probably responsible for the relatively slight increase in T_c compared to the remarkable enhancement of T_c in $LaO_{0.5}F_{0.5}BiS_2$.

The text and data presented in this chapter are reprints of material that appears in "Upper critical magnetic field of $Ln\mathrm{O}_{0.5}\mathrm{F}_{0.5}\mathrm{BiS}_2$ (*Ln* = La, Nd) superconductors at ambient and high pressure," Y. Fang, C. T. Wolowiec, A. J. Breindel D. Yazici, P.-C. Ho, and M. B. Maple, *Supercond. Sci. Technol.* **30**, 115004 (2017). The dissertation author is the primary investigator and author of this article.

Bibliography

[1] Y. Mizuguchi, H. Fujihisa, Y. Gotoh, K. Suzuki, H. Usui, K. Kuroki, S. Demura, Y. Takano, H. Izawa, and O. Miura, Phys. Rev. B **86**, 220510 (2012).

[2] S. Demura, Y. Mizuguchi, K. Deguchi, H. Okazaki, H. Hara, T. Watanabe, S. James Denholme, M. Fujioka, T. Ozaki, H. Fujihisa, G. Yoshito, M. Osuke, Y. Takahide, T. Hiroyuki, and T. Yoshihiko, J. Phys. Soc. Jpn. **82**, 033708 (2013).

[3] Y. Mizuguchi, S. Demura, K. Deguchi, Y. Takano, H. Fujihisa, Y. Gotoh, H. Izawa, and O. Miura, J. Phys. Soc. Jpn. **81**, 114725 (2012).

[4] D. Yazici, K. Huang, B. D. White, A. H. Chang, A. J. Friedman, and M. B. Maple, Phil. Mag. **93**, 673 (2013).

[5] Y. Fang, D. Yazici, B. D. White, and M. B. Maple, Phys. Rev. B **91**, 064510 (2015).

[6] D. Yazici, K. Huang, B. D. White, I. Jeon, V. W. Burnett, A. J. Friedman, I. K. Lum, M. Nallaiyan, S. Spagna, and M. B. Maple, Phys. Rev. B **87**, 174512 (2013).

[7] Y. Fang, C. T. Wolowiec, D. Yazici, and M. B. Maple, Novel Superconducting Materials **1** (2015).

[8] K. Kuroki, JPSJ News and Comments **11**, 02 (2014).

[9] Y. Mizuguchi, J. Phys. Chem. Solids **84**, 34 (2015).

[10] D. Yazici, I. Jeon, B. D. White, and M. B. Maple, Physica C **514**, 218 (2015).

[11] H. Kotegawa, Y. Tomita, H. Tou, H. Izawa, Y. Mizuguchi, O. Miura, S. Demura, K. Deguchi, and Y. Takano, J. Phys. Soc. Jpn. **81**, 103702 (2012).

[12] C. T. Wolowiec, B. D. White, I. Jeon, D. Yazici, K. Huang, and M. B. Maple, J. Phys.: Condens. Matter **25**, 422201 (2013).

[13] C. T. Wolowiec, D. Yazici, B. D. White, K. Huang, and M. B. Maple, Phys. Rev. B **88**, 064503 (2013).

[14] R. Jha, B. Tiwari, and V. P. S. Awana, J. Phys. Soc. Jpn. **83**, 063707 (2014).

[15] C. Y. Guo, Y. Chen, M. Smidman, S. A. Chen, W. B. Jiang, H. F. Zhai, Y. F. Wang, G. H. Cao, J. M. Chen, X. Lu, and H. Q. Yuan, Phys. Rev. B **91**, 214512 (2015).

[16] M. Fujioka, M. Tanaka, S. J. Denholme, T. Yamaki, H. Takeya, T. Yamaguchi, and Y. Takano, Europhys. Lett. **108**, 47007 (2014).

[17] Y. K. Luo, H. F. Zhai, P. Zhang, Z. A. Xu, G. H. Cao, and J. D. Thompson, Phys. Rev. B **90**, 220510 (2014).

[18] Y. Fang, D. Yazici, B. D. White, and M. B. Maple, Phys. Rev. B (2015).

[19] T. Tomita, M. Ebata, H. Soeda, H. Takahashi, H. Fujihisa, Y. Gotoh, Y. Mizuguchi, H. Izawa, O. Miura, S. Demura, K. Deguchi, and Y. Takano, J. Phys. Soc. Jpn. **83**, 063704 (2014).

[20] Y. Mizuguchi, A. Miyake, K. Akiba, M. Tokunaga, J. Kajitani, and O. Miura, Phys. Rev. B **89**, 174515 (2014).

[21] T. F. Smith, C. W. Chu, and M. B. Maple, Cryogenics **9**, 53 (1969).

[22] M. Nagao, S. Demura, K. Deguchi, A. Miura, S. Watauchi, T. Takei, Y. Takano, N. Kumada, and I. Tanaka, J. Phys. Soc. Jpn. **82**, 113701 (2013).

[23] A. Miura, M. Nagao, T. Takei, S. Watauchi, Y. Mizuguchi, Y. Takano, I. Tanaka, and N. Kumada, Cryst. Growth Des. **15**, 39 (2014).

[24] M. Nagao, A. Miura, S. Demura, K. Deguchi, S. Watauchi, T. Takei, Y. Takano, N. Kumada, and I. Tanaka, Solid State Commun. **178**, 33 (2014).

[25] R. Jha, A. Kumar, S. Kumar Singh, and V. P. S. Awana, J. Appl. Phys. **113**, 056102 (2013).

[26] R. Higashinaka, R. Miyazaki, Y. Mizuguchi, O. Miura, and Y. Aoki, J. Phys. Soc. Jpn. **83**, 5004 (2014).

[27] P. K. Biswas, A. Amato, C. Baines, R. Khasanov, H. Luetkens, H. Lei, C. Petrovic, and E. Morenzoni, Phys. Rev. B **88**, 224515 (2013).

[28] A. Gurevich, Physica C: Superconductivity **456**, 160 (2007).

[29] K. Suzuki, H. Usui, and K. Kuroki, Physics Procedia **45**, 21 (2013).

[30] T. Yildirim, Phys. Rev. B **87**, 020506 (2013).

[31] J. Kajitani, A. Omachi, T. Hiroi, O. Miura, and Y. Mizuguchi, Physica C **504**, 33 (2014).

[32] Y. Mizuguchi, A. Miura, J. Kajitani, T. Hiroi, O. Miura, K. Tadanaga, N. Kumada, E. Magome, C. Moriyoshi, and Y. Kuroiwa, Sci. Rep. **5**, 14968 (2015).

[33] I. Jeon, D. Yazici, B. D. White, A. J. Friedman, and M. B. Maple, Phys. Rev. B **90**, 054510 (2014).

[34] K. Deguchi, Y. Mizuguchi, S. Demura, H. Hara, T. Watanabe, S. J. Denholme, M. Fujioka, H. Okazaki, T. Ozaki, H. Takeya, T. Yamaguchi, O. Miura, and Y. Takano, Europhys. Lett. **101**, 17004 (2013).

[35] J. Kajitani, T. Hiroi, A. Omachi, O. Miura, and Y. Mizuguchi, J. Supercond. Nov. Magn. **28**, 1129 (2015).

[36] J. Kajitani, K. Deguchi, A. Omachi, T. Hiroi, Y. Takano, H. Takatsu, H. Kadowaki, O. Miura, and Y. Mizuguchi, Solid State Commun. **181**, 1 (2014).

[37] J. Kajitani, K. Deguchi, T. Hiroi, A. Omachi, S. Demura, Y. Takano, O. Miura, and Y. Mizuguchi, J. Phys. Soc. Jpn. **83**, 065002 (2014).

[38] E. Paris, B. Joseph, A. Iadecola, T. Sugimoto, L. Olivi, S. Demura, Y. Mizuguchi, Y. Takano, T. Mizokawa, and N. L. Saini, J. Phys.: Condens. Matt. **26**, 435701 (2014).

Chapter VI

High pressure effects on non-fluorinated BiS_2-based superconductors $La_{1-x}M_xOBiS_2$ (M = Ti and Th)

VI.A Introduction

Following the discovery of superconductivity in the layered bismuth oxysulfide compound $Bi_4O_4S_3$, an intense effort to find new BiS_2-based superconductors quickly ensued as a result of the remarkable flexibility of the BiS_2-layers in forming compounds with new chemical compositions [1–4]. By doping the BiS_2-layers with electrons via appropriate chemical substitutions, superconductivity was found in *Ln*(O, F)BiS_2 (*Ln* =

La-Nd, Yb), (Sr, La)$FBiS_2$, (La, *M*)$OBiS_2$ (*M* = Ti, Zr, Hf, Th), $Bi_3O_2S_3$, La(O, F)$BiSe_2$, $EuBiS_2F$, and $Eu_3Bi_2S_4F_4$ with values of the superconducting transition temperature T_c ranging from 2.7 to 10.6 K [2, 5–12]. One of the fascinating features in the behavior of several of the BiS_2-based superconductors, including $LnO_{0.5}F_{0.5}BiS_2$ (*Ln* = La-Nd, Yb), (La,Sm)$O_{0.5}F_{0.5}BiS_2$, $Sr_{0.5}R_{0.5}FBiS_2$ (*R* = La-Pr, Sm), $LaO_{0.5}F_{0.5}BiSe_2$, and $EuBiS_2F$, is the pressure-induced enhancement of T_c that occurs at about 0.5-2.2 GPa, revealing the existence of two distinct superconducting phases [13–19]. This phenomenon is believed to be associated with a structural phase transition, which has been demonstrated in the case of $LaO_{0.5}F_{0.5}BiS_2$, from a tetragonal structure to a monoclinic structure with a sudden change in unit cell volume at an external pressure (P) of $\sim$0.5 GPa [20].

In addition to the requisite superconducting BiS_2 layers, there are other similarities in the compounds reported to have a second superconducting phase under high pressure: 1) all of these compounds contain F, which resides in blocking layers and donates conduction electrons to the BiS_2 layers, and 2) the high pressure phase has a significantly larger value of T_c than the low pressure phase. These similarities raise the issue of whether F is essential for the formation of the pressure-induced high-T_c phase. Recently, superconductivity was also found in single crystalline $CeOBiS_2$ at 1.3 K, and the value of T_c could be gradually enhanced under an external pressure [21]. This phenomenon was suggested to be related to Ce valence fluctuations, which can be tuned via the application of pressure; however, it is still not clear if there are concomitant phase transitions. On the other hand, the compounds $La_{1-x}M_xOBiS_2$ (M = Ti, Zr, Hf, Th) were reported to have the same crystal structure, very similar lattice parameters, and

values of T_c ($\sim$3 K) similar to that of $LaO_{0.5}F_{0.5}BiS_2$ [8]. The M ions in $La_{1-x}M_xOBiS_2$ are tetravalent and contribute conduction electrons to the BiS_2 layers in the absence of F; hence, this system is ideal for investigating whether non-F substituted BiS_2 compounds have a second pressure-induced high T_c phase. High pressure studies of $La_{1-x}M_xOBiS_2$ also have the potential of uncovering new superconducting phases in BiS_2-based superconductors and will be very helpful in developing an understanding of the nature of the pressure-induced low-T_c to high-T_c phase transition in these materials.

VI.B Experimental Details

Polycrystalline samples of $La_{0.80}Ti_{0.20}OBiS_2$ and $La_{0.85}Th_{0.15}OBiS_2$ were synthesized by solid state reaction as described elsewhere [8]. Geometric factors used in determining the electrical resistivity for each sample were measured before applying pressure. Hydrostatic pressure was generated by using a clamped piston-cylinder cell (PCC) in which a 1:1 mixture of n-pentane and isoamyl alcohol by volume was used as the pressure-transmitting medium. The pressures applied to the samples were estimated by measuring the T_c of a high purity ($>$99.99%) Sn disk inside the sample chamber of the cell and comparing the measured values with the well-determined $T_c(P)$ of high purity Sn [22]. Electrical resistance measurements under high pressure up to $\sim$2.4 GPa were performed in a temperature range between 1.5 and 280 K using a standard four-probe method in a pumped ^{4}He dewar.

VI.C Results and Discussion

The resistive superconducting transition curves $\rho(T)$, normalized to the value of ρ in the normal state at 4.2 K, for polycrystalline $La_{0.80}Ti_{0.20}OBiS_2$ and $La_{0.85}Th_{0.15}OBiS_2$ samples are shown in the upper and lower panels of Fig. VI.1, respectively. The superconducting transitions are very sharp for pressures below 0.95 GPa for both samples; however, the transitions become quite broad at higher pressures and the values of ρ remain finite down to 1.5 K. The relationship between T_c and pressure for the two compounds can be seen in Fig. VI.2. ${T_c}^{99\%}$, ${T_c}^{90\%}$, ${T_c}^{50\%}$, and ${T_c}^{10\%}$ represent the temperatures where ρ falls to 99%, 90%, 50%, and 10% of its normal-state value, respectively. The value of ${T_c}^{99\%}$ is 3.5 K for $La_{0.80}Ti_{0.20}OBiS_2$ at ambient pressure and increases slightly with increasing pressure to 3.7 K at 0.95 GPa, above which ${T_c}^{99\%}$ starts decreasing gradually. A similar dome-shaped T_c vs. P superconducting phase boundary can also be observed in the case of $La_{0.85}Th_{0.15}OBiS_2$, although the values of T_c are slightly different than those of $La_{0.80}Ti_{0.20}OBiS_2$. For both compounds, the difference between ${T_c}^{99\%}$ and ${T_c}^{90\%}$ (indicated by the green vertical lines in Fig. VI.2), which is related to the width of superconducting transition, becomes much larger at pressures at which T_c starts decreasing (0.95 GPa), reflecting dramatic changes in the superconductivity. During the pressure releasing cycle, the values of T_c are reversible and the superconducting transitions become sharp again when the samples have returned to low pressures as can be seen in Figs. VI.1 and VI.2 (data represented by crosses). These features in the T_c vs. P data indicate that there are significant differences in the superconducting behavior

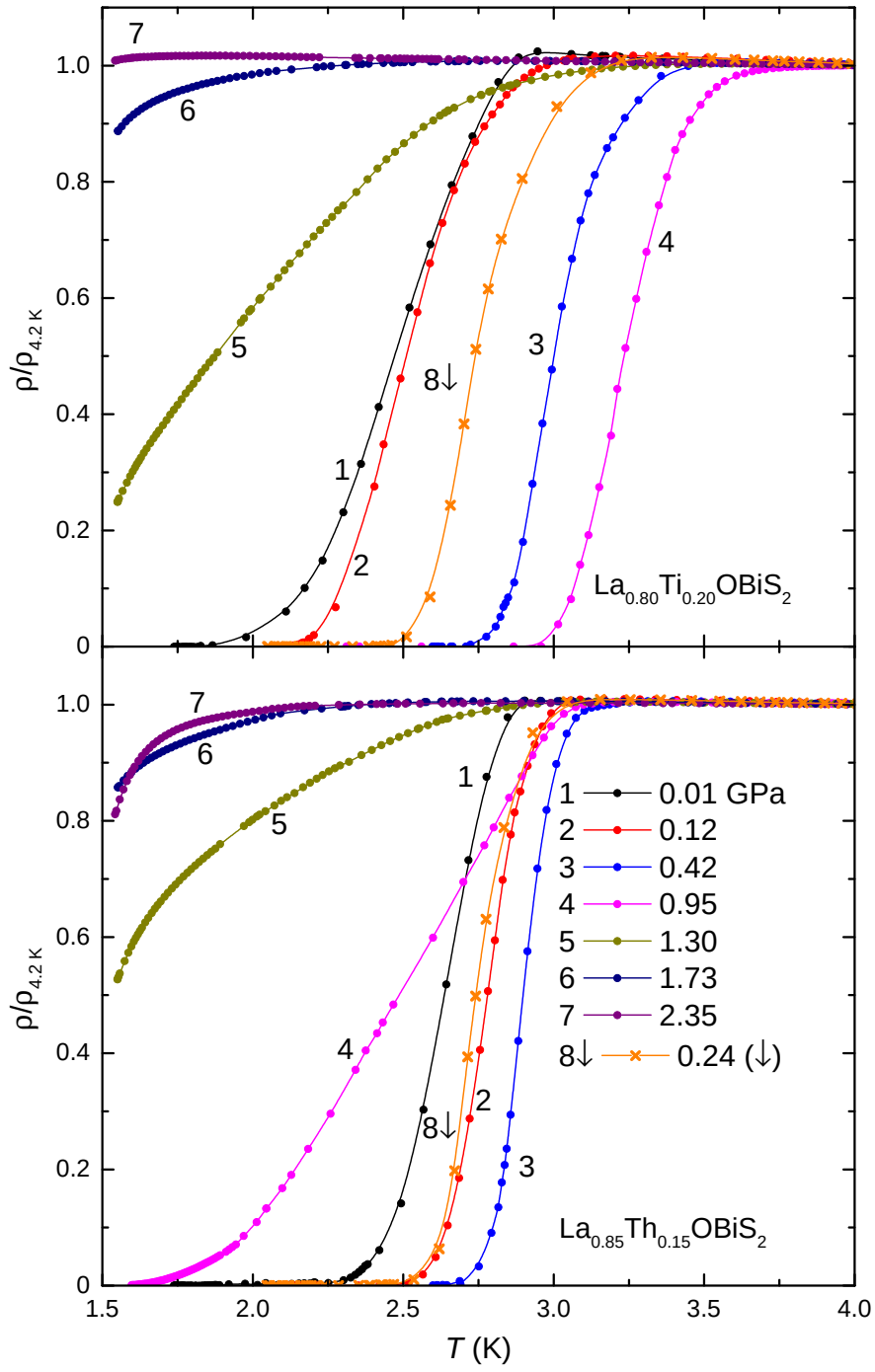

Figure VI.1: Temperature T dependence of electrical resistivity ρ, normalized to its normal state value at 4.2 K, below 4 K for $La_{0.80}Ti_{0.20}OBiS_2$ (upper panel) and $La_{0.85}Th_{0.15}OBiS_2$ (lower panel). The numbers and symbols with different colors in both panels are used to indicate the pressures listed in the lower panel. Most of the $\rho(T)$ data (represented by circles) were obtained upon increasing pressure. Crosses and the $\downarrow$ behind the number 8 in this figure as well as the following figures throughout this paper are used to represent data taken upon decreasing pressure.

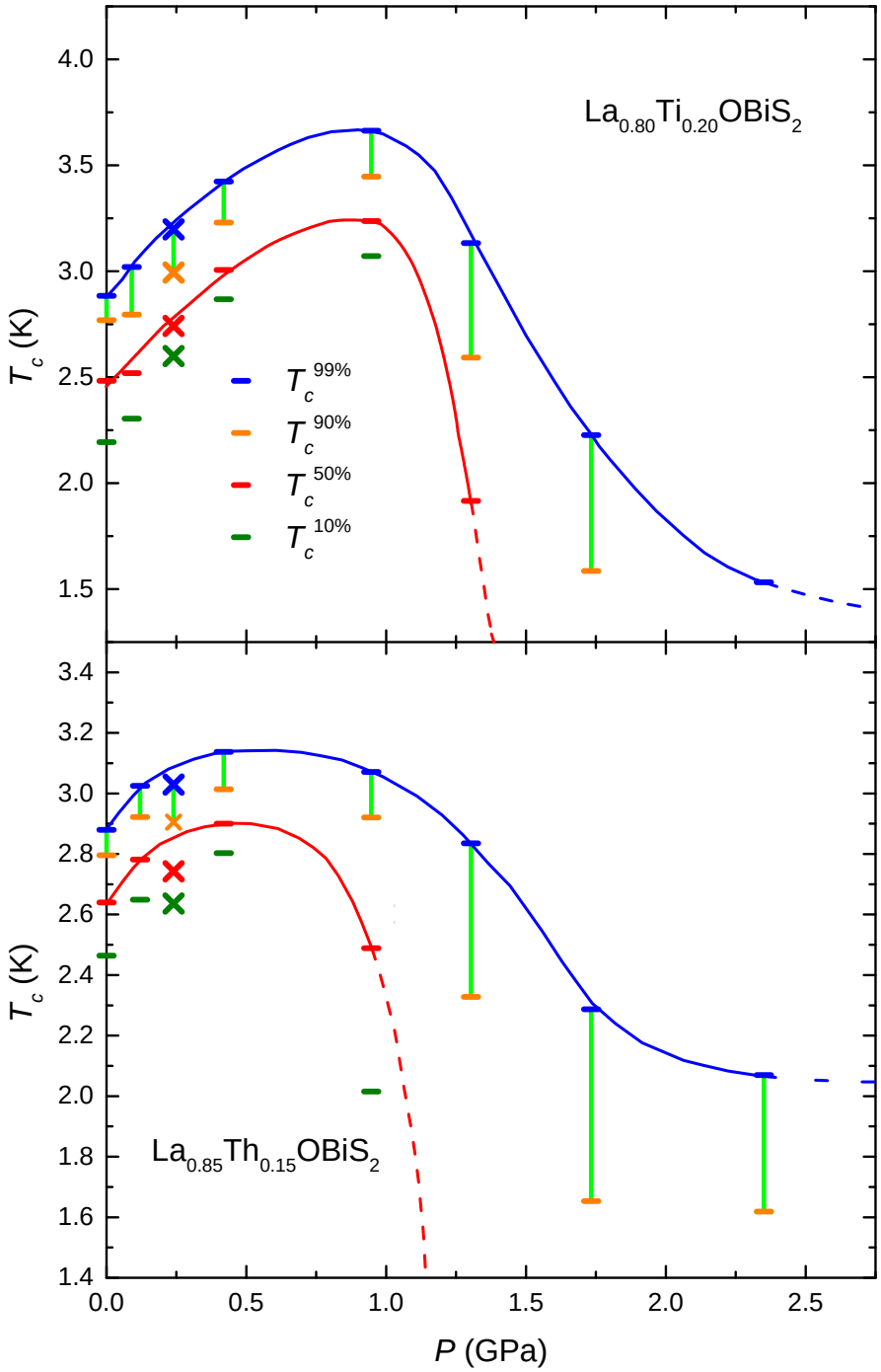

Figure VI.2: Superconducting transition temperature T_c vs. pressure for $La_{0.80}Ti_{0.20}OBiS_2$ (upper panel) and $La_{0.85}Th_{0.15}OBiS_2$ (lower panel). The temperature at which ρ drops to 99%, 90%, 50%, and 10% of its normal state value above the superconducting transition is indicated by symbols $T_c^{99\%}$, $T_c^{90\%}$, $T_c^{50\%}$, and $T_c^{10\%}$, respectively. The length of the vertical lines represents the difference between $T_c^{99\%}$ and $T_c^{90\%}$ and is a measure of the broadening of the superconducting transition under pressure. Crosses represent data taken upon decreasing pressure. The solid and dashed lines are guides to the eye for the experimental data and the corresponding extrapolations, respectively.

below and above 0.95 GPa.

To obtain further information about the origin of the suppression of superconductivity at high pressure, we investigated the normal state resistivity of the two compounds under pressure. Upon warming, $\rho(T)$ of $La_{0.85}Th_{0.15}OBiS_2$ first decreases significantly, passes through a minimum, and then increases nearly linearly at higher temperatures, as shown in Fig. VI.3. Such minima in the normal state resistivity are also observed for $La_{0.80}Ti_{0.20}OBiS_2$ under pressure and other BiS_2-based superconductors [8, 11, 13, 23, 24]. In addition, subtle anomalies in resistivity, indicated by black arrows in Fig. VI.3, were observed in both compounds when pressure was applied to the samples. Upon further increase in pressure, the temperature at which the anomaly displays a kink (T_a) increases with increasing pressure (see the lower inset of Fig. VI.3); however, at pressures above 0.42 GPa, such anomalies in $\rho(T)$ can no longer be observed. Very recently, a similar kink in $\rho(T)$ was reported in non-superconducting $LaOBiSe_2$ at ambient pressure, which may related to a charge density wave transition and can be suppressed by F substitution [25]. In this study, the appearance of these anomalies is possibly due to a temperature-driven phase transition; however, the nature of the transition will require further investigation.

In this work, we use the parameter $a(T)$, which represents the slope of $\rho(T)$, (dρ/dT), at a certain temperature to characterize the tendency of the compound to exhibit metallic- or semiconducting-like behavior. For simple metals at high temperatures, a is closely related to the scattering of conduction electrons by phonons. Although the value of a does not have a clear physical significance for semiconductors, a positive

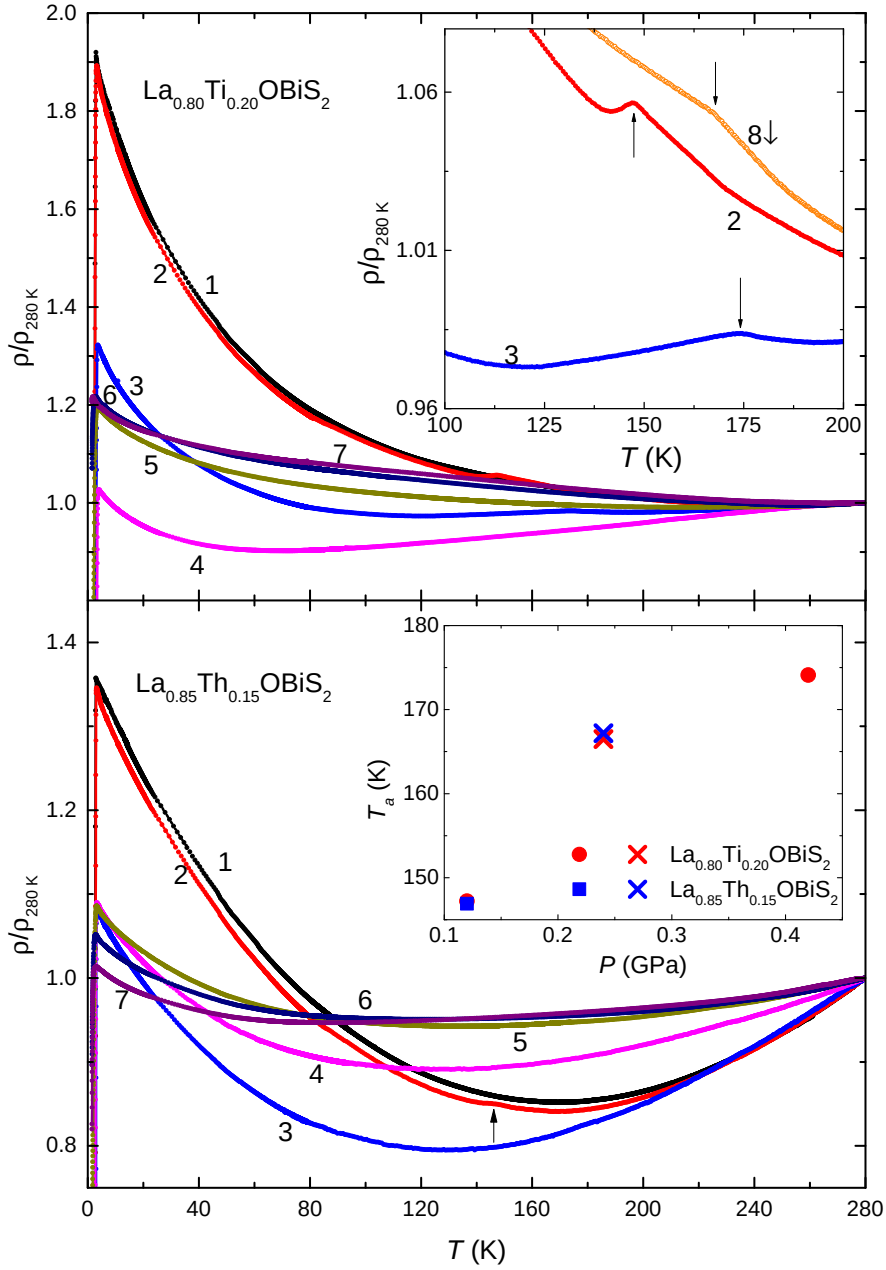

Figure VI.3: Temperature T dependence of the electrical resistivity ρ, normalized to the value of ρ at 280 K, ($\rho/\rho_{280\mathrm{K}}$), of $La_{0.80}Ti_{0.20}OBiS_2$ (upper panel) and $La_{0.85}Th_{0.15}OBiS_2$ (lower panel) at various pressures. The pressure corresponding to each ($\rho/\rho_{280\mathrm{K}}$) curve is indicated in Fig. VI.1 with the same color. Upper inset: enlargement of the T dependence of $\rho/\rho_{280\mathrm{K}}$ where the anomalies in $\rho(T)$ can be observed. The orange curve represents the data obtained at 0.24 GPa during the pressure releasing cycle. Lower inset: temperature at which the anomaly in $\rho(T)$ occurs, (T_a), vs. pressure (P). Black arrows in the figure indicate the location of anomalies in the resistivity.

value of a suggests that the sample is metallic-like and a negative value of a means it is semiconducting-like. In this work, the quantity $a(T)$ represents the tendency of the compounds to exhibit metallic- or semiconducting-like behavior at different pressures. As shown in Fig. VI.4(a), the values of a at $\sim$10 K ($a_{10\,\mathrm{K}}$) for the two compounds are negative at ambient pressure, suggesting semiconducting-like behavior at low temperatures. Upon application of an external pressures, $a_{10\,\mathrm{K}}$ first increases rapidly at low pressures but relatively moderately at high pressures, resulting in a kink in the pressure dependence of $a_{10\,\mathrm{K}}$ at $\sim$0.7 GPa. Although the values of $a_{10\,\mathrm{K}}$ are all negative at pressures up to 2.4 GPa, the increase of $a_{10\,\mathrm{K}}$ with pressure clearly indicates suppression of the semiconducting-like behavior. The kinks in $a_{10\,\mathrm{K}}(P)$ found at $\sim$0.7 GPa suggests there are some fundamental differences between behavior of the two compounds at low and high pressure, which are consistent with the decrease of T_c and broadening of the superconducting transitions at high pressure discussed previously.

Although the pressure dependences of a at low temperature are quite similar for the two compounds, the values of a at 250 K ($a_{250\,\mathrm{K}}$) for $La_{0.85}Th_{0.15}OBiS_2$ are positive and almost the same at low pressures, in contrast to the remarkable enhancement of $a_{250\,\mathrm{K}}$ from negative to positive values in the case of $La_{0.80}Ti_{0.20}OBiS_2$ as shown in Fig. VI.4(b). As indicated by the dashed lines in Fig. VI.4(b), the pressure dependence of $a_{250\,\mathrm{K}}$ dramatically decreases at higher pressures for both compounds, which suggests not only pressure-induced suppression of metallic-like behavior at high temperatures for the two compounds but also indicates the appearance of high pressure phases that exhibit different types of electronic conduction compared to the corresponding low pressure

phases. This behavior can be observed (Fig. VI.3) at high temperatures above $\sim$ 60 K for the Ti substituted sample and above $\sim$140 K for the Th substituted sample. It should be noted that the values of $a_{250\,\mathrm{K}}$ for $La_{0.80}Ti_{0.20}OBiS_2$ are even negative above 1.3 GPa, indicating the reappearance of semiconducting-like behavior at high temperatures.

Either the suppression of metallic conductivity or reappearance of semiconducting-like behavior is unusual for solids under pressure, since applying external pressures generally decreases the distance between neighboring atoms and results in an increase in the carrier density as well as a suppression of the semiconducting energy gap. For a better understanding of the normal state resistivity, we plotted representative ρ at 4.2 K ($\rho_{4.2\,\mathrm{K}}$) vs. pressure data for the two compounds in Fig. VI.5. It can be observed that $\rho_{4.2\,\mathrm{K}}$ for both compounds is significantly suppressed when pressure is first applied, which can be easily understood due to the increase of the electron density under pressures. With further increase in pressure, however, $\rho_{4.2\,\mathrm{K}}$ of $La_{0.80}Ti_{0.20}OBiS_2$ increases slowly, while $\rho_{4.2\,\mathrm{K}}$ of $La_{0.85}Ti_{0.15}OBiS_2$ decreases very slightly, resulting in kinks in $\rho_{4.2\,\mathrm{K}}(P)$ at $\sim$0.6 GPa for both compounds, as indicated by the arrows in Fig. VI.5. Consistent with previous discussions about the behavior of superconductivity and a under pressure, a different phase whose normal state resistivity exhibits an unusual response to pressure appears at pressures above $\sim$0.6 GPa.

As mentioned in the introduction, all of the BiS_2-based superconductors which were reported to show pressure-induced low-T_c to high-T_c phase transitions contain F. The previous study of Sm substituted $LaO_{0.5}F_{0.5}BiS_2$ suggested that the pressure dependences of T_c in BiS_2-based superconductors are closely related to the lattice parameter a rather

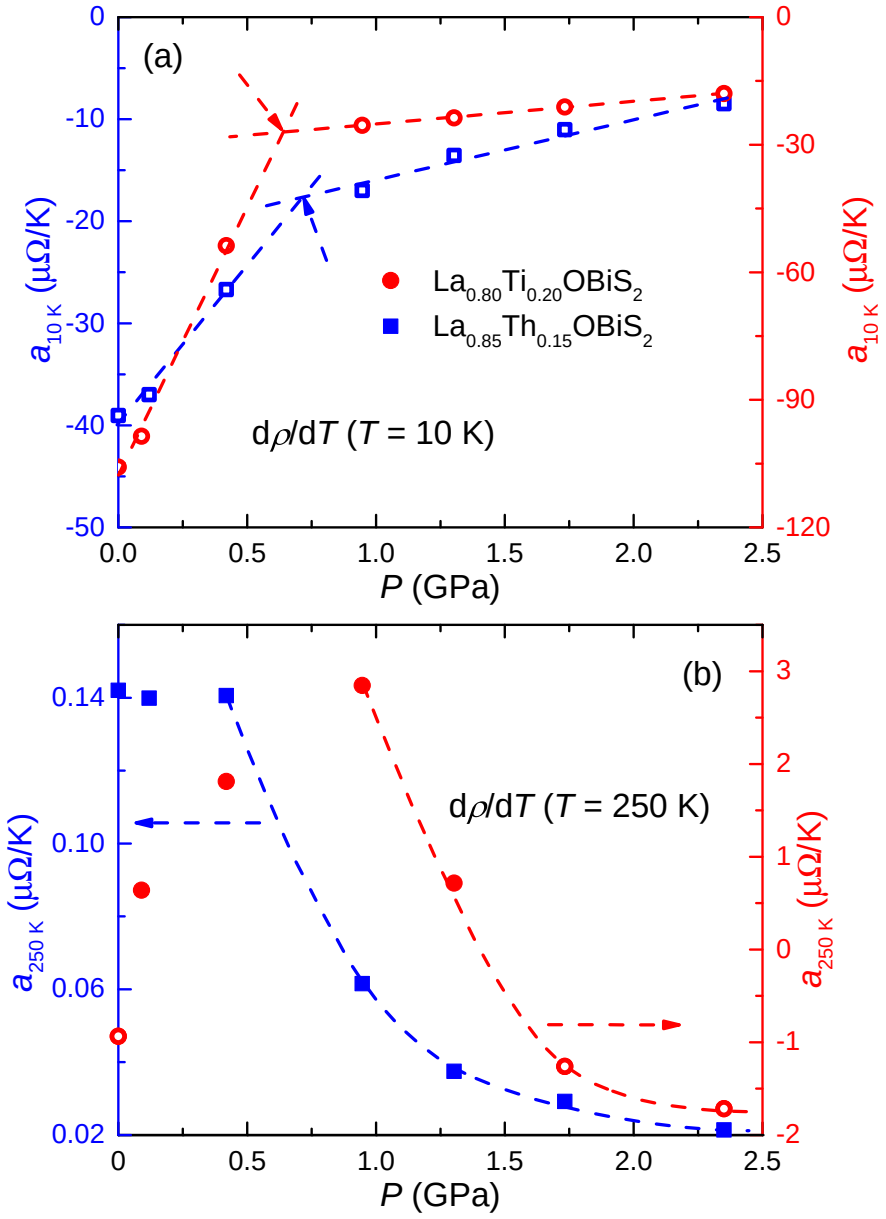

Figure VI.4: Evolution of the slopes of $\rho(T)$ at ~10 K (a) and at ~250 K (b) with increasing pressure for $La_{0.80}Ti_{0.20}OBiS_2$ (red circles) and $La_{0.85}Th_{0.15}OBiS_2$ (blue squares), respectively. The open circles indicate that the values are negative, suggesting semiconducting-like behavior. Dashed lines are guides to the eye.

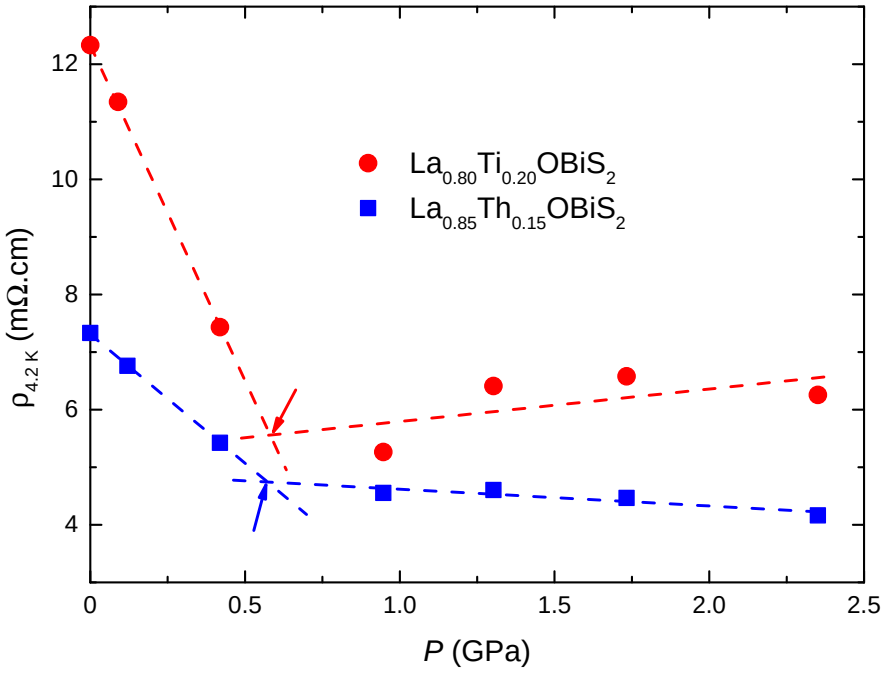

Figure VI.5: Normal state electrical resistivity ρ at 4.2 K for $La_{0.80}Ti_{0.20}OBiS_2$ (red circles) and $La_{0.85}Th_{0.15}OBiS_2$ (blue squares) under pressure. The dashed lines are linear fits of $\rho_{4.2\,\mathrm{K}}$ vs. P data whose slopes change at $\sim$0.6 GPa (indicated by the arrows) for both compounds.

than the chemical composition of the blocking layers [13]. In this study, although phase transitions were clearly observed in $La_{0.80}Ti_{0.20}OBiS_2$ and $La_{0.85}Th_{0.15}OBiS_2$ via investigations of the behavior of both the superconducting transitions and normal state electrical resistivity under pressure, the high pressure phases of the two compounds are apparently unfavorable for superconductivity. The results indicate that F in the blocking layer of BiS_2-based compounds plays a critical role of not only providing conduction electrons but also the sudden pressure-induced enhancement of superconductivity. This is presumably associated with a structural phase transition from tetragronal to orthorhombic symmetry, as has been shown for $LaO_{0.5}F_{0.5}BiS_2$.

Although superconductivity is suppressed and ρ remains finite to 1.5 K, the decrease of ρ signaling the appearance of superconducting currents can still be observed up to the highest pressure obtained in this study. For homogeneous samples, in general, pressure-induced phase transitions (either structural or electronic, first or second order) usually occur in a rather narrow hydrostatic pressure range. The abrupt changes in normal state resistivity presented in this study also suggest the phase transition should be complete before 1 GPa; this raises the question of why the superconducting transitions of the two compounds remain broad at pressures above 1 GPa. Considering the fact that bulk superconductivity of the samples at ambient pressure has been verified by means of specific heat and magnetization measurements[8], it is possible that the high pressure phase is not superconducting and the superconducting currents observed above $\sim$1 GPa are associated with small regions of the low-pressure phase that remain at high pressure due to slight inhomogeneities in the samples. However, the possibility that the high

pressure state of the compounds is still superconducting at lower temperature cannot be ruled out. Further studies need to be performed to determine whether the compounds are superconducting at lower temperatures.

VI.D Concluding Remarks

In summary, the observed phenomena including suppression and broadening of the superconducting transition, changes of the normal state electrical resistivity with pressure, and the dramatic changes in the behavior of the normal state electronic conduction between 0.42-0.95 GPa strongly suggest a pressure-induced phase transition occurs in the $La_{1-x}M_xOBiS_2$ compounds. In contrast to the pressure-induced low-T_c to high T_c phase transitions reported in F-containing BiS_2 superconductors, the high-pressure phase observed in this work does not favor superconductivity. The results suggest that fluorine plays a critical role for the pressure-induced enhancement of T_c for BiS_2-based compounds. For the low-pressure phase, anomalies in the normal state resistivity, which seem to be pressure dependent, were observed in the pressure range from 0.24 to 0.45 GPa. Another unusual phenomenon observed in this study is the tendency toward more semiconducting behavior with increasing pressure in the high-pressure phase at temperatures above $\sim$140 K. Further studies of these unusual phenomena are expected to enrich our understanding of the physics of solids at high-pressure.

The text and data presented in this chapter are reprints of material that appears in "High pressure effects on non-fluorinated BiS_2-based superconductors $La_{1-x}M_xOBiS_2$ (M = Ti and Th)," Y. Fang, D. Yazici, I. Jeon, and M. B. Maple, *Phys. Rev. B* **96**, 214505 (2017). The dissertation author is the primary investigator and author of this article.

Bibliography

[1] Y. Mizuguchi, H. Fujihisa, Y. Gotoh, K. Suzuki, H. Usui, K. Kuroki, S. Demura, Y. Takano, H. Izawa, and O. Miura, Phys. Rev. B **86**, 220510 (2012).

[2] D. Yazici, K. Huang, B. D. White, A. H. Chang, A. J. Friedman, and M. B. Maple, Phil. Mag. **93**, 673 (2013).

[3] Y. Fang, C. T. Wolowiec, D. Yazici, and M. B. Maple, Novel Superconducting Materials **1** (2015).

[4] D. Yazici, I. Jeon, B. D. White, and M. B. Maple, Physica C **514**, 218 (2015).

[5] Y. Fang, D. Yazici, B. D. White, and M. B. Maple, Phys. Rev. B **91**, 064510 (2015).

[6] I. Jeon, D. Yazici, B. D. White, A. J. Friedman, and M. B. Maple, Phys. Rev. B **90**, 054510 (2014).

[7] X. Lin, X. X. Ni, B. Chen, X. F. Xu, X. X. Yang, J. H. Dai, Y. K. Li, X. J. Yang, Y. K. Luo, Q. Tao, G. H. Cao, and Z. Xu, Phy. Rev. B **87**, 020504 (2013).

[8] D. Yazici, K. Huang, B. D. White, I. Jeon, V. W. Burnett, A. J. Friedman, I. K. Lum, M. Nallaiyan, S. Spagna, and M. B. Maple, Phys. Rev. B **87**, 174512 (2013).

[9] Y. Yu, J. F. Shao, S. Tan, C. J. Zhang, and Y. H. Zhang, J. Phys. Soc. Jpn. **82**, 034718 (2013).

[10] M. Tanaka, M. Nagao, Y. Matsushita, M. Fujioka, S. J. Denholme, T. Yamaguchi, H. Takeya, and Y. Takano, J. Solid State Chem. **219**, 168 (2014).

[11] H. F. Zhai, Z. T. Tang, H. Jiang, K. Xu, K. Zhang, P. Zhang, J. K. Bao, Y. L. Sun, W. H. Jiao, I. Nowik, I. Felner, Y. K. Li, X. F. Xu, Q. Tao, C. M. Feng, Z. A. Xu, and G. H. Cao, Phys. Rev. B **90**, 064518 (2014).

[12] H. F. Zhai, P. Zhang, S. Q. Wu, C. Y. He, Z. T. Tang, H. Jiang, Y. L. Sun, J. K. Bao, I. Nowik, I. Felner, Y. W. Zeng, Y. K. Li, X. F. Xu, Q. Tao, Z. A. Xu, and G. H. Cao, J. Am. Chem. Soc. **136**, 15386 (2014).

[13] Y. Fang, D. Yazici, B. D. White, and M. B. Maple, Phys. Rev. B **92**, 094507 (2015).

[14] C. T. Wolowiec, B. D. White, I. Jeon, D. Yazici, K. Huang, and M. B. Maple, J. Phys.: Condens. Matter **25**, 422201 (2013).

[15] Y. Fang, C. T. Wolowiec, A. J. Breindel, D. Yazici, P.-C. Ho, and M. B. Maple, Supercond Sci. Technol. **30**, 115004 (2017).

[16] R. Jha, B. Tiwari, and V. P. S. Awana, J. Phys. Soc. Jpn. **83**, 063707 (2014).

[17] R. Jha, B. Tiwari, and V. P. S. Awana, J. Appl. Phys. **117**, 013901 (2015).

[18] M. Fujioka, M. Tanaka, S. J. Denholme, T. Yamaki, H. Takeya, T. Yamaguchi, and Y. Takano, Europhys. Lett. **108**, 47007 (2014).

[19] C. Y. Guo, Y. Chen, M. Smidman, S. A. Chen, W. B. Jiang, H. F. Zhai, Y. F. Wang, G. H. Cao, J. M. Chen, X. Lu, and H. Q. Yuan, Phys. Rev. B **91**, 214512 (2015).

[20] T. Tomita, M. Ebata, H. Soeda, H. Takahashi, H. Fujihisa, Y. Gotoh, Y. Mizuguchi, H. Izawa, O. Miura, S. Demura, K. Deguchi, and Y. Takano, J. Phys. Soc. Jpn. **83**, 063704 (2014).

[21] M. Tanaka, M. Nagao, R. Matsumoto, N. Kataoka, I. Ueta, H. Tanaka, S. Watauchi, I. Tanaka, and Y. Takano, J. Alloys Compd. **722**, 467 (2017).

[22] T. F. Smith, C. W. Chu, and M. B. Maple, Cryogenics **9**, 53 (1969).

[23] S. Demura, Y. Mizuguchi, K. Deguchi, H. Okazaki, H. Hara, T. Watanabe, S. James Denholme, M. Fujioka, T. Ozaki, H. Fujihisa, G. Yoshito, M. Osuke, Y. Takahide, T. Hiroyuki, and T. Yoshihiko, J. Phys. Soc. Jpn. **82**, 033708 (2013).

[24] G. C. Kim, M. Cheon, Y. C. Kim, and R.-K. Ko, arXiv preprint arXiv:1512.05070 (2015).

[25] S. Wu, Z. Sun, F. Chiang, C. Ma, H. Tian, R. Zhang, B. Zhang, J. Li, and H. Yang, Solid State Communications **205**, 14 (2015).

Chapter VII

Chemical Substitution and High Pressure Effects on Superconductors in the *Ln*OBiS$_2$ (*Ln* = La-Nd) System

VII.A Introduction

Following the discovery of superconductivity by Kammerlingh Onnes in 1911, efforts in the search for new superconducting materials during the past century have shown that most of the pure metals and an enormous number of alloys and compounds become superconducting at low temperatures. The highest superconducting critical temperature T_c that has been reported is 133 K for the cuprates at ambient pressure and 203 K in sulfur hydride at 155 GPa, although the latter claim has not yet been independently verified [1, 2]. In order to experimentally realize new superconducting materials with properties

suitable for practical applications, there is still much to accomplish in both theory and experiment. The recently discovered family of BiS_2-based superconductors exhibit a layered crystal structure which is characterized by an alternating pattern of BiS_2 double layers that are separated by blocking layers [3]. This layered structure provides new hope and opportunity to enrich the class of layered superconductors with higher values of T_c.

Chemical substitution may induce significant change in materials to their lattice parameters, crystal structure and electronic structure. It has been broadly used as a strategy to tune physical properties of materials including electronic transport, magnetic, thermal, mechanical, and luminescent properties. Chemical substitution has been found to induce superconductivity via electron or hole doping in LnFeAsO compounds by replacing F for O [4–10], Co for Fe [11], Sr for La [12], Th for Gd [13], and also through the introduction of oxygen vacancies [14, 15]. Similar to the LnFeAsO compounds, it has been reported that electron carriers are essential for the emergence of superconductivity in the BiS_2-based materials [3, 16]. By modifying the blocking layers of the BiS_2-based compounds, electron carriers can be generated within the structures. As a result, a large number of novel BiS_2-based superconductors, such as $Bi_4O_4S_3$, $Bi_3O_2S_3$, $LnO_{1-x}F_xBiS_2$ (*Ln* = La, Ce, Pr, Nd, Yb), $La_{1-x}M_xOBiS_2$ (M = Ti, Zr, Hf, Th), $Sr_{1-x}La_xFBiS_2$, $EuBiS_2F$, and $Eu_3Bi_2S_4F_4$, have been developed with T_c's ranging from 2.7 to 10.6 K [3, 10, 17–26].

The superconducting properties of BiS_2-based compounds are also sensitive to the environment in which they are synthesized or being measured. For example, polycrystalline samples of $LaO_{1-x}F_xBiS_2$ subjected to high pressure (HP) annealing have

T_c values significantly higher than as-grown (AG) samples. Also, with the application of external hydrostatic pressure, a monotonic decrease in T_c is observed for both the $Bi_4O_4S_3$ and $SrFBiS_2$ compounds [27, 28]; in contrast, the compounds $LnO_{1-x}F_xBiS_2$, $Eu_3Bi_2S_4F_4$, $EuFBiS_2$, $LaO_{0.5}F_{0.5}BiSe_2$ and $Sr_{0.5}La_{0.5}FBiS_2$ were reported to have a sharp jump in T_c under applied pressure, indicating a pressure-induced transition from a low-T_c to high-T_c superconductor phase [27, 29–34]. It is also observed that superconductivity in the BiS_2-based compounds is very sensitive to chemical composition and to the level of electron doping in particular. As a result, T_c values of the samples with the same nominal chemical composition are not always the same since there might be slight differences in the actual chemical composition.

At present, there have been more than one hundred research papers published regarding superconductivity in the BiS_2-based compounds, which have helped increase our understanding of these novel materials and superconductivity in general. The peculiar crystal structure of these BiS_2-based compounds as a landscape for studying and optimizing superconductivity has fostered a healthy competition within the scientific community to explore the important critical parameters that affect T_c as well as to understand the nature of superconductivity itself in these layered structures. In this article, we will review some of the recent progress in both the study of chemical substitution and external pressure effects on the BiS_2-based compounds. Discussions about some of the parameters that are essential for superconductivity in these compounds will also be presented.

VII.B $Bi_4O_4S_3$

As the first discovered superconductor in the BiS_2-based compounds, $Bi_4O_4S_3$ is a bulk superconductor with a T_c of about 4.5 K [3, 35]. The structure of $Bi_4O_4S_3$ is derived from the structure of the parent $Bi_6O_8S_5$ with a 50% deficiency in SO_4 units; this results in the presence of electron carriers in the BiS_2 layers which induce the superconductivity in $Bi_4O_4S_3$ [3, 36]. Interestingly, the parent phase, $Bi_6O_8S_5$, which was initially regarded as a band insulator, was soon found to show superconductivity at $\sim$4.2 K when the sample is annealed in vacuum [37].

Chemical substitutions have been found to suppress T_c in the superconducting compound $Bi_4O_4S_3$. Substitution of Se at the S site results in a slight increase in the lattice parameter c and a remarkable enhancement of the normal state resistivity [38]. The T_c of the $Bi_4O_4S_{3-x}Se_x$ compound decreases with increasing Se concentration from 4.4 K at x = 0 to 3.5 K at x = 0.15, while the upper critical field at 0 K, $H_{c2}(0)$, determined by fitting the conventional one-band Werthamer–Helfand–Hohenberg (WHH) equation to the $H_{c2}(T)$ data, is also suppressed from 2.3 to 1.8 T [39]. Similarly, T_c of the $Bi_{4-x}Ag_xO_4S_3$ compound gradually decreases with increasing Ag concentration and a subtle shrinkage of both the a and c lattice parameters were observed up to x = 0.2 [40]. It should be noted that the chemical pressure generated by Ag substitution is negligible in $Bi_4O_4S_3$ and the suppression of T_c most likely arises from the substitution of the Ag ions into the superconducting BiS_2 layers and the resultant change in the electronic structure of the compound.

VII.C $LnO_{1-x}F_xBiS_2$ (*Ln* = La, Ce, Pr, Nd, Yb)

The parent compounds in the *Ln*OBiS$_2$ family are band insulators. The substitution of F for O induces superconductivity via electron doping into the BiS$_2$ layers. By applying relatively small magnetic fields ($\sim$1 T) to polycrysatlline specimens of these superconductors, the superconducting state can be destroyed [21]. Due to the chemical similarity of the rare earth elements, there is considerable flexibility in modifications that can be made to the blocking layers of these compounds which facilitates the investigation of the superconducting and normal state properties of BiS$_2$-based compounds. The *Ln*OBiS$_2$ compounds crystallize in a tetragonal structure with space group *P4/nmm* [20]. Between each *Ln*O blocking layer, there is a double BiS$_2$ superconducting layer in which there are two distinct positions for the S ions: in-plane position (S1) and out-of-plane position (S2), as indicated in Fig. VII.1.

Currently, superconductivity has been induced in five different parent compounds *Ln*(O,F)BiS$_2$ (*Ln* = La, Ce, Pr, Nd, Yb), with the substitution of F for O [21]. Polycrystalline samples of these compounds can be synthesized by using solid state reactions in sealed quartz tubes. However, along with the main superconducting phase, small amounts of secondary phases including *Ln*F$_3$ and BiF$_3$ may also be formed in the polycrystalline samples [10, 19–21, 41, 42]. As a result, the actual chemical composition of these compounds may be different from the nominal chemical composition, particularly regarding the concentration of F, resulting in an overestimated level of electron doping into the BiS$_2$ layers. This concern has also been raised in the study of single-crystalline samples

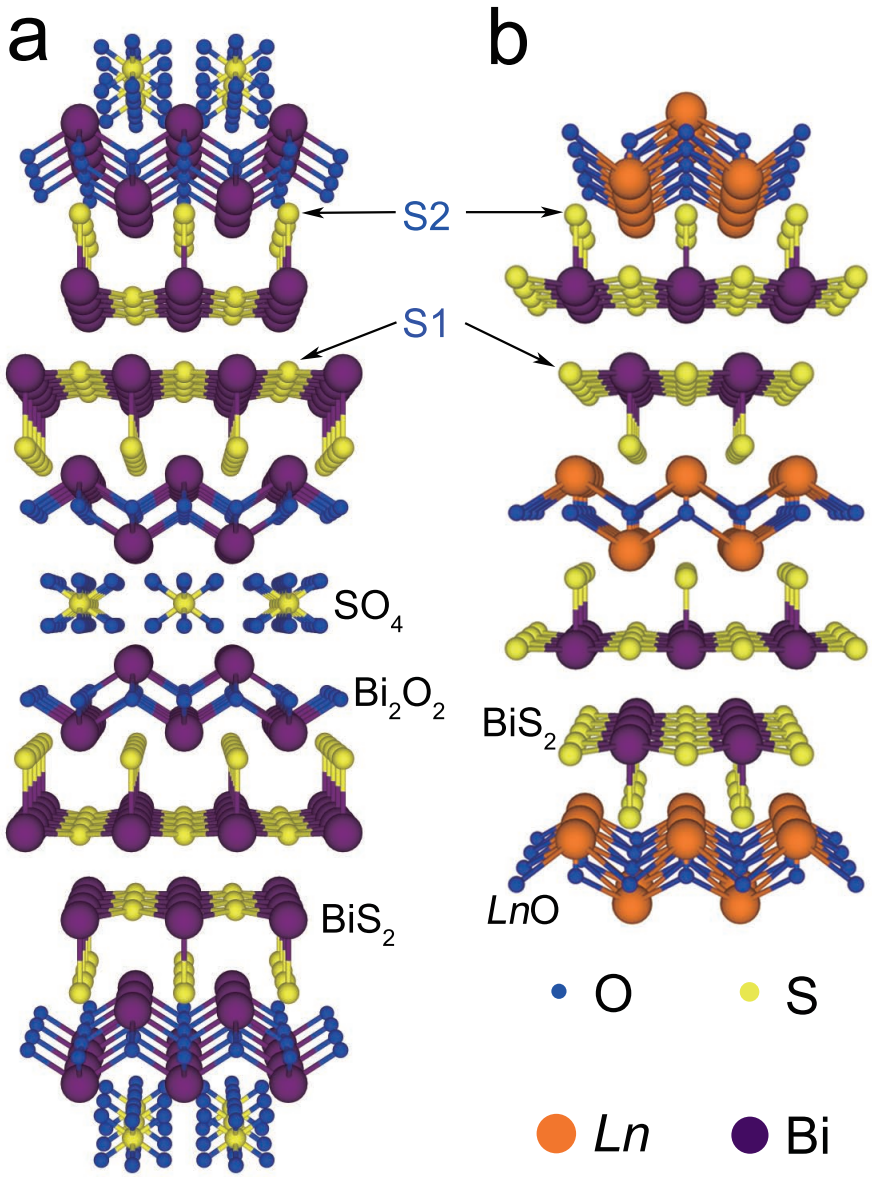

Figure VII.1: Representative crystal structure of (a) $Bi_4O_4S_3$ and (b) *Ln*OBiS_2. O^{2-} ions in the *Ln*O blocking layer can be partially replaced by F^-. S1 and S2 indicate the in-plane and out-of-plane positions of S, respectively, in the superconducting BiS_2 layers of the two structures.

of $NdO_{1-x}F_xBiS_2$, in which case, the actual electron doping level was reported to be much lower than anticipated [43]. Hence, T_c values of samples with the same nominal chemical composition reported by different authors may differ from one another [21, 22]. Although conclusive evidence of inhomogeneity in polycrystalline samples of the BiS_2-based superconductors has not been reported, measurements of electrical resistivity (ρ), magnetic susceptibility (χ), and specific heat (C), etc. may still be partially affected by possible inhomogeneity of the samples, and thus compromise reports of some of the intrinsic properties of these compounds. In addition, the existence of defects and disorder in these materials may also complicate the analysis of experiments and comparison with theoretical models. As mentioned by Kuroki, establishing the intrinsic phase diagram of the BiS_2-based superconductors is still a significant challenge in research on BiS_2-based superconductors [44].

VII.C.1 Electronic and crystal structures, and their correlation with T_c

The T_c vs F concentration plots for *Ln*$O_{1-x}F_xBiS_2$, displayed in Fig. VII.2, show a broad range of F concentration in which superconductivity can be induced; there is also an apparent enhancement of T_c with increasing *Ln* atomic number. The optimal F concentration for superconductivity in these compounds falls within the range of $0.4 \leqslant x \leqslant 0.7$. As the concentration of F is increased, the superconductivity of these compounds was also found to be more resistant to the destructive effects of an external magnetic field up to the F solubility limit [47, 48]. As an example, the upper critical field of $NdO_{1-x}F_xBiS_2$ increases from 0.9 T at x = 0.3 to 3.3 T at x = 0.7 [48]. For

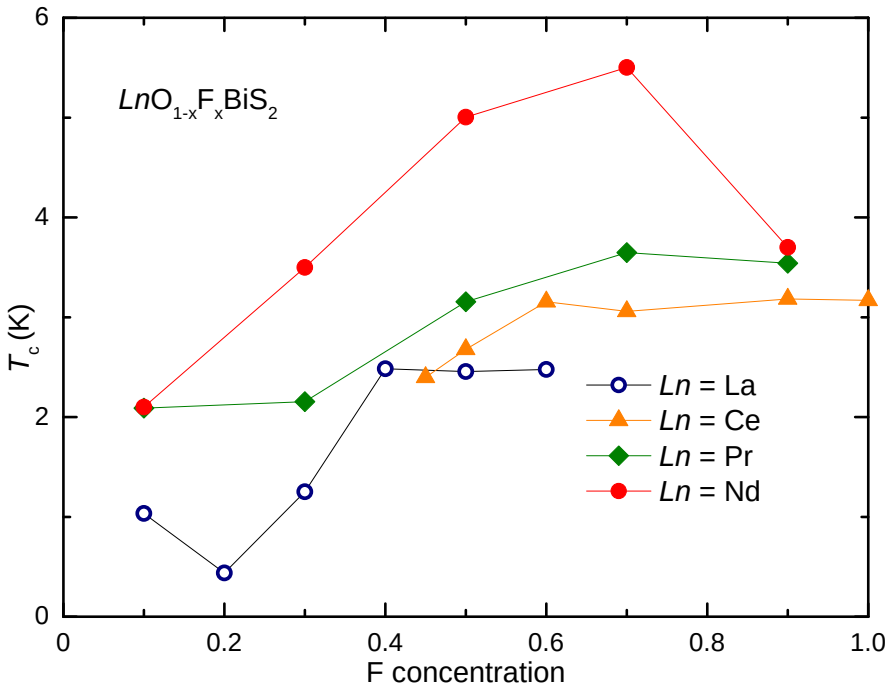

Figure VII.2: Dependence of T_c on nominal F concentration for $Ln\mathrm{O}_{1-x}\mathrm{F}_x\mathrm{BiS}_2$ (*Ln* = La-Nd). The T_c values for *Ln* = La, Ce, Pr, Nd are obtained from Ref. [45–48], respectively. For interpretation of the definition of T_c of each sample, the reader is referred to the corresponding articles.

$LaO_{1-x}F_xBiS_2$, first-principles calculations suggest that the density of states at the Fermi level increases with increasing F substitution and attains its maximum value at x = 0.5 [16]. Hence, a large number of studies have been made on compounds with a nominal composition given by $LnO_{0.5}F_{0.5}BiS_2$ [10, 19, 20].

Electronic structure calculations for $LnO_{1-x}F_xBiS_2$, and, in particular, for the compound $LaO_{0.5}F_{0.5}BiS_2$, have been widely reported [49, 50]. It was suggested that $LaOBiS_2$ is an insulator with an energy gap of $\sim$0.8 eV [51], which is consistent with experimental evidence revealing significantly high values of ρ and negative temperature coefficients ($d\rho/dT < 0$) in polycrystalline samples [52]. As F is substituted into the O site (see Fig. VII.1), it is expected that electrons will be doped into the conduction bands which consist mainly of Bi-6p orbitals, resulting in an increase in charge carrier density in the BiS_2 layers [3, 50]. The possibility of conventional strong coupling s-wave superconductivity for $Bi_4O_4S_3$, $LaO_{0.5}F_{0.5}BiS_2$, and $NdO_{1-x}F_xBiS_2$ has been supported by measurements of magnetic penetration depth using muon-spin spectroscopy or tunnel diode resonator techniques [53–56]. In addition, some theoretical studies suggest that the superconductivity observed in the BiS_2-based compounds occurs via strong electron-phonon coupling [16, 51, 57]. However, other unconventional pairing mechanisms including extended s- or d-wave pairing, g-wave pairing, and triplet spin pairing were also proposed [58–62]. While evidence for both electron-phonon coupling [16, 51, 53–57] and strong electron-electron interactions [58–64] has been reported, the concentration of charge carriers in the BiS_2 layers is considered to be essential for the superconductivity in the $LnO_{1-x}F_xBiS_2$ compounds [18, 20, 21, 24, 27, 51, 52, 54, 65].

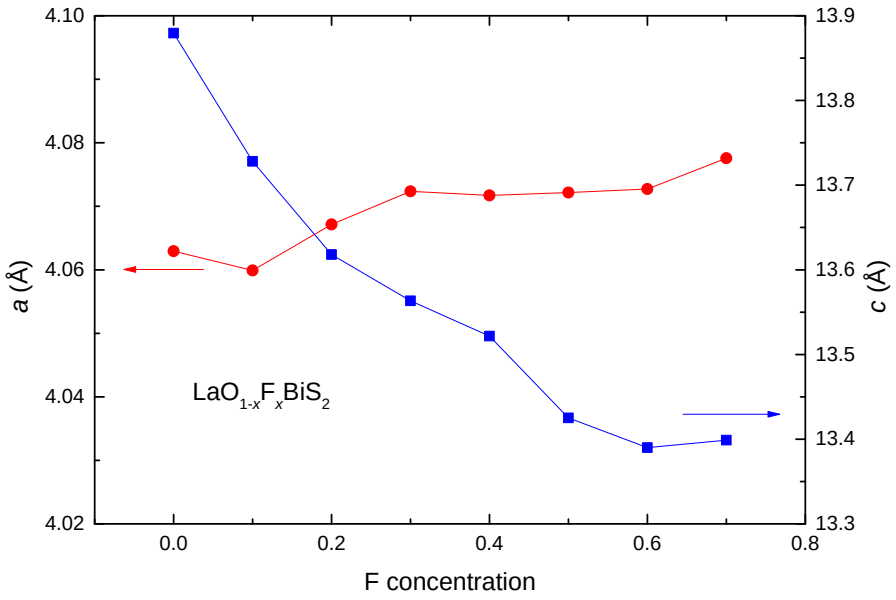

Figure VII.3: Nominal F concentration dependence of the lattice constants a (red) and c (blue) of AG $LaO_{1-x}F_xBiS_2$. The data are obtained from Ref. [24].

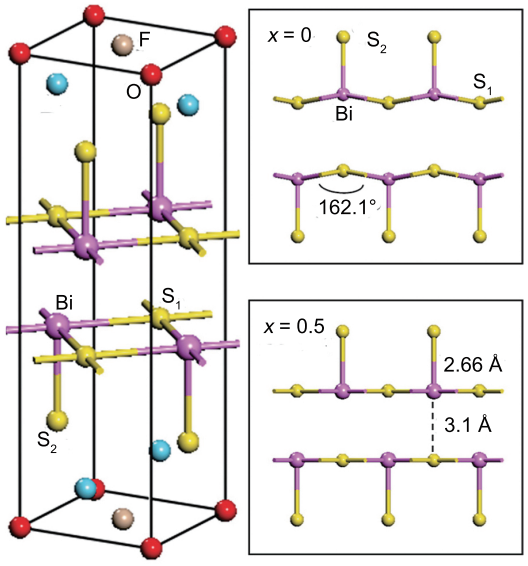

Figure VII.4: (left) Crystal structure of $LaO_{0.5}F_{0.5}BiS_2$. (right) The side view of the BiS_2 layers for $x = 0$ and $x = 0.5$ is displayed in the top and bottom panel, respectively. Adapted with permission from Ref. [16]. Copyrighted by the American Physical Society.

The substitution of F for O in *Ln*OBiS$_2$ may also induce a change in lattice parameters due to the smaller size of the F^- ions compared with O^{2-} ions. For *Ln*O$_{1-x}$F$_x$BiS$_2$, the length of the a-axis does not change significantly upon F substitution; however, the c-axis decreases monotonically until the F concentration reaches the solubility limit (typically around 50%) as illustrated by the example of LaO$_{1-x}$F$_x$BiS$_2$ shown in Fig. VII.1 [10, 19, 20, 47, 48]. The highest value of T_c was reported when c attains its minimum value, and the evolution of T_c seems consistent with the change in lattice parameter c [20, 47, 48]. However, it should be noted that these results do not necessarily indicate an exclusive role of the lattice parameter c in affecting T_c, since it is observed that the level of electron doping also reaches a maximum when the c parameter is smallest.

Local distortion of the lattice may also be induced by F substitution. Asymmetric broadening of the diffraction peaks with increasing F concentration in LaO$_{1-x}$F$_x$BiS$_2$ was observed in neutron scattering measurements, suggesting that strain may be induced along the c-axis due to a random substitution of the F ions at O sites [52]. It is also possible for a distortion to occur in the BiS$_2$ plane as a result of F substitution. For the LaO$_{1-x}$F$_x$BiS$_2$ compounds, first-principles calculations show that the z coordinate of the in-plane S and Bi atoms in the unit cell decreases with doping, yielding a nearly perfect planar structure at x = 0.5 (see Fig. VII.4). In fact, by using single crystal x-ray diffraction, nearly flat in-plane S-Bi-S angles were observed in LaO$_{1-x}$F$_x$BiS$_2$ at x = 0.46, which is close to the optimal F concentration value (x = 0.5) that yields the highest value of T_c [67, 68]. A flat Bi–S plane would result in an increase in hybridization of the p_x/p_y orbitals of Bi and S and, in turn, enhanced superconductivity.

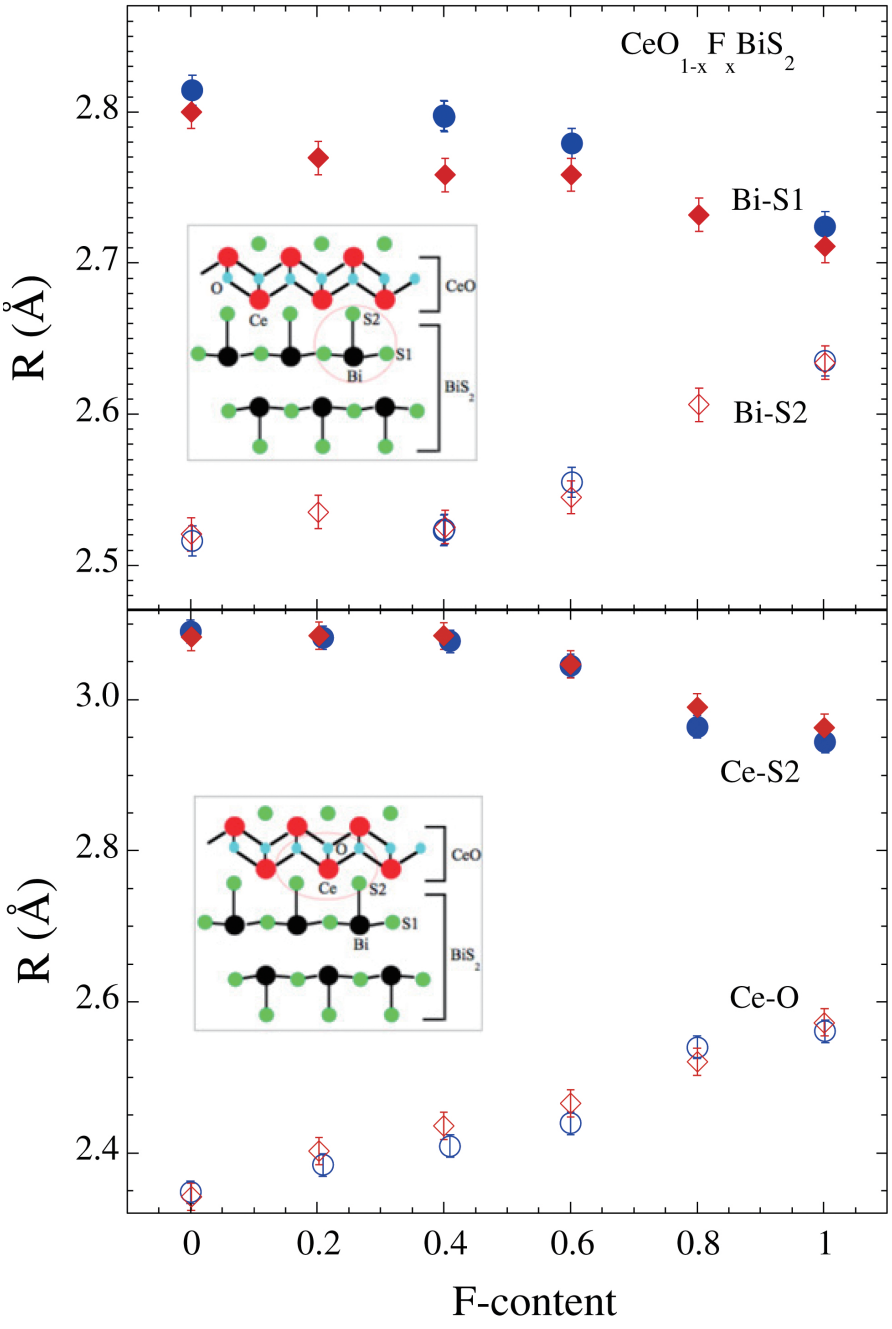

Figure VII.5: Near-neighbor distances from Bi (upper) and Ce (lower) as a function of F concentration. Blue circles and red diamonds represent the data taken from the as-grown and high pressure annealed samples, respectively. The insets show structural cartoons with near-neighbour atomic clusters (encircled) around Bi and Ce. Reprinted with permission from Ref. [66]: Determination of local atomic displacements in $CeO_{1-x}F_xBiS_2$ system, J. Phys.: Condens. Matter 26 (2014) 435701. Copyright (2014) by the IOP Publishing.

Investigation of extended x-ray absorption fine structure (EXAFS) of the $CeO_{1-x}F_xBiS_2$ compounds reveals that the local structure of both the BiS_2 superconducting layer and the Ce(O,F) blocking layer changes systematically with increasing F concentration [66]. The Bi-S2 distance increases with F concentration while the Ce-S2 distance decreases with F concentration (see Fig. VII.5), leading to the breaking of the Ce-S-Bi coupling channel [69]. Consequently, the hybridization between the Ce $4f$ orbital and the Bi $6p$ conduction band decreases with F concentration and the Ce^{3+}/Ce^{4+} valence fluctuations are suppressed, resulting in a completely localized $4f^1$ (Ce^{3+}) state at $x > 0.4$, where the samples exhibit superconductivity and ferromagnetism [69]. Therefore, it has been suggested that the valence of Ce, i.e., the coupling between the Ce $4f$ and Bi $6p$ states, is not beneficial to the superconductivity.

Considering the contraction in radius for the *Ln* ions, one may expect changes in both lattice parameters a and c as well as changes in T_c with increasing atomic number of *Ln*. Figure VII.6 displays typical values of T_c, defined as the temperature at which ρ falls to 50% of its normal-state value, for the compounds in the *Ln*(O,F)BiS_2 system as a function of lattice constant a. Except for the *Ln* = Yb and Nd cases, the T_c values of the samples after HP annealing are higher than the values of the AG samples. In addition, the dependence of T_c on the lattice paramter a for the AG samples are completely different from the HP annealed samples: for the AG samples, T_c increases with decreasing a (heavier *Ln*); however, the value of T_c for $LaO_{0.5}F_{0.5}BiS_2$ after HP annealing (a larger value of a) is significantly higher than the value of other HP annealed samples (smaller values of a). While the values of T_c for both AG and HP annealed samples appear to be

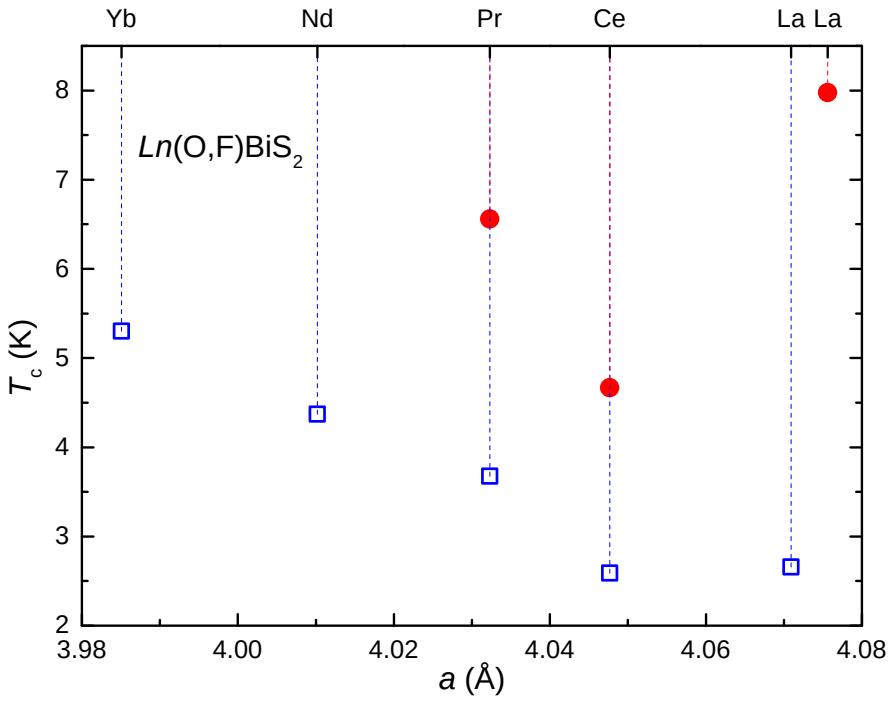

Figure VII.6: Correlation between T_c and a-axis of $Ln\mathrm{O}_{1-x}\mathrm{F}_x\mathrm{BiS}_2$ (x = 0.5 for *Ln* = La, Pr, Nd, Yb, x = 0.3 for *Ln* = Ce) superconductors. The open squares and filled circles represent the data obtained from as-grown samples and high pressure annealed samples, respectively. Dashed lines are guides to the eye. The T_c and a values for *Ln* = Nd, Yb samples are obtained from Ref. [21] and the data for *Ln* = La, Ce, Pr samples are taken from Refs. [65, 70, 71], respectively.

correlated, although differently, with the length of the a-axis [36], no structural phase transition was observed by HP annealing and the lattice parameters a and c for the AG and HP annealed samples are similar; this suggests that there should be other factors which have a significant effect on T_c. The markedly different values in T_c between the AG and HP annealed samples currently has no satisfactory explanation. However, evidence of a local distortion in the lattice has been reported, and this distortion is likely to be a source of the difference in T_c. For the HP annealed samples of $CeO_{1-x}F_xBiS_2$, the in-plane Bi-S1 distance is shorter; however, the out-of-plane Bi-S2 distance and the sizing of the blocking layers appear to be marginally effected by the HP annealing (see Fig. VII.5) [66]. It was also suggested that the crystal structure within the ab plane of the $CeO_{0.3}F_{0.7}BiS_2$ compound evolved to a higher symmetry after HP annealing, resulting in a better tetragonal phase [70]. Finally, the uniaxial strain along the c-axis, which was found in annealed samples of the $LaO_{0.5}F_{0.5}BiS_2$ and $PrO_{0.5}F_{0.5}BiS_2$ compounds, was reported to be positively correlated with the enhancement of superconductivity [65, 71]. These results indicate that the optimization of the local structure is important for realizing higher T_c values in the BiS_2-based superconductors.

VII.C.2 Normal state electrical resistivity, magnetic susceptibility, and specific heat

Given that F substitution enhances the charge carrier density of BiS_2-based parent compounds, one would expect that F-substitution may induce more metallic-like behavior in these materials. The temperature dependence of $\rho(T)$ in the normal state for single

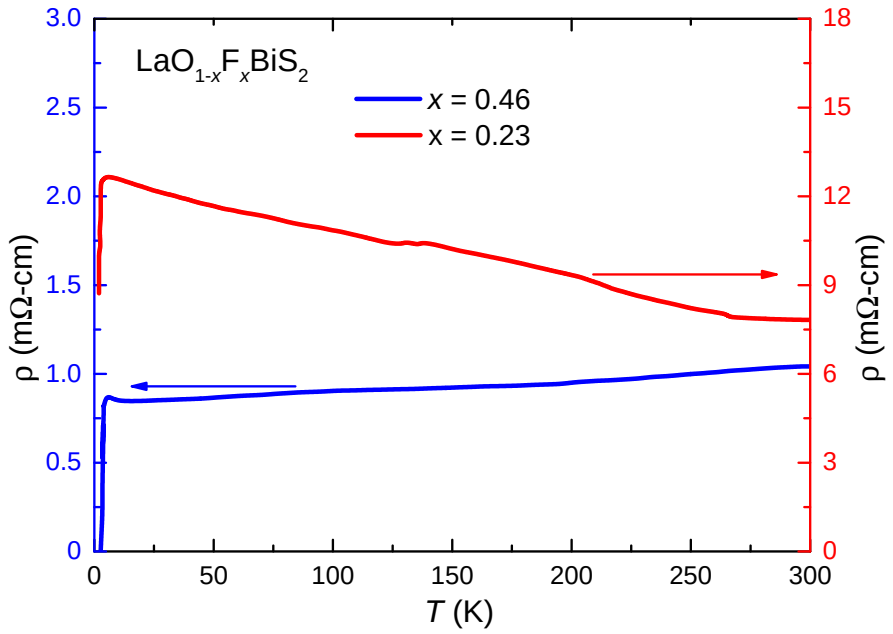

Figure VII.7: Temperature dependence of the electrical resistivity for $LaO_{1-x}F_xBiS_2$ (x = 0.23 and 0.46) single crystals. The data are obtained from Ref. [67].

crystals of $LaO_{1-x}F_xBiS_2$ (x = 0.23, 0.46) is shown in Fig. VII.7; while the crystal with x = 0.23 exhibits semiconducting-like behavior ($d\rho/dT < 0$), the crystal with x = 0.46 shows metallic behavior ($d\rho/dT > 0$) with significantly reduced values of resistivity [67]. These results are consistent with electronic band structure calculations which indicate that the parent compounds in this system should behave as band insulators but become metallic upon doping electron carriers into the BiS_2 layers [50]. However, the theoretical calculations do not fit well with measurements of $\rho(T)$ of polycrystalline samples of *Ln*OBiS$_2$ which tend to exhibit strong sample dependent results. Some of the *Ln*OBiS$_2$ parent compounds, which are in polycrystalline form, have been reported to show semimetallic behavior in contrast to the semiconducting-like behavior of the corresponding F-doped polycrystalline samples [10, 25, 46–48]. This behavior may be related to the quality of these polycrystalline samples, since complete semiconducting-

like behavior is also reported in the case of $LaOBiS_2$ and in the case of polycrystalline $CeOBiS_2$, the resistivity can be significantly increased together with the appearance of semiconducting-like behavior after HP annealing [46, 52].

Substitution of F into the lattice does not always result in a suppression of semiconducting-like behavior in polycrystalline samples. In fact, F substitution can enhance semiconducting-like behavior which has been observed in AG samples of $CeO_{1-x}F_xBiS_2$ and HP annealed samples of $LaO_{1-x}F_xBiS_2$ [10, 24]; this is in contrast to observations of suppressed semiconducting-like behavior by F substitution in single-crystalline samples of $CeO_{1-x}F_xBiS_2$ and $LaO_{1-x}F_xBiS_2$ [67, 72]. Although the cause of such unusual behavior is still unclear, the existence of grain boundaries as well as poor intergrain contacts in polycrystalline samples may contribute significantly to the semiconducting-like behavior of the F-substituted compounds. In addition to the semiconducting-metallic transition induced by F substitution in single crystals of $LaO_{1-x}F_xBiS_2$, research on single crystals of $NdO_{1-x}F_xBiS_2$ reveals metallic behavior in the normal state along the ab-plane of the crystal; this is different from the semiconducting behavior observed in polycrystalline samples of $NdO_{1-x}F_xBiS_2$ [43, 48, 64, 72, 73]. However, reports of the electrical transport properties in the normal state of single crystals of $CeO_{1-x}F_xBiS_2$ reveal semiconducting-like behavior in the ab-plane which is consistent with measurements on polycrystalline samples of the same compound [68]. Hence, the intrinsic electrical transport properties of the $LnO_{1-x}F_xBiS_2$ compounds seem to be dependent on a combination of lanthanide element *Ln*, F concentration x, and quality of the samples.

Both zero-field-cooled (ZFC) and field-cooled (FC) measurements of $\chi(T)$ were performed for *Ln*$O_{1-x}F_xBiS_2$ samples with different *Ln* and F concentrations. As shown in Fig. VII.8, ZFC measurements on *Ln*$O_{0.5}F_{0.5}BiS_2$ (*Ln* = La, Pr, Nd) yield a significant shielding volume fraction with T_c onset values that are consistent with the $\rho(T)$ data, while FC measurements reveal that $\chi(T)$ remains nearly unchanged in the superconducting state relative to the normal state, indicating strong vortex pinning [21]. For the case of samples with *Ln* = Ce and Yb and nominal F concentrations of $x \geqslant 0.7$ and x = 0.5, respectively, magnetic phase transitions were also observed, apart from diamagnetic signals arising from the appearance of superconductivity [21, 70, 72]. In addition to the induction of superconductivity and enhancement of T_c as a result of F substitution, the shielding volume fraction may be significantly enhanced at those temperatures where it has begun to saturate as a result of the increase in F concentration; a typical example of this behavior was found for $NdO_{1-x}F_xBiS_2$ reported in Ref. [47].

Figure VII.9 displays specific heat $C(T)$ data for the polycrystalline $LaO_{0.5}F_{0.5}BiS_2$ compound in the temperature range 1.8 K $\leqslant T \leqslant$ 50 K [21]. The expression $C(T)/T = \gamma + \beta T^2$, where γ is the electronic specific heat coefficient and β is the coefficient of the lattice contribution, was used in to fit the C/T vs T^2 data in the normal state which is displayed in the inset in the lower right hand side of Fig. VII.9. Shown in the inset in the upper left hand side of Fig. VII.9 are C_e/T vs T data, where C_e is the electronic contribution to the specific heat. Bulk superconductivity in polycyrstalline $LaO_{0.5}F_{0.5}BiS_2$ was confirmed with the appearance of a clear jump in the C_e/T vs T data at T_c. The ratio of the observed jump to the electronic contribution to the specific

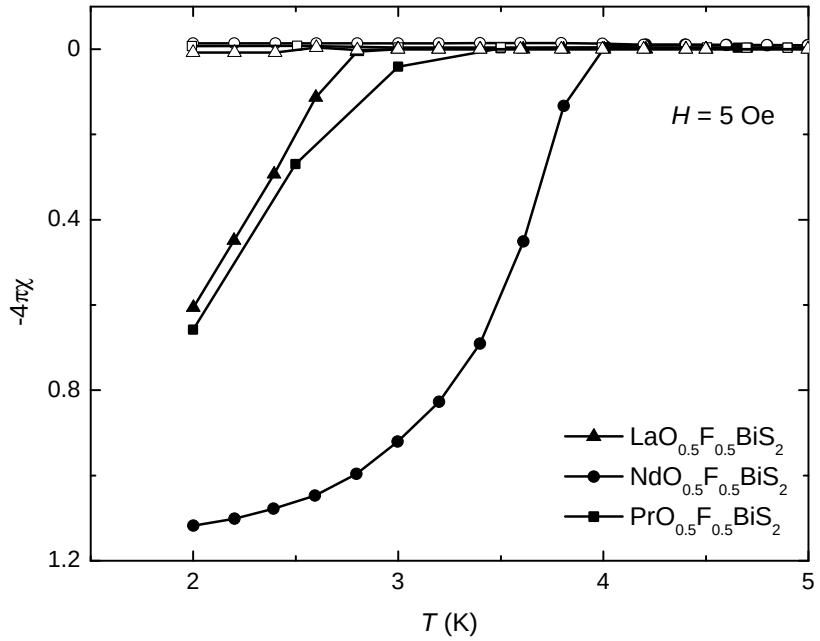

Figure VII.8: Temperature dependence of the magnetic susceptibility χ for $Ln\mathrm{O}_{0.5}\mathrm{F}_{0.5}\mathrm{BiS}_2$ (*Ln* = La, Pr, Nd) measured in the field-cooled (FC) (open symbols) and zero-field-cooled (ZFC) (filled symbols) processes. The data are taken from Ref. [21].

heat at T_c is estimated to be $\Delta C/\gamma T_c$ = 0.94, which is lower than the weak coupling BCS value of 1.43, but large enough to confirm bulk superconductivity in this compound. For the other *Ln*$O_{0.5}F_{0.5}BiS_2$ compounds with *Ln* = Ce, Pr, Nd, and Yb, the significant upturns in the C/T vs T data observed at low temperature are likely due to the presence of a Schottky-like anomaly for *Ln* = Pr and Nd or magnetic ordering for *Ln* = Ce and Yb [21, 74]. No clear $C(T)/T$ jump related to the appearance of superconductivity was observed in these samples [21]. The jumps in $C(T)/T$ in these compounds may not be readily observable because they may be reduced by the pairbreaking interaction due to the magnetic ions; the jumps may also be obscured by the broadening of the superconducting transitions by sample inhomogeneity or by the large upturns in $C(T)/T$. More rigorous experimental and theoretical studies on higher quality samples are needed to establish the nature of superconductivity in these compounds.

VII.D $La_{1-x}M_xOBiS_2$ (M = Th, Hf, Zr, and Ti)

As an alternative to F substitution, electron doping in the $LaOBiS_2$ system is possible by partially replacing trivalent La with tetravalent M (M = Th, Hf, Zr, and Ti) [25]. It has been reported that the $La_{1-x}M_xOBiS_2$ system exhibits superconductivity with values of T_c up to 2.85 K. A comparison of T_c values observed in the various compounds is displayed in the inset of Fig. VII.10 in which 20% (x = 0.2) of M = Th, Hf, Zr, and Ti was substituted for La in $La_{1-x}M_xOBiS_2$; there appears to be no clear correlation between T_c and the atomic radius of the tetravalent atom that replaces the La ion. The lowest value of T_c is observed for the $La_{0.8}Zr_{0.2}OBiS_2$ compound;

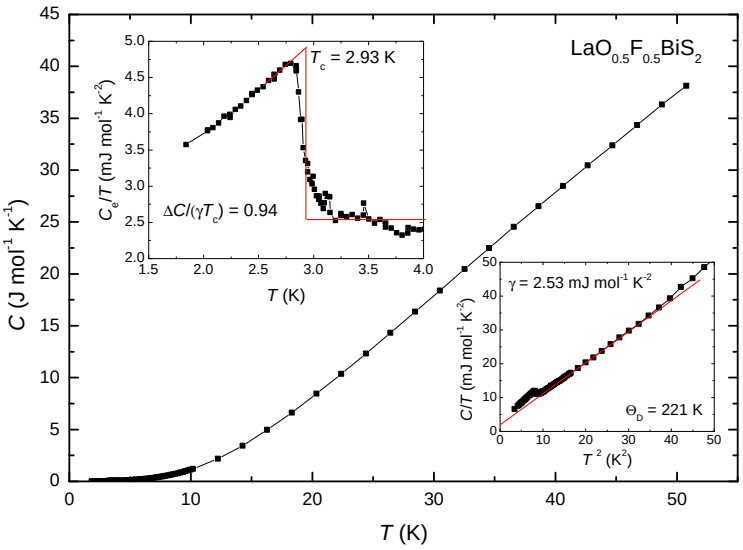

Figure VII.9: Specific heat C vs temperature T for $LaO_{0.5}F_{0.5}BiS_2$. A plot of C/T vs T^2 is shown in the inset in the lower right hand part of the figure. The red line is a fit of the expression $C(T)/T = \gamma + \beta T^2$. A plot of C_e/T vs T, where C_e is the electronic contribution to the specific heat, in the vicinity of the superconducting transition is shown in the inset in the upper left hand side of the figure. The data are taken from Ref. [21].

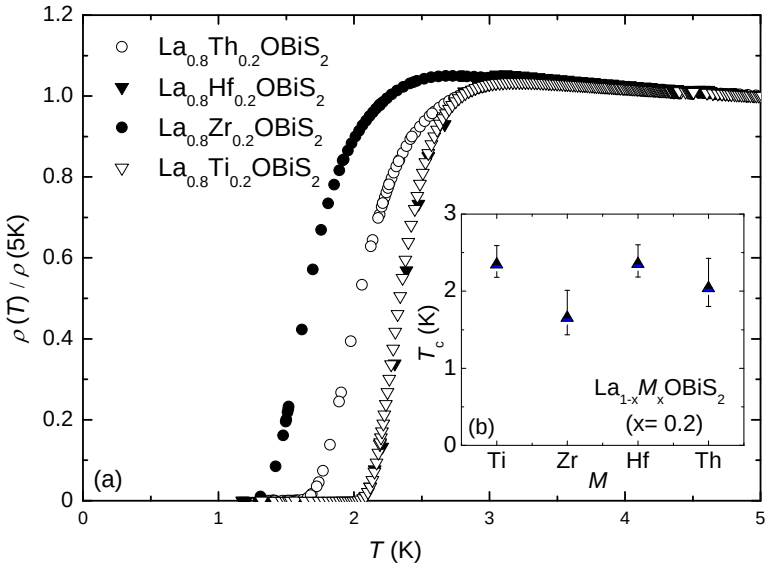

Figure VII.10: Resistive superconducting transitions and (inset) superconducting transition temperatures T_c for $La_{1-x}M_xOBiS_2$ compounds with M = Th, Hf, Zr, Ti and $x = 0.2$. T_c is defined as the temperature where ρ drops to 50% of its normal state value, and the width of the transition is determined from the temperatures where the resistivity drops to 90% and 10% of its normal state value. Reprinted with permission from Ref. [25]. Copyright (2013) by the American Physical Society.

while sharper superconducting transitions are observed for the $La_{0.8}Hf_{0.2}OBiS_2$ and $La_{0.8}Ti_{0.2}OBiS_2$ compounds, broader transitions are observed for the $La_{0.8}Zr_{0.2}OBiS_2$ and $La_{0.8}Th_{0.2}OBiS_2$ compounds. X-ray diffraction experiments show that both the a and c lattice parameters do not change significantly with different M^{4+} substitutions at the x = 0.2 concentration. However, with increasing M concentration, both values of a and c for $La_{1-x}M_xOBiS_2$ were observed to decrease gradually. For $La_{1-x}Th_xOBiS_2$, T_c first decreases with x from 2.85 K at x = 0.15 to 2.05 K at x = 0.20 and then remains roughly constant at higher concentration. A similar evolution of T_c with increasing M was also observed for $La_{1-x}M_xOBiS_2$ (M = Hf, Ti); however, after partially replacing La^{3+} with Sr^{2+}, no superconductivity was observed in $La_{1-x}Sr_xOBiS_2$ down to $\sim$1 K in the range $0.1 \leqslant x \leqslant 0.3$, which is in agreement with the behavior reported for $La_{1-x}Mg_xOBiS_2$ (x = 0-0.2) samples [25, 75]. These results suggest that hole doping is not sufficient to induce superconductivity and reveals the importance of electron doping in achieving superconductivity in BiS_2-based compounds.

Measurements of $\rho(T)$ for the $La_{0.85}Th_{0.15}OBiS_2$ and $La_{0.8}Hf_{0.2}OBiS_2$ compounds were performed in various magnetic fields down to 0.36 K [25]. As magnetic field is increased, the superconducting transition width broadens and the onset of superconductivity gradually shifts to lower temperatures. The orbital critical fields $H_{c2}(0)$ for the $La_{0.85}Th_{0.15}OBiS_2$ and $La_{0.8}Hf_{0.2}OBiS_2$ compounds were inferred from their initial slopes of H_c with respect to T using the conventional one-band WHH theory [39], yielding values of 1.09 and 1.12 T, respectively. These values of $H_{c2}(0)$ are close to the values of 1.9 T for $H_{c2}(0)$ observed in $LaO_{0.5}F_{0.5}BiS_2$ [18, 21], suggesting that there is a

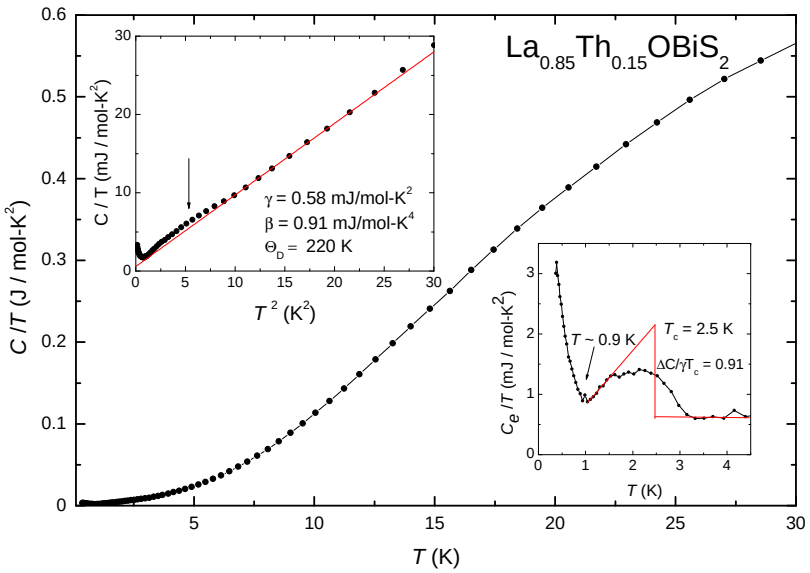

Figure VII.11: Specific heat C divided by temperature T, C/T, vs T for $La_{0.85}Th_{0.15}OBiS_2$. C/T vs T^2 is shown in the inset in the upper left hand part of the figure. The red line is a fit of the expression $C(T)/T = \gamma + \beta T^2$ to the data. The inset in the lower right part of the figure shows a plot of $C_e(T)$ vs T in the vicinity of the superconducting transition. Reprinted with permission from Ref. [25]. Copyright (2013) by the American Physical Society.

common superconducting phase characteristic of BiS_2-based superconductors.

Specific heat measurements were performed for the $La_{0.85}Th_{0.15}OBiS_2$ and $La_{0.8}Hf_{0.2}OBiS_2$ compounds in the temperature range of 0.36 K $\leqslant T \leqslant$ 30 K [25]. A clear feature is observed between 1 and 3 K for $La_{0.85}Th_{0.15}OBiS_2$ as shown in the inset at the lower right hand side of Fig. VII.11. A value of T_c = 2.5 K was estimated from an idealized entropy conserving construction, which is close to the T_c obtained from $\rho(T)$ measurement (T_c = 2.85 K). The presence of the feature suggests that superconductivity is a bulk phenomenon in this compound. The value of $\Delta C/\gamma T_c$ for $La_{0.85}Th_{0.15}OBiS_2$ is estimated to be $\sim$0.91, which is less than the value of 1.43 predicted by the BCS theory, but similar to that seen in $LaO_{0.5}F_{0.5}BiS_2$ [21]. However, only a small feature in C_e/T data for $La_{0.8}Hf_{0.2}OBiS_2$ is observed around the T_c (2.36 K) obtained from $\rho(T)$ measurements. The absence of a well-defined superconducting jump at T_c for $La_{0.8}Hf_{0.2}OBiS_2$ is likely to be a consequence of the superconducting transition being spread out in temperature due to sample inhomogeneity [21].

VII.E Chemical substitution effects on *Ln*(O,F)BiS_2

It has been demonstrated that the charge carrier (electron) density is important for the superconductivity of BiS_2-based compounds. In addition, values of T_c for AG samples of $LnO_{0.5}F_{0.5}BiS_2$ increase with increasing atomic number of the *Ln* component as shown in Fig. VII.6 [21, 22]. (The ionic size of the Ln^{3+} ion decreases with increasing atomic number.) This size contraction has the effect of reducing the dimensions of the blocking layers which contain the Ln^{3+} ions, thereby squeezing the neighboring BiS_2 layers,

i.e., effectively generating chemical pressure on the superconducting BiS_2 layers. As discussed in section 3.1, it appears that there is a correlation between T_c and the decrease in the size of the a-axis in the *Ln*(O,F)BiS_2 system. Hence, substitution of the element La with heavier lanthanide elements such as Sm, Eu, and Gd holds promise as a strategy for further enhancement of T_c in the BiS_2-based superconducting compounds. Recently, the compound with nominal chemical composition $SmO_{0.5}F_{0.5}BiS_2$ was synthesized and reported to be nonsuperconducting [76]; attempts have been unsuccessful in synthesizing other $LnO_{0.5}F_{0.5}BiS_2$ compounds with *Ln* = Eu-Tm. However, there has been recent success in synthesizing compounds in which there is a partial substitution at the *Ln* site with relatively smaller atoms as a method for enhancing T_c and further determining which parameters are relevant in affecting superconductivity [41, 42, 75–79].

As an example, partial substitution of La with the smaller Y ions in the compound of $La_{1-x}Y_xO_{0.5}F_{0.5}BiS_2$ allows one to study of the effects of chemical pressure on superconductivity [42]. Similar to La, Y has a trivalent electronic configuration and no magnetic moment, making Y^{3+} a suitable replacement for the La^{3+} ions. As a result of the substitution of Y for La in $La_{1-x}Y_xO_{0.5}F_{0.5}BiS_2$, T_c was found to gradually decrease from 2.8 K at x = 0 to 1.8 K at x = 0.1 and then remain roughly constant at $\sim$3.0 K for $x \geqslant 0.125$ as shown in Fig. VII.12. The lattice parameter a and the unit cell volume of $La_{1-x}Y_xO_{0.5}F_{0.5}BiS_2$ monotonically decrease with increasing Y concentration until the solubility limit x = 0.20. Interestingly, the evolution of the La-O-La bond angle with increasing x closely follows the evolution of $T_c(x)$ as shown in Fig. VII.12. It should be mentioned that the lattice constant c changes in the opposite manner (decreasing

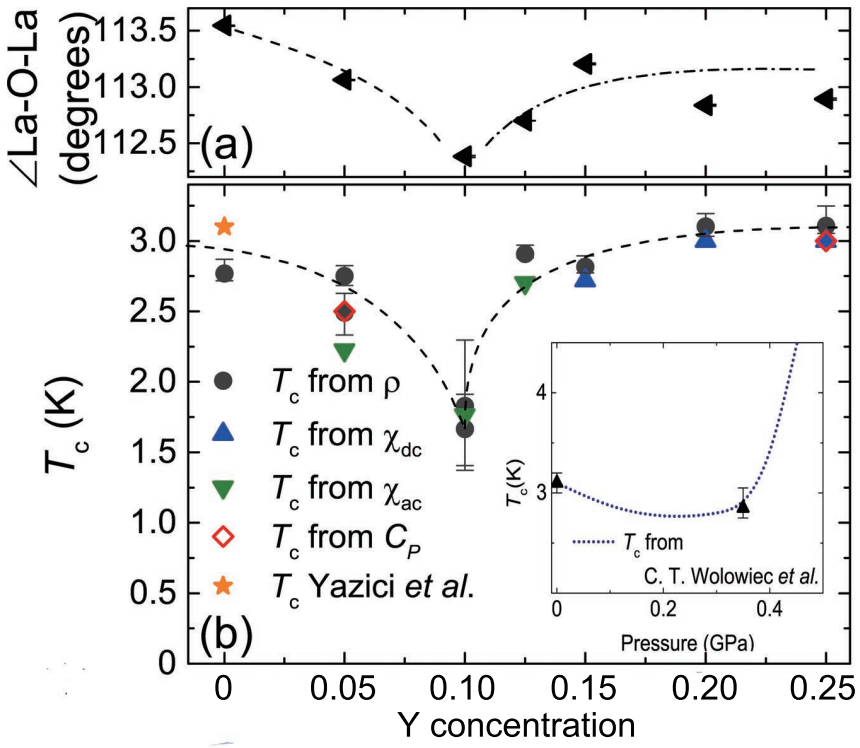

Figure VII.12: (a) La(Y)-O(F)-La(Y) bond angle vs nominal yttrium concentration. (b) Dependence of T_c on Y concentration for the $La_{1-x}Y_xO_{0.5}F_{0.5}BiS_2$ system. The orange star is the T_c of $LaO_{0.5}F_{0.5}BiS_2$ reported in Ref. [21]. The inset shows the behavior of T_c under hydrostatic pressure [30]. Reprinted with permission from Ref. [42]. Copyright (2014) by the American Physical Society.

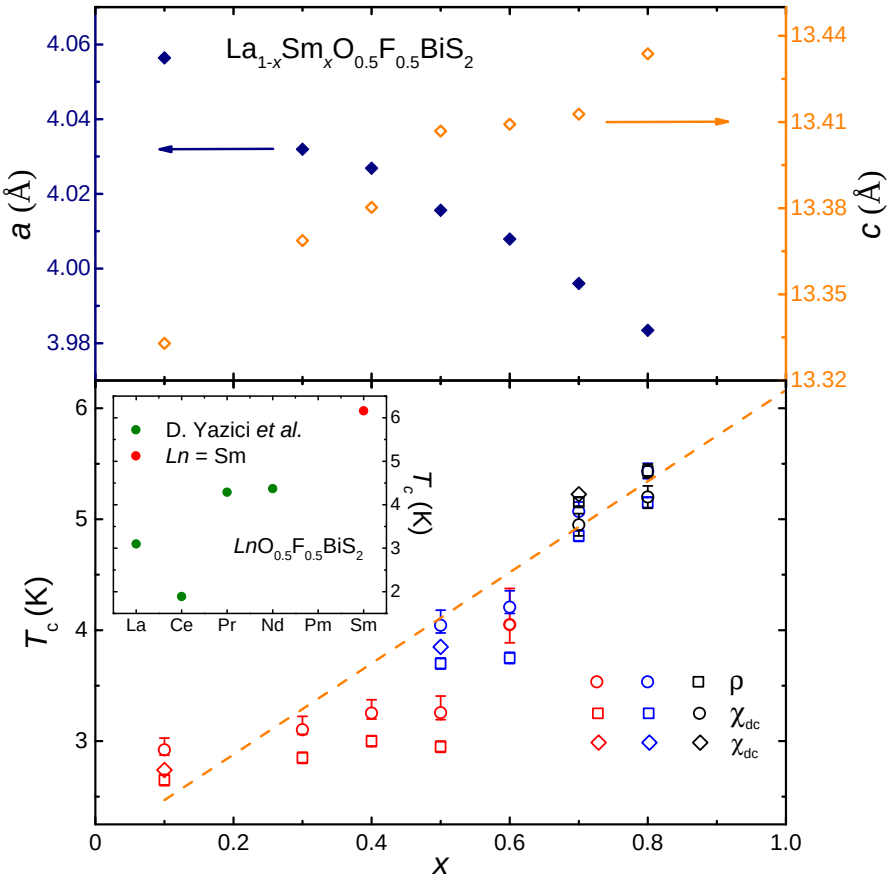

Figure VII.13: Dependence of the lattice constants a and c (upper panel) and T_c (lower panel) on Sm concentration x of $La_{1-x}Sm_xO_{0.5}F_{0.5}BiS_2$. Red, blue, and purple symbols in the lower panel represent results for samples annealed at 800°C, 750°C, and 710°C, respectively. The inset shows representative values of T_c of *Ln*(O,F)BiS_2 reported in Ref. [21]. The other data are obtained from Ref. [41].

with increasing Y concentration), which suggests that T_c may also be affected by the value of c. Unfortunately, due to the solubility limit of Y in $La_{1-x}Y_xO_{0.5}F_{0.5}BiS_2$, further investigation of the relation between lattice parameters, bond angle, and T_c by the method of substitution is not possible and the highest chemical pressure obtained in $La_{0.8}Y_{0.2}O_{0.5}F_{0.5}BiS_2$ is still lower than 0.7 GPa, above which a structural phase transition from tetragonal ($P4/nmm$) to monoclinic ($P21/m$) has been observed in $LaO_{0.5}F_{0.5}BiS_2$ under applied external hydrostatic pressure [30, 80].

Figure VII.13 shows the Sm concentration of T_c for $La_{1-x}Sm_xO_{0.5}F_{0.5}BiS_2$. An enhancement of superconductivity is observed in the $La_{1-x}Sm_xO_{0.5}F_{0.5}BiS_2$ compound in which T_c increases from ∼2.8 K at x = 0.1 to 5.4 K at the solubility limit of x = 0.8 [41]. A linear extrapolation of the $T_c(x)$ data beyond the x = 0.8 solubility limit to x = 1.0 allows for an estimate of the value of T_c for the parent compound $SmO_{0.5}F_{0.5}BiS_2$ to be as high as ∼6.2 K; this value of T_c is significantly higher than values of T_c reported for other AG samples of the *Ln*$O_{0.5}F_{0.5}BiS_2$ compound and is therefore consistent with the trend that higher values of T_c are observed in *Ln*$O_{0.5}F_{0.5}BiS_2$ compounds containing a *Ln* element having a larger atomic number (see the inset of Fig. VII.13). As the Sm concentration increases from x = 0.1 to 0.8, the lattice constant c increases while the lattice constant a gradually decreases, resulting in an overall suppression of the unit cell volume of ∼3%, however, no structural phase transition is observed. In comparison, there is only a ∼2% decrease in the unit cell volume of $LaO_{0.5}F_{0.5}BiS_2$ before the pressure-induced structure phase transition [80]. Hence, the effects of Sm substitution for La and applied hydrostatic pressure on the compound $LaO_{0.5}F_{0.5}BiS_2$ seem somewhat different.

Effects of substitutions at the *Ln* site in the *Ln*$O_{0}.5F_{0}.5BiS_2$ compounds were also investigated at various F concentrations which allows for the study of the tuning of the lattice constant c and its effects on superconductivity. Phase diagrams of T_c vs *Ln* substitution for the $Ce_{1-x}Nd_xO_{1-y}F_yBiS_2$ and $Nd_{1-z}Sm_zO_{1-y}F_yBiS_2$ systems were determined from measurements of magnetization at nominal F concentrations of y = 0.7, 0.5, and 0.3 as shown in Fig. VII.14 [78]. Superconductivity is induced and noticeably enhanced for those compounds containing higher concentrations of *Ln* elements with

relatively smaller atomic size (or larger atomic number), i.e., higher concentrations of Nd and Sm atoms. The shift in the phase boundary to the right for decreasing F concentration suggests the importance of F concentration in the induction of superconductivity in these BiS_2-based compounds. For a given F concentration, it appears that superconductivity is enhanced in compounds with Ln ions of smaller ionic size; however, there is no appreciable increase in T_c for greater concentrations of F. It is interesting to note that samples with different nominal values of F concentration that share similar values of T_c also exhibit similar values of the ratio of the length of the c axis to that of the a axis (see Fig. VII.14(b)); this implies that the superconductivity observed in the BiS_2-based compounds is closely related with the lattice constant ratio c/a. The effect of charge carrier density on the enhancement of superconductivity in these BiS_2 compounds seems to be of less importance in comparison to the lattice parameter a and the c/a ratio.

The role of the charge carrier density in the enhancement of superconductivity is emphasized in the study of the $La_{1-x}Mg_xO_{1-2x}F_{2x}BiS_2$ system in which Mg^{2+} and F^- are substituted for La^{3+} and O^{2-}, respectively [75]. Superconductivity is observed for nominal $x \geqslant 0.2$ where T_c continues to increase up to $\sim$3 K at x = 0.3 which is slightly beyond the solubility limit of x = 0.25. For a fixed F concentration at $2x$ = 0.4, the introduction of Mg^{2+} ions into the $LaO_{0.6}F_{0.4}BiS_2$ compound generates holes in the BiS_2 superconducting layers which have the effect of suppressing superconductivity and thereby reducing T_c despite the reduction in lattice parameters. The research also indicates that a reduction in lattice parameters leads to an enhancement of T_c. For instance, a reduction in the values of the lattice parameters appears to enhance superconductivity

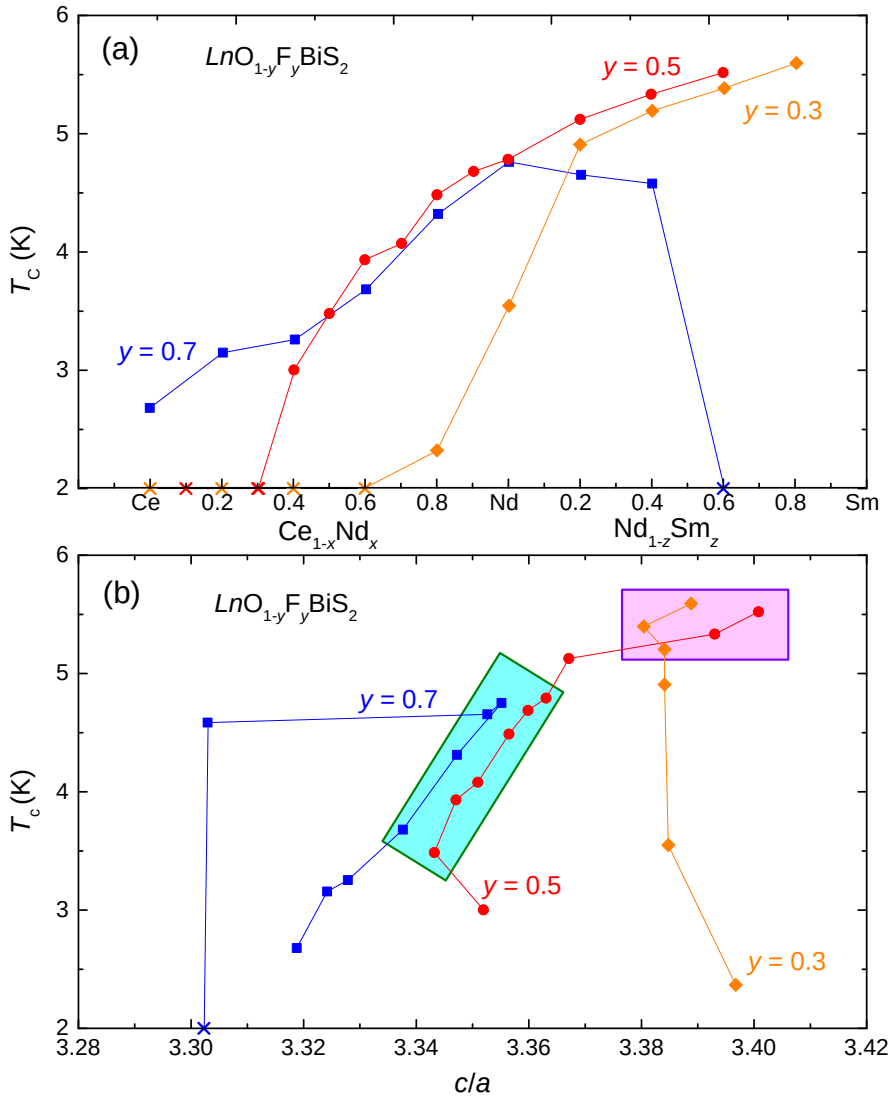

Figure VII.14: Superconducting critical temperature T_c of $LnO_{1-y}F_yBiS_2$ (y = 0.7, 0.5, and 0.3) as a function of *Ln* concentration. The cross symbols indicate that a superconducting transition is not observed above 2 K. Reprinted with permission from Ref. [78] J. Kajitani, T. Hiroi, A. Omachi, O. Miura, Y. Mizuguchi, J. Phys. Soc. Jpn. 84 (2015) 044712. Copyrighted by the Physical Society of Japan.

when comparing the $La_{0.8}Ca_{0.2}O_{0.6}F_{0.4}BiS_2$ and $La_{0.8}Mg_{0.2}O_{0.6}F_{0.4}BiS_2$ compounds which have T_c values of 2.07 K and 2.54 K, respectively.

VII.F Superconductivity of *Ln*$O_{0.5}F_{0.5}BiS_2$ under applied pressure

In addition to chemical substitution, the application of external pressure is another means to induce fundamental change to both the crystalline and electronic structure which can have a significant impact on the superconducting properties of the layered BiS_2-based compounds. The first report of a dramatic and abrupt increase in T_c from $\sim$3 to 10.7 K for the $LaO_{0.5}F_{0.5}BiS_2$ compound under pressure is shown in the upper panel of Fig. VII.15(a). In the $T_c(P)$ phase diagram, there is an obvious transition from a low-T_c superconducting phase to a high-T_c superconducting phase [30]. The phenomenon was soon reported to be associated with a pressure-induced first order phase transition from a tetragonal to a monoclinic crystal structure in which there is a relative shift or sliding of the two neighboring BiS_2 layers along the a axis [80]. Similar behavior in the evolution of T_c with pressure has also been observed in other *Ln*$O_{0.5}F_{0.5}BiS_2$ (*Ln* = Ce, Pr, Nd) compounds as shown in the $T_c(P)$ phase diagrams of Fig. VII.16 [29].

Interestingly, the critical transition pressure, P_t, that marks the low-T_c to high-T_c phase transition in the superconducting state is coincident with changes in the normal state electrical transport properties in the *Ln*$O_{0.5}F_{0.5}BiS_2$ system; the pressure-induced phase transition corresponds with a saturation in the rate of suppression of semiconducting-like behavior in the normal state [30]. In the case of the $NdO_{0.5}F_{0.5}BiS_2$ compound, a semiconductor-metal transition occurs at P_t as shown in Fig. VII.15(b) [29]. Such

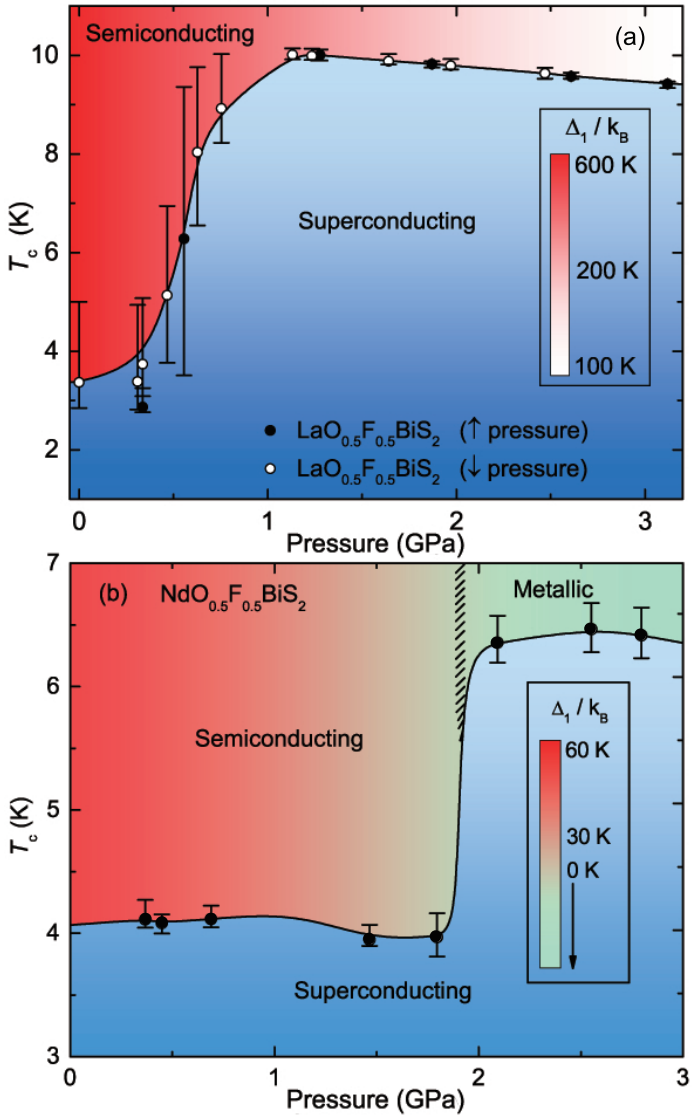

Figure VII.15: $T_c(P)$ phase diagrams for (a) $LaO_{0.5}F_{0.5}BiS_2$ and (b) $NdO_{0.5}F_{0.5}BiS_2$. The red color gradient represents the suppression of the semiconducting behavior with pressure as manifested in the decrease of the semiconducting energy gap Δ_1/k_B whose values are indicated in the legend. The green region to the right of the crosshatching in (b) corresponds to the metallization of $NdO_{0.5}F_{0.5}BiS_2$. (a), (b) Reprinted with permission from Ref. [30] (copyright (2013) American Physical Society) and Ref. [29] (Enhancement of superconductivity near the pressure-induced semiconductor-metal transition in the BiS_2-based superconductors $LnO_{0.5}F_{0.5}BiS_2$ (*Ln* = La, Ce, Pr, Nd), J. Phys.: Condens. Matter 25 (2013) 422201. Copyright (2013) by the IOP Publishing.), respectively.

changes in the behavior of the normal state $\rho(T)$ indicate that there may be increases in the density of charge carriers that correspond to the rapid increase in T_c.

AG samples from the series of *Ln*$O_{0.5}F_{0.5}BiS_2$ compounds with *Ln* elements of smaller atomic radius (i.e., larger atomic number) exhibit higher T_c values when compared with compounds containing *Ln* elements of larger atomic radius suggesting that T_c correlates with the lattice parameters. Given the correlation between T_c and the lattice parameters, one might expect that the pressure-induced phase transitions observed for the various *Ln*$O_{0.5}F_{0.5}BiS_2$ compounds would occur at a characteristic and consistent value of the lattice parameter a across the *Ln*$O_{0.5}F_{0.5}BiS_2$ series. Furthermore, considering the results from substitution studies discussed earlier in this article, one would expect a smaller applied pressure to induce the phase transition for those *Ln*$O_{0.5}F_{0.5}BiS_2$ compounds with *Ln* elements exhibiting smaller values of the lattice parameter a. To the contrary, the a-axis lattice parameters at P_t are not constant across the series *Ln*$O_{0.5}F_{0.5}BiS_2$. The lattice parameter a for the $LaO_{0.5}F_{0.5}BiS_2$ compound just before the transition pressure, $P_t \sim 0.7$ GPa, is estimated to be 4.08 $\AA$ which is larger than the values of a for other members of the *Ln*$O_{0.5}F_{0.5}BiS_2$ series at ambient pressure [21, 80]. The $T_c(P)$ phase diagrams depicted in Fig. VII.16 indicate that the critical transition pressure P_t increases as the atomic size of the *Ln* ions decreases and that the jump in T_c during the phase transition (ΔT_c) is smaller for smaller *Ln* ions in *Ln*$O_{0.5}F_{0.5}BiS_2$ [29, 30]. Heavier *Ln* ions seem to help stabilize the structure of the *Ln*$O_{0.5}F_{0.5}BiS_2$ against external pressure.

Figure VII.17 shows the evolution of T_c for the $La_{1-x}Sm_xO_{0.5}F_{0.5}BiS_2$ compound as a function of both pressure and Sm concentration x [81]. Similar to the *Ln*$O_{0.5}F_{0.5}BiS_2$

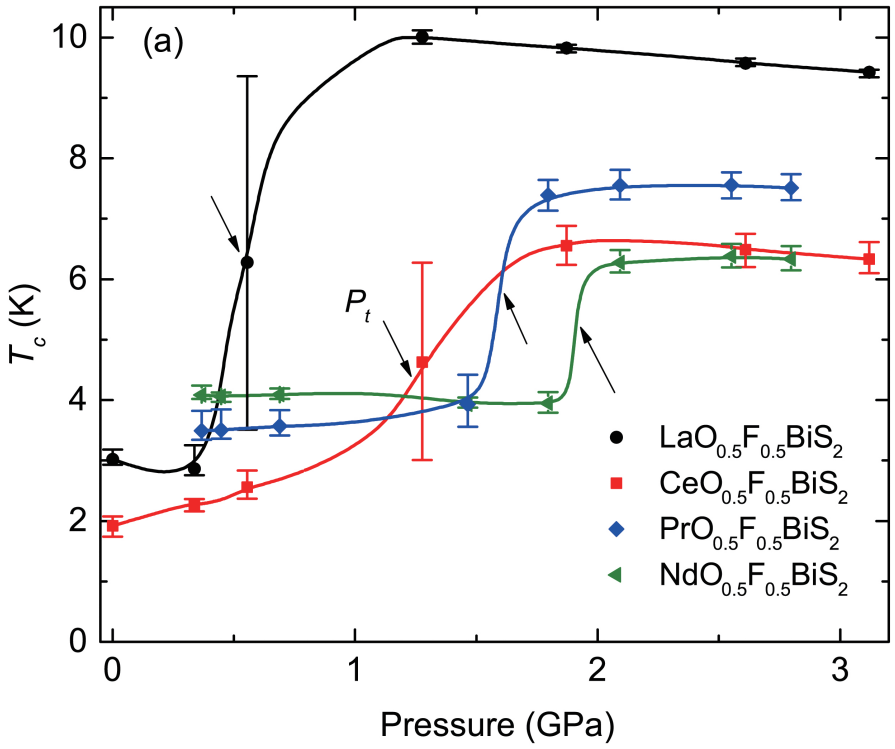

Figure VII.16: Pressure dependence of T_c for LnO$_{0.5}$F$_{0.5}$BiS$_2$ (Ln = La, Ce, Pr, Nd). The black arrows indicate the critical transition pressures from the low-T_c to high-T_c superconducting phases. Reprinted with permission from Ref. [29]: Enhancement of superconductivity near the pressure-induced semiconductor-metal transition in the BiS$_2$-based superconductors LnO$_{0.5}$F$_{0.5}$BiS$_2$ (Ln = La, Ce, Pr, Nd), J. Phys.: Condens. Matter 25 (2013) 422201. Copyright (2013) by the IOP Publishing.

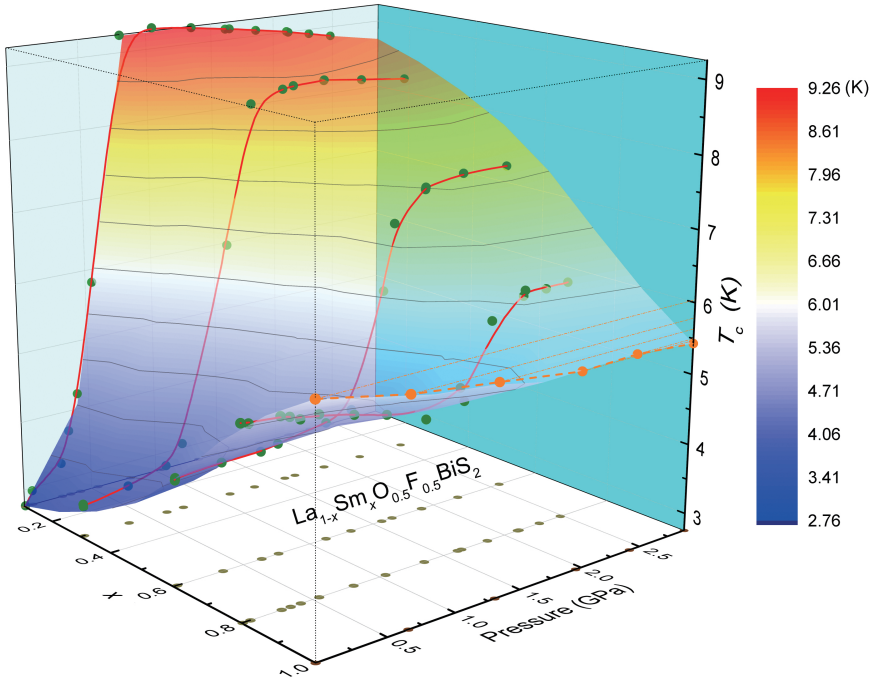

Figure VII.17: Superconducting critical temperature T_c of $La_{1-x}Sm_xO_{0.5}F_{0.5}BiS_2$ (x = 0.1-0.8) plotted as a function of pressure and nominal Sm concentration x. Filled circles in the x-y plane are projections of T_c. The data are taken from Ref. [81]. (For interpretation of the estimated T_c values of $SmO_{0.5}F_{0.5}BiS_2$, the reader is referred to Ref. [81].)

compounds, the $La_{1-x}Sm_xO_{0.5}F_{0.5}BiS_2$ system exhibits a reversible pressure-induced transition from a low-T_c (SC1) to a high-T_c (SC2) superconducting phase. It has been shown that the lattice parameter a in the $La_{1-x}Sm_xO_{0.5}F_{0.5}BiS_2$ compound is significantly reduced by increasing the Sm concentration x [41]. The results for the SC1 to SC2 phase transition in the $La_{1-x}Sm_xO_{0.5}F_{0.5}BiS_2$ system indicate that optimization of T_c could be achieved in $La_{1-x}Sm_xO_{0.5}F_{0.5}BiS_2$ by decreasing the a lattice parameter (high Sm concentration) in the SC1 phase at ambient pressure or by increasing a (low Sm concentration) in the SC2 phase under pressure.

Although the chemical composition of the blocking layers in the $LnO_{0.5}F_{0.5}BiS_2$

and $La_{1-x}Sm_xO_{0.5}F_{0.5}BiS_2$ compounds are different, their evolution of T_c with pressure is similar. As displayed in Fig. VII.18(a), P_t increases with decreasing atomic size of the *Ln* ion for $LnO_{0.5}F_{0.5}BiS_2$ (*Ln* = La, Ce, Pr, Nd) compounds in the same way that P_t increases with increasing Sm concentration for $La_{1-x}Sm_xO_{0.5}F_{0.5}BiS_2$ under pressure [29, 81]. If we plot ΔT_c for $LnO_{0.5}F_{0.5}BiS_2$ and $La_{1-x}Sm_xO_{0.5}F_{0.5}BiS_2$ as a function of lattice parameter a, they follow the same linear trend, despite the differences in the chemical composition of their blocking layer. This suggests the importance of the in-plane separation between ions in the superconducting BiS_2 layers and its effect on superconductivity in the BiS_2-based compounds under pressure. However, there is no clear relationship observed between the c lattice parameter and superconductivity in these BiS_2-based compounds under pressure.

Partial substitution of *Ln* ions with smaller ions typically results in a reduction of the a lattice parameter and along with (but not always) a slight increase in the c lattice parameter; however, it has been reported that both the a and c lattice parameters can be simultaneously suppressed with the application of hydrostatic pressure [80]. This has implications for the behavior of superconductivity under external pressure as being fundamentally different when compared to the behavior of superconductivity in response to chemical substitution in the BiS_2-based compounds. As an example, it was reported that a structural phase transition from the tetragonal phase to the monoclinic phase occurs at $\sim$0.7 GPa in $LaO_{0.5}F_{0.5}BiS_2$ under pressure, whereas it is known that all BiS_2-based superconductors at ambient pressure exhibit the tetragonal phase, including those compounds subject to heavy chemical substitution. As another example, the T_c of AG

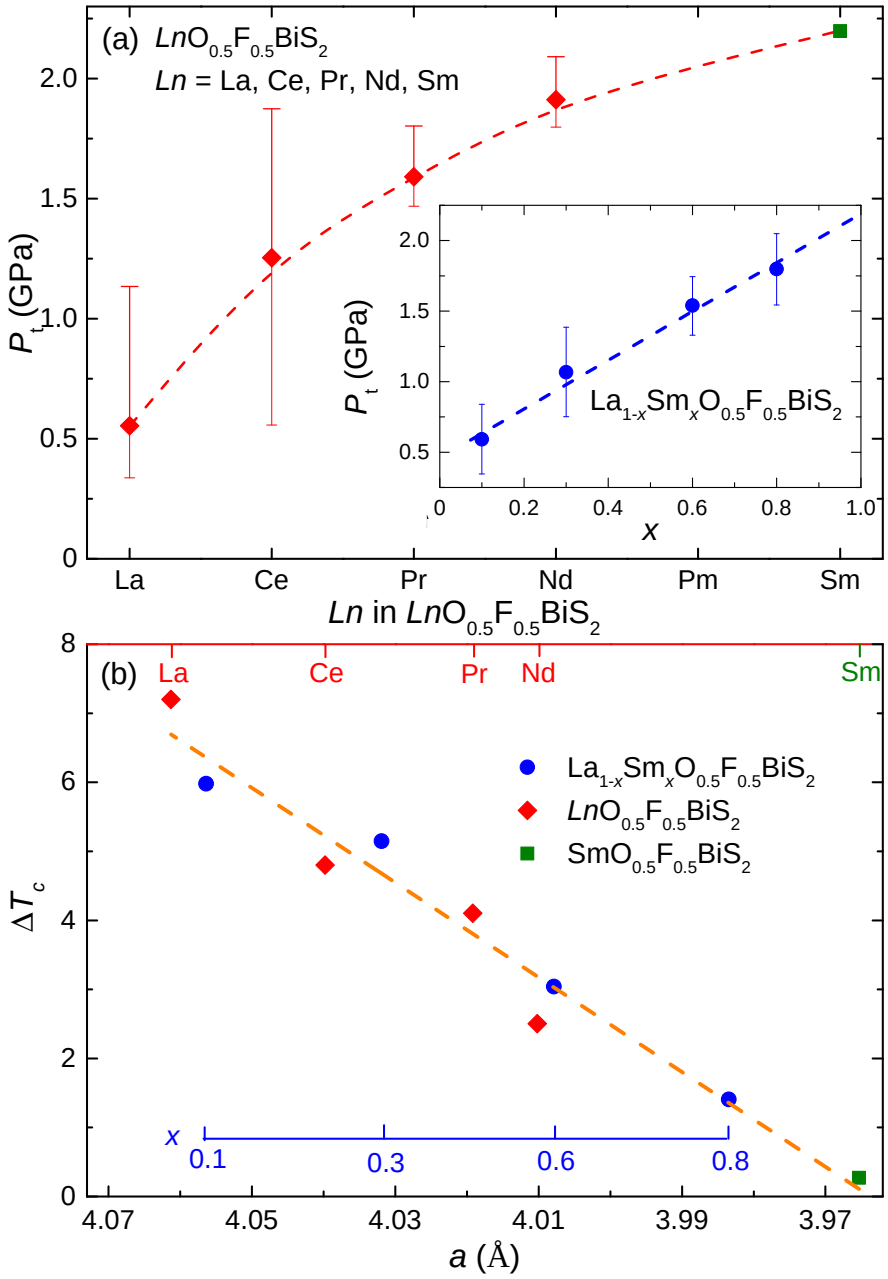

Figure VII.18: (a) Evolution of $P_{\rm t}$ as a function of *Ln* in $LnO_{0.5}F_{0.5}BiS_2$. The inset in panel (a) shows Sm concentration dependence of $P_{\rm t}$ for $La_{1-x}Sm_xO_{0.5}F_{0.5}BiS_2$. (b) ΔT_c vs lattice parameter a of $La_{1-x}Sm_xO_{0.5}F_{0.5}BiS_2$ and $LnO_{0.5}F_{0.5}BiS_2$. Dashed lines are guides to the eye. ΔT_c and $P_{\rm t}$ values of $LnO_{0.5}F_{0.5}BiS_2$ and $La_{1-x}Sm_xO_{0.5}F_{0.5}BiS_2$ are taken from Refs. [29] and [81], respectively. The values of the lattice parameter a for $LnO_{0.5}F_{0.5}BiS_2$ and $La_{1-x}Sm_xO_{0.5}F_{0.5}BiS_2$ are obtained from Refs. [74] and [41], respectively. (For interpretation of the estimated data of $SmO_{0.5}F_{0.5}BiS_2$, the reader is referred to Refs. [41, 81].)

samples of $LaO_{0.5}F_{0.5}BiS_2$ increases with a reduction in the lattice parameter a through a partial or full replacement of La with heavier (smaller) *Ln*, whereas further reduction of the lattice parameter a by increasing external hydrostatic pressure up to 1.5 GPa results in a gradual decrease in the T_c of $La_{0.2}Sm_{0.8}O_{0.5}F_{0.5}BiS_2$ [81]. Rather than adopting a single lattice parameter determination in explaining the effects of applied pressure on superconductivity in these BiS_2-based compounds, these observations suggest that there is a complex interplay of various parameters and their effects on superconductivity under pressure. In addition to the importance of the size of the lattice constant a in affecting superconductivity, reduction of the lattice constant c also appears to affect the superconducting state of BiS_2-based compounds. By applying uniaxial pressure along the c-axis in single crystalline $PrO_{0.5}F_{0.5}BiS_2$, a low-T_c to high-T_c phase transition is also observed at 0.7 GPa, which is significantly lower than the P_t of $PrO_{0.5}F_{0.5}BiS_2$ under hydrostatic pressure [82]. Until now, although a large number of compounds in the BiS_2 family have been investigated in terms of their transport behavior under pressure, reports on the evolution of crystal structure with pressure are very limited. To clarify correlations between the crystal structure of BiS_2-based compounds and their superconductivity under pressure, further experiments involving the use of in-situ x-ray diffraction/absorption measurements under pressure need to be performed on different BiS_2-based samples in both polycrystal and single crystal form.

VII.G Se-substituted *Ln*$O_{0.5}F_{0.5}BiS_2$

Most of the research regarding chemical substitution and superconductivity in the *Ln*(O,F)BiS_2 compounds has been devoted to studying the effects of elemental substitution in the blocking *Ln*O layers. There has been much less effort and only a few reports regarding the effects on superconductivity that result from modification of the superconducting BiS_2 layers. Substitution of Sb for Bi appears to be an ineffective means for enhancing superconductivity. While $LaO_{0.5}F_{0.5}BiS_2$ has a $T_c \sim 3$ K, $LaO_{0.5}F_{0.5}SbS_2$ does not exhibit superconductivity above 1.7 K [83]. Furthermore, it appears that a small amount of Sb substitution (10%) in the $NdO_{0.5}F_{0.5}BiS_2$ compound strongly suppresses superconductivity [84]. Alternatively, it is possible to completely replace S with either Se or Te in $LaO_{0.5}F_{0.5}BiS_2$; however, only the $LaO_{0.5}F_{0.5}BiSe_2$ compound was found to exhibit superconductivity with a $T_c \sim 2.6$ K [83]. The Se^{2-} and S^{2-} ions are chemically similar; however, the Se^{2-} ionic radius of 1.98 $\mathring{A}$ is larger than the S^{2-} ionic radius of 1.84 $\mathring{A}$ (assuming a coordination number of 6) [79]. This distinction may prove useful in studies on the effects of Se substitution in the *Ln*$O_{0.5}F_{0.5}BiS_2$ system from which new insights and perspectives might be gained regarding the relationship between crystal structure and superconductivity in the *Ln*(O,F)BiS_2 compounds.

The dependence of T_c on the Se concentration, substituted for S in *Ln*$O_{0.5}F_{0.5}BiS_2$, exhibits complicated behavior when the *Ln* element changes. For polycrystalline sample of $NdO_{0.5}F_{0.5}Bi(S_{1-x}Se_x)_2$ ($x \leqslant 0.2$), it has been reported that, as the Se concentration is increased, there is a noticeable change in the lattice constant a, but no significant

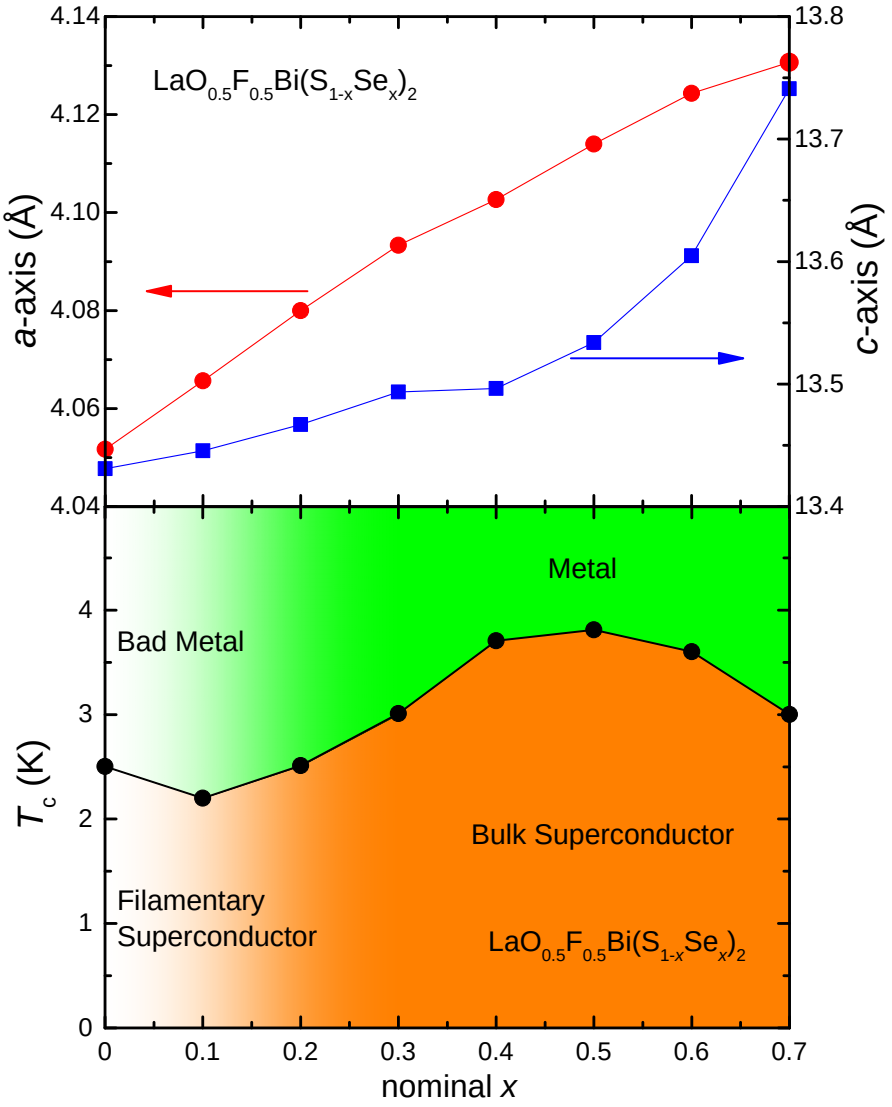

Figure VII.19: Nominal Se concentration dependence of lattice constants a and c (upper) and T_c (lower). Reprinted with permission from Ref. [85] T. Hiroi, J. Kajitani, A. Omachi, O. Miura, Y. Mizuguchi, J. Phys. Soc. Jpn. 84 (2015) 024723. Copyrighted by the Physical Society of Japan.

change in the lattice constant c; in addition, both T_c and the shielding volume fraction of $NdO_{0.5}F_{0.5}Bi(S_{1-x}Se_x)_2$ decrease with increasing Se concentration [84]. These results are consistent with the previous discussion regarding modification of the *Ln*O blocking layers in which superconductivity is enhanced as the lattice parameters are reduced. In the case of $LaO_{0.5}F_{0.5}Bi(S_{1-x}Se_x)_2$, T_c increases from 2.4 K at x = 0.2 to 3.8 K at x = 0.5 with a large shielding volume fraction followed by a slight decrease in T_c for $x > 0.5$ [79, 85]. Synchrotron x-ray diffraction experiments performed on the $LaO_{0.5}F_{0.5}Bi(S_{1-x}Se_x)_2$ compound show that Se atoms are more likely to occupy in-plane S1 sites rather than the out-of-plane S2 sites, resulting in an expansion in both the a and c axes with increasing Se concentration [79]. This behavior complicates the picture we have regarding the correlation between the crystal structure and superconductivity in the BiS_2-based compounds.

VII.H Concluding remarks

There is already a significant amount of interesting behavior reported on the effects of chemical substitution in the recently discovered family of BiS_2-based compounds; and many of these interesting properties are often not exhibited in the parent form of these compounds. The *Ln*$BiOS_2$ compounds were synthesized and reported as early as 1995 [86]; however, no superconductivity was found in the *Ln*$BiOS_2$ system until electron doping studies were performed in 2012 [10, 19–21]. Hence, the introduction of charge carriers (electrons) into the parent compound is regarded to be essential for the emergence of superconductivity in BiS_2-based superconductors [20, 74]. Measurements

of $\rho(T)$ under pressure provide supporting evidence that the dramatic enhancement of superconductivity in various *Ln*$O_{0.5}F_{0.5}BiS_2$ compounds is coincident with an increase in the charge carrier density [29, 30].

Substitution for ions in either the BiS_2 superconducting layers or the blocking *Ln*O layers with ions of different atomic size allows one to tune the lattice parameters as well as the local lattice structure of the BiS_2-based compounds and thereby generate chemical pressure. An increase in chemical pressure in the superconducting BiS_2 layers would result in a shorter Bi-S1 bond distance thereby enhancing the overlap of the Bi-6p and S-p orbitals; this would allow superconductivity to be tuned without a dramatic change of charge carrier density. Experimental evidence suggests that both the contraction along the a axis and the c/a ratio play an essential role in the emergence of superconductivity in some *Ln*Bi(O,F)S_2 compounds [21, 41, 75, 77, 78]. However, the clear correlation between lattice contraction and superconductivity does not apply to all BiS_2-based compounds and fails to hold when samples are subjected to hydrostatic pressure. At present, finding a universal relationship between the crystal structure and superconductivity in the BiS_2-based compounds is still one of the main challenges in this research area. Recently, Mizuguchi *et.al.* defined a value of in-plane chemical pressure as (R_{Bi} + R_{S1})/Bi-S1(in-plane), where R_{Bi} is the estimated ionic radius of $Bi^{2.5+}$, R_{S1} is the estimated average ionic radius of the chalcogen at the S1 site, and the Bi-S1 bond distance is obtained from the Rietveld refinement of experimental XRD data [79]. A clear correlation between T_c and the in-plane chemical pressure is observed in the *Ln*$O_{0.5}F_{0.5}BiS_2$ (*Ln* = $Ce_{1-x}Nd_x$, $Nd_{1-x}Sm_x$) and $LaO_{0.5}F_{0.5}Bi(S_{1-x}Se_x)_2$ systems;

however, such a relationship needs to be further confirmed with studies of the effects of in-plane chemical pressure on other BiS_2-based systems. Additional experimental and theoretical effects are also needed to elucidate the relationship between in-plane chemical pressure and the resultant enhancement of T_c [79].

At present, the highest reported T_c among the BiS_2-based compounds is $\sim$10.7 K for $LaO_{0.5}F_{0.5}BiS_2$ under pressure [30, 80]; however, the BSCCO cuprate superconductors, in which Bi ions are located in the blocking layers of the structures, can have T_c values higher than 100 K [87–89]. The $Ba_{1-x}K_xBiO_3$ family, another system containing Bi ions, was reported to have T_c values as high as $\sim$30 K and the BiO_2 planes are regarded to be essential for the superconductivity in the compounds [90, 91]. The speed at which new members of BiS_2-based superconductors are being synthesized and studied holds promise for the discovery of new superconducting compounds with values of T_c significantly higher than 11 K. Nevertheless, some challenging but essential problems regarding the intrinsic behavior of the BiS_2-based superconductors remain to be solved. As the debate over the nature of the pairing mechanism for superconductivity in the BiS_2-based superconductors continues, it is difficult to develop an effective strategy for enhancing T_c. The intrinsic transport and thermal properties, which may shed light on the nature of the pairing mechanism, need to be established through further studies on high quality single-crystalline samples. Theoretical calculations, which investigate electronic structure and related properties of BiS_2-based superconductors, should be more focused on the actual chemical compositions of the compounds. Another interesting but unclarified issue is the remarkable difference in T_c between the AG and HP annealed

samples of *Ln*(O,F)BiS_2 (*Ln* = La, Ce, Pr). The similarity in both chemical composition and crystal structure of the HP annealed samples and their AG counterparts suggests that the local environment of the crystals may play an essential role in the superconductivity of these BiS_2-based compounds. It is hopeful that T_c values for the family of BiS_2-based superconductors can be further enhanced if the factors responsible for an increase in T_c such as those affected by HP annealing and the application of external pressure are clarified. Amidst the abundance of physical phenomena thus far observed, at this early stage of discovery and research there remain unanswered questions and opportunities to develop a fundamental understanding of superconductivity in the BiS_2-based compounds.

The text and data presented in this chapter are reprints of material that appears in "Chemical Substitution and High Pressure Effects on Superconductors in the *Ln*OBiS_2 (*Ln* = La-Nd) System," Y. Fang, C. T. Wolowiec, D. Yazici, and M. B. Maple, *Nov. Supercond. Mater.* **1**, 79 (2015). The dissertation author is the primary investigator and author of this article.

Bibliography

[1] J. G. Bednorz and K. A. Müller, Z. Phys. B: Condens. Matter **64**, 189 (1986).

[2] A. P. Drozdov, M. I. Eremets, I. A. Troyan, V. Ksenofontov, and S. I. Shylin, arXiv preprint arXiv:1506.08190 (2015).

[3] Y. Mizuguchi, H. Fujihisa, Y. Gotoh, K. Suzuki, H. Usui, K. Kuroki, S. Demura, Y. Takano, H. Izawa, and O. Miura, Phys. Rev. B **86**, 220510 (2012).

[4] Y. Kamihara, T. Watanabe, M. Hirano, and H. Hosono, J. Am. Chem. Soc. **130**, 3296 (2008).

[5] G. F. Chen, Z. Li, D. Wu, G. Li, Z. Hu, J. Dong, P. Zheng, J. L. Luo, and N. L. Wang, Phys. Rev. Lett. **100**, 247002 (2008).

[6] Z. A. Ren, W. Lu, J. Yang, W. Yi, X. L. Shen, Z. C. Li, G. C. Che, X. L. Dong, L. L. Sun, F. Zhou, and Z. X. Zhao, Chin. Phys. Lett. **25**, 2215 (2008).

[7] Z. A. Ren, J. Yang, W. Lu, W. Yi, G. C. Che, X. L. Dong, L. L. Sun, and Z.-X. Zhao, Mater. Res. Innovations **12**, 105 (2008).

[8] Z. Ren, J. Yang, W. Lu, W. Yi, X. L. Shen, Z. C. Li, G. C. Che, X. L. Dong, L. L. Sun, F. Zhou, and Z. X. Zhao, Europhys. Lett. **82**, 57002 (2008).

[9] X. H. Chen, T. Wu, R. H. Liu, H. Chen, and D. F. Fang, Nature **453**, 761 (2008).

[10] J. Xing, S. Li, X. X. Ding, H. Yang, and H.-H. Wen, Phys. Rev. B **86**, 214518 (2012).

[11] A. S. Sefat, A. Huq, M. A. McGuire, R. Jin, B. C. Sales, D. Mandrus, L. M. D. Cranswick, P. W. Stephens, and K. H. Stone, Phys. Rev. B **78**, 104505 (2008).

[12] H.-H. Wen, G. Mu, L. Fang, H. Yang, and Y. Zhu, Europhys. Lett. **82**, 17009 (2008).

[13] C. Wang, L. Li, S. Chi, Z. Zhu, Z. Ren, Y. Li, Y. Wang, X. Lin, Y. Luo, S. Jiang, X. Xu, G. Cao, and Z. Xu, Europhys. Lett. **83**, 67006 (2008).

[14] Z.-A. Ren, G.-C. Che, X.-L. Dong, J. Yang, W. Lu, W. Yi, X.-L. Shen, Z.-C. Li, L.-L. Sun, F. Zhou, and Z.-X. Zhao, Europhys. Lett. **83**, 17002 (2008).

[15] J. Yang, Z.-C. Li, W. Lu, W. Yi, X.-L. Shen, Z.-A. Ren, G.-C. Che, X.-L. Dong, L.-L. Sun, F. Zhou, and Z.-X. Zhao, Supercond. Sci. Technol. **21**, 082001 (2008).

[16] T. Yildirim, Phys. Rev. B **87**, 020506 (2013).

[17] J. Shao, Z. Liu, X. Yao, L. Pi, S. Tan, C. Zhang, and Y. Zhang, physica status solidi (RRL)-Rapid Research Letters **8**, 845 (2014).

[18] V. P. S. Awana, A. Kumar, R. Jha, S. Kumar Singh, A. Pal, J. Saha, and S. Patnaik, Solid State Commun. **157**, 21 (2013).

[19] S. Demura, Y. Mizuguchi, K. Deguchi, H. Okazaki, H. Hara, T. Watanabe, S. James Denholme, M. Fujioka, T. Ozaki, H. Fujihisa, G. Yoshito, M. Osuke, Y. Takahide, T. Hiroyuki, and T. Yoshihiko, J. Phys. Soc. Jpn. **82**, 033708 (2013).

[20] Y. Mizuguchi, S. Demura, K. Deguchi, Y. Takano, H. Fujihisa, Y. Gotoh, H. Izawa, and O. Miura, J. Phys. Soc. Jpn. **81**, 114725 (2012).

[21] D. Yazici, K. Huang, B. D. White, A. H. Chang, A. J. Friedman, and M. B. Maple, Phil. Mag. **93**, 673 (2013).

[22] Y. Mizuguchi, Physics Procedia **58**, 94 (2014).

[23] H. F. Zhai, Z. T. Tang, H. Jiang, K. Xu, K. Zhang, P. Zhang, J. K. Bao, Y. L. Sun, W. H. Jiao, I. Nowik, I. Felner, Y. K. Li, X. F. Xu, Q. Tao, C. M. Feng, Z. A. Xu, and G. H. Cao, Phys. Rev. B **90**, 064518 (2014).

[24] K. Deguchi, Y. Mizuguchi, S. Demura, H. Hara, T. Watanabe, S. J. Denholme, M. Fujioka, H. Okazaki, T. Ozaki, H. Takeya, T. Yamaguchi, O. Miura, and Y. Takano, Europhys. Lett. **101**, 17004 (2013).

[25] D. Yazici, K. Huang, B. D. White, I. Jeon, V. W. Burnett, A. J. Friedman, I. K. Lum, M. Nallaiyan, S. Spagna, and M. B. Maple, Phys. Rev. B **87**, 174512 (2013).

[26] X. Lin, X. X. Ni, B. Chen, X. F. Xu, X. X. Yang, J. H. Dai, Y. K. Li, X. J. Yang, Y. K. Luo, Q. Tao, G. H. Cao, and Z. Xu, Phy. Rev. B **87**, 020504 (2013).

[27] H. Kotegawa, Y. Tomita, H. Tou, H. Izawa, Y. Mizuguchi, O. Miura, S. Demura, K. Deguchi, and Y. Takano, J. Phys. Soc. Jpn. **81**, 103702 (2012).

[28] R. Jha, B. Tiwari, and V. P. S. Awana, J. Phys. Soc. Jpn. **83**, 105001 (2014).

[29] C. T. Wolowiec, B. D. White, I. Jeon, D. Yazici, K. Huang, and M. B. Maple, J. Phys.: Condens. Matter **25**, 422201 (2013).

[30] C. T. Wolowiec, D. Yazici, B. D. White, K. Huang, and M. B. Maple, Phys. Rev. B **88**, 064503 (2013).

[31] R. Jha, B. Tiwari, and V. P. S. Awana, J. Phys. Soc. Jpn. **83**, 063707 (2014).

[32] C. Y. Guo, Y. Chen, M. Smidman, S. A. Chen, W. B. Jiang, H. F. Zhai, Y. F. Wang, G. H. Cao, J. M. Chen, X. Lu, and H. Q. Yuan, arXiv preprint arXiv:1505.04704 (2015).

[33] Y. K. Luo, H. F. Zhai, P. Zhang, Z. A. Xu, G. H. Cao, and J. D. Thompson, Phys. Rev. B **90**, 220510 (2014).

[34] M. Fujioka, M. Tanaka, S. J. Denholme, T. Yamaki, H. Takeya, T. Yamaguchi, and Y. Takano, Europhys. Lett. **108**, 47007 (2014).

[35] S. K. Singh, A. Kumar, B. Gahtori, G. Sharma, S. Patnaik, and V. P. S. Awana, J. Am. Chem. Soc. **134**, 16504 (2012).

[36] Y. Mizuguchi, J. Phys. Chem. Solids **84**, 34 (2015).

[37] Y. Yu, J. F. Shao, S. Tan, C. J. Zhang, and Y. H. Zhang, J. Phys. Soc. Jpn. **82**, 034718 (2013).

[38] R. Jha and V. P. S. Awana, Physica C **498**, 45 (2014).

[39] N. R. Werthamer, E. Helfand, and P. C. Hohenberg, Phys. Rev. **147**, 295 (1966).

[40] S. G. Tan, P. Tong, Y. Liu, W. J. Lu, L. J. Li, B. C. Zhao, and Y. P. Sun, Eur. Phys. J. B **85**, 1 (2012).

[41] Y. Fang, D. Yazici, B. D. White, and M. B. Maple, Phys. Rev. B **91**, 064510 (2015).

[42] I. Jeon, D. Yazici, B. D. White, A. J. Friedman, and M. B. Maple, Phys. Rev. B **90**, 054510 (2014).

[43] Z. R. Ye, H. F. Yang, D. W. Shen, J. Jiang, X. H. Niu, D. L. Feng, Y. P. Du, X. G. Wan, J. Z. Liu, X. Y. Zhu, W. H. H., and J. M. H., Phys. Rev. B **90**, 045116 (2014).

[44] K. Kuroki, JPSJ News and Comments **11**, 02 (2014).

[45] R. Higashinaka, R. Miyazaki, Y. Mizuguchi, O. Miura, and Y. Aoki, J. Phys. Soc. Jpn. **83**, 5004 (2014).

[46] S. Demura, K. Deguchi, Y. Mizuguchi, K. Sato, R. Honjyo, A. Yamashita, T. Yamaki, H. Hara, T. Watanabe, S. J. Denholme, M. Fujioka, H. Okazaki, T. Ozaki, O. Miura, T. Yamaguchi, H. Takeya, and Y. Takano, J. Phys. Soc. Jpn. **84**, 024709 (2015).

[47] R. Jha, H. Kishan, and V. P. S. Awana, J. Appl. Phys. **115**, 013902 (2014).

[48] R. Jha and V. P. S. Awana, Mater. Res. Express **1**, 016002 (2014).

[49] C. Morice, E. Artacho, S. E. Dutton, D. Molnar, H.-J. Kim, and S. S. Saxena, arXiv preprint arXiv:1312.2615 (2013).

[50] H. Usui, K. Suzuki, and K. Kuroki, Phys. Rev. B **86**, 220501 (2012).

[51] B. Li, Z. W. Xing, and G. Q. Huang, Europhys. Lett. **101**, 47002 (2013).

[52] J. Lee, M. B. Stone, A. Huq, T. Yildirim, G. Ehlers, Y. Mizuguchi, O. Miura, Y. Takano, K. Deguchi, S. Demura, and S.-H. Lee, Phys. Rev. B **87**, 205134 (2013).

[53] Shruti, P. Srivastava, and S. Patnaik, J. Phys.: Condens. Matt. **25**, 312202 (2013).

[54] G. Lamura, T. Shiroka, P. Bonfa, S. Sanna, R. De Renzi, C. Baines, H. Luetkens, J. Kajitani, Y. Mizuguchi, O. Miura, K. Deguchi, S. Demura, Y. Takano, and M. Putti, Phys. Rev. B **88**, 180509 (2013).

[55] L. Jiao, Z. Weng, J. Liu, J. Zhang, G. Pang, C. Guo, F. Gao, X. Zhu, H.-H. Wen, and H. Yuan, J. Phys.: Condens. Matt. **27**, 225701 (2015).

[56] P. K. Biswas, A. Amato, C. Baines, R. Khasanov, H. Luetkens, H. Lei, C. Petrovic, and E. Morenzoni, Phys. Rev. B **88**, 224515 (2013).

[57] X. G. Wan, H. C. Ding, S. Y. Savrasov, and C. G. Duan, Phys. Rev. B **87**, 115124 (2013).

[58] G. B. Martins, A. Moreo, and E. Dagotto, Phys. Rev. B **87**, 081102 (2013).

[59] Y. Yang, W.-S. Wang, Y.-Y. Xiang, Z.-Z. Li, and Q.-H. Wang, Phys. Rev. B **88**, 094519 (2013).

[60] Y. Liang, X. Wu, W.-F. Tsai, and J. Hu, Frontiers Phys. **9**, 194 (2014).

[61] X. Wu, J. Yuan, Y. Liang, H. Fan, and J. Hu, EPL (Europhysics Letters) **108**, 27006 (2014), URL `http://stacks.iop.org/0295-5075/108/i=2/a=27006`.

[62] T. Zhou and Z. D. Wang, J. Supercond. Nov. Magn. **26**, 2735 (2013).

[63] S. Li, H. Yang, D. Fang, Z. Wang, J. Tao, X. Ding, and H. Wen, Science China Physics, Mechanics and Astronomy **56**, 2019 (2013).

[64] J. Z. Liu, D. L. Fang, Z. Y. Wang, J. Xing, Z. Y. Du, S. Li, X. Y. Zhu, H. Yang, and H.-H. Wen, Europhys. Lett. **106**, 67002 (2014).

[65] J. Kajitani, K. Deguchi, A. Omachi, T. Hiroi, Y. Takano, H. Takatsu, H. Kadowaki, O. Miura, and Y. Mizuguchi, Solid State Commun. **181**, 1 (2014).

[66] E. Paris, B. Joseph, A. Iadecola, T. Sugimoto, L. Olivi, S. Demura, Y. Mizuguchi, Y. Takano, T. Mizokawa, and N. L. Saini, J. Phys.: Condens. Matt. **26**, 435701 (2014).

[67] A. Miura, M. Nagao, T. Takei, S. Watauchi, I. Tanaka, and N. Kumada, J. Solid State Chem. **212**, 213 (2014).

[68] A. Miura, M. Nagao, T. Takei, S. Watauchi, Y. Mizuguchi, Y. Takano, I. Tanaka, and N. Kumada, Cryst. Growth Des. **15**, 39 (2014).

[69] T. Sugimoto, B. Joseph, E. Paris, A. Iadecola, T. Mizokawa, S. Demura, Y. Mizuguchi, Y. Takano, and N. L. Saini, Phys. Rev. B **89**, 201117 (2014).

[70] J. Kajitani, T. Hiroi, A. Omachi, O. Miura, and Y. Mizuguchi, J. Supercond. Nov. Magn. **28**, 1129 (2015).

[71] J. Kajitani, K. Deguchi, T. Hiroi, A. Omachi, S. Demura, Y. Takano, O. Miura, and Y. Mizuguchi, J. Phys. Soc. Jpn. **83**, 065002 (2014).

[72] M. Nagao, A. Miura, S. Demura, K. Deguchi, S. Watauchi, T. Takei, Y. Takano, N. Kumada, and I. Tanaka, Solid State Commun. **178**, 33 (2014).

[73] M. Nagao, S. Demura, K. Deguchi, A. Miura, S. Watauchi, T. Takei, Y. Takano, N. Kumada, and I. Tanaka, J. Phys. Soc. Jpn. **82**, 113701 (2013).

[74] D. Yazici, I. Jeon, B. D. White, and M. B. Maple, Physica C **514**, 218 (2015).

[75] H. J. Chen, G. H. Zhang, T. Hu, G. Mu, W. Li, F. Q. Huang, X. M. Xie, and M. H. Jiang, Inorg. Chem. **53**, 9 (2013).

[76] G. S. Thakur, G. K. Selvan, Z. Haque, L. C. Gupta, S. L. Samal, S. Arumugam, and A. K. Ganguli, Inorg. Chem. **54**, 1076 (2015).

[77] J. Kajitani, A. Omachi, T. Hiroi, O. Miura, and Y. Mizuguchi, Physica C **504**, 33 (2014).

[78] J. Kajitani, T. Hiroi, A. Omachi, O. Miura, and Y. Mizuguchi, J. Phys. Soc. Jpn. **84**, 044712 (2015).

[79] Y. Mizuguchi, A. Miura, J. Kajitani, T. Hiroi, O. Miura, K. Tadanaga, N. Kumada, E. Magome, C. Moriyoshi, and Y. Kuroiwa, arXiv preprint arXiv:1504.01208 (2015).

[80] T. Tomita, M. Ebata, H. Soeda, H. Takahashi, H. Fujihisa, Y. Gotoh, Y. Mizuguchi, H. Izawa, O. Miura, S. Demura, K. Deguchi, and Y. Takano, J. Phys. Soc. Jpn. **83**, 063704 (2014).

[81] Y. Fang, D. Yazici, B. D. White, and M. B. Maple, Physical Review B **92**, 094507 (2015).

[82] M. Fujioka, M. Nagao, S. J. Denholme, M. Tanaka, H. Takeya, T. Yamaguchi, and Y. Takano, Appl. Phys. Lett. **105**, 052601 (2014).

[83] A. Krzton-Maziopa, Z. Guguchia, E. Pomjakushina, V. Pomjakushin, R. Khasanov, H. Luetkens, P. K. Biswas, A. Amato, H. Keller, and K. Conder, J. Phys: Condens. Matter **26**, 215702 (2014).

[84] T. Hiroi, J. Kajitani, A. Omachi, O. Miura, and Y. Mizuguchi, J. Supercond. Nov. Magn. **28**, 1149 (2015).

[85] T. Hiroi, J. Kajitani, A. Omachi, O. Miura, and Y. Mizuguchi, J. Phys. Soc. Jpn. **84**, 024723 (2015).

[86] V. S. Tanryverdiev, O. M. Aliev, and I. I. Aliev, Inorg. Mater. **31** (1995).

[87] H. Maeda, Y. Tanaka, M. Fukutomi, and T. Asano, Jpn. J. Appl. Phys. **27**, L209 (1988).

[88] M. A. Subramanian, C. C. Torardi, J. C. Calabrese, J. Gopalakrishnan, K. J. Morrissey, T. R. Askew, R. B. Flippen, U. Chowdhry, and A. W. Sleight, Science **239**, 1015 (1988).

[89] J. L. Tallon, R. G. Buckley, P. W. Gilberd, M. R. Presland, I. W. M. Brown, M. E. Bowden, L. A. Christian, and R. Goguel, Nature **333**, 153 (1988).

[90] R. J. Cava, B. Batlogg, J. J. Krajewski, R. Farrow, L. W. Rupp, A. E. White, K. Short, W. F. Peck, and T. Kometani, Nature **332**, 814 (1988).

[91] L. F. Mattheiss and D. R. Hamann, Phys. Rev. Lett. **60**, 2681 (1988).

Chapter VIII

Evidence for a conducting surface ground state in high-quality single crystalline FeSi

VIII.A Introduction

The transition metal silicides FeSi, MnSi, CoSi, and CrSi, have the B20 crystal structure, which is the only group in the cubic system without an inversion center. These compounds exhibit a rich variety of physical phenomena that are of great interest for fundamental understanding and potential applications. For example, the d-electron compound FeSi shows a remarkable similarity to f-electron Kondo insulators, and the electrical resistivity $\rho(T)$ evolves continuously with decreasing temperature from metallic behavior ($\mathrm{d}\rho/\mathrm{d}T > 0$) to semiconducting behavior ($\mathrm{d}\rho/\mathrm{d}T < 0$) [1–5]. A considerable

amount of theoretical effort [6–10] has been expended to explain the strong temperature dependence of the magnetic susceptibility $\chi(T)$ of FeSi which reaches a maximum value at around 500 K [1] that is not due to magnetic order [11, 12].

The ground state of FeSi is considered to be non-magnetic; however, experimental investigations of FeSi at low temperature reveal features that are sample dependent and are not well understood [5, 13, 14]. The published results are consistent in terms of the small semiconducting energy gap of 50-60 meV inferred from $\rho(T)$ measurements in the temperature range 70-170 K. However, upon further decrease of the temperature, the following features in $\rho(T)$ of FeSi have been reported: Saturation steps [5], a hump (shoulder) at 70 K [14, 15] or $\sim$ 35 K [16], a moderate increase with decreasing temperature below 40 K [17] or 50 K [18], or a saturation below about 5 K [19]. Moreover, the values of ρ below 70 K reported in these references are also very different, indicating strong sample dependence of the electrical transport behavior. It has been well established in experiments that the electrical properties of semiconductors can be very sensitive to external dopants [20–24]. To investigate the intrinsic physical properties of FeSi, we prepared high quality single-crystal samples of FeSi and performed various types of measurements over a wide temperature range of 1.8-400 K. Anomalous electrical transport behavior associated with a change in primary charge carriers and negative magneto-resistivity at low temperatures were observed in all of the samples. We also report metallic conducting behavior of FeSi single crystals below $\sim$20 K, yielding evidence for a conducting surface state, consistent with specific heat, magneto-resistivity, and magnetization measurements.

VIII.B Experimental Details

Single-crystalline samples of FeSi were grown in a high-temperature Sn flux with Fe: Si molar ratio of 1: 1. The quality of the FeSi samples was assessed by means of single crystal X-ray diffraction at room temperature. A Bruker Apex II X-ray diffractometer with Mo $K_{\alpha 1}$ (λ = 0.71073 Å) radiation was used to measure the scattering intensity. The crystal structure was refined with the SHELXTL package [25]. Electrical resistivity, magneto-resistivity, Hall effect, and specific heat measurements were performed using a Quantum Design Physical Property Measurement System (PPMS) DynaCool. The magnetization and magnetic susceptibility measurements were carried out with a Quantum Design Magnetic Property Measurement System (MPMS) [26]. SEM and EDX were taken with a FEI Scios DualBeam FIB/SEM operated at 15 kV.

VIII.C Results and Discussion

The FeSi single crystals grow along the [111] direction in the Sn flux, resulting in bar-shaped samples. The results of single-crystalline X-ray diffraction measurements on FeSi are shown in Fig. VIII.1. Consistent with previous studies, stoichiometric FeSi crystallizes in the cubic chiral structure with space group $P2_13$ ($B20$-type) and lattice parameter a = 4.4860(5) Å. No vacancies were observed according to the refinement. The profile residual Rp is 1.79% with a weighted profile residual Rwp = 4.11%. No electron density residual was detected, revealing the high quality of the FeSi crystals. Scanning electron microscope (SEM) and energy dispersive X-ray spectroscopy (EDX)

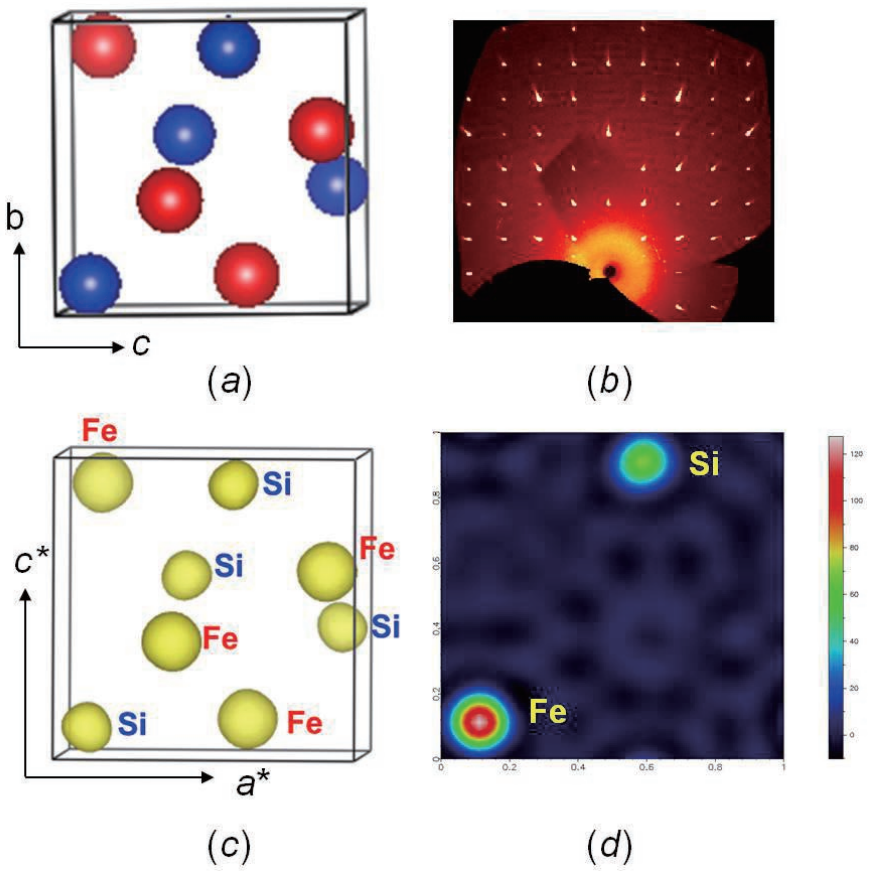

Figure VIII.1: (a) The crystal structure of FeSi (Red: Fe; Blue: Si). (b) Single crystal X-ray diffraction precession image of the $(h0l)$ plane in the reciprocal lattice of FeSi at 300 K. All of the resolved spots correspond to the cubic chiral crystal structure $P2_13$. (c) 3D Fourier map showing the electron density in $B20$-FeSi. (d) 2D Fourier map showing the electron density on Fe and Si along the z-axis.

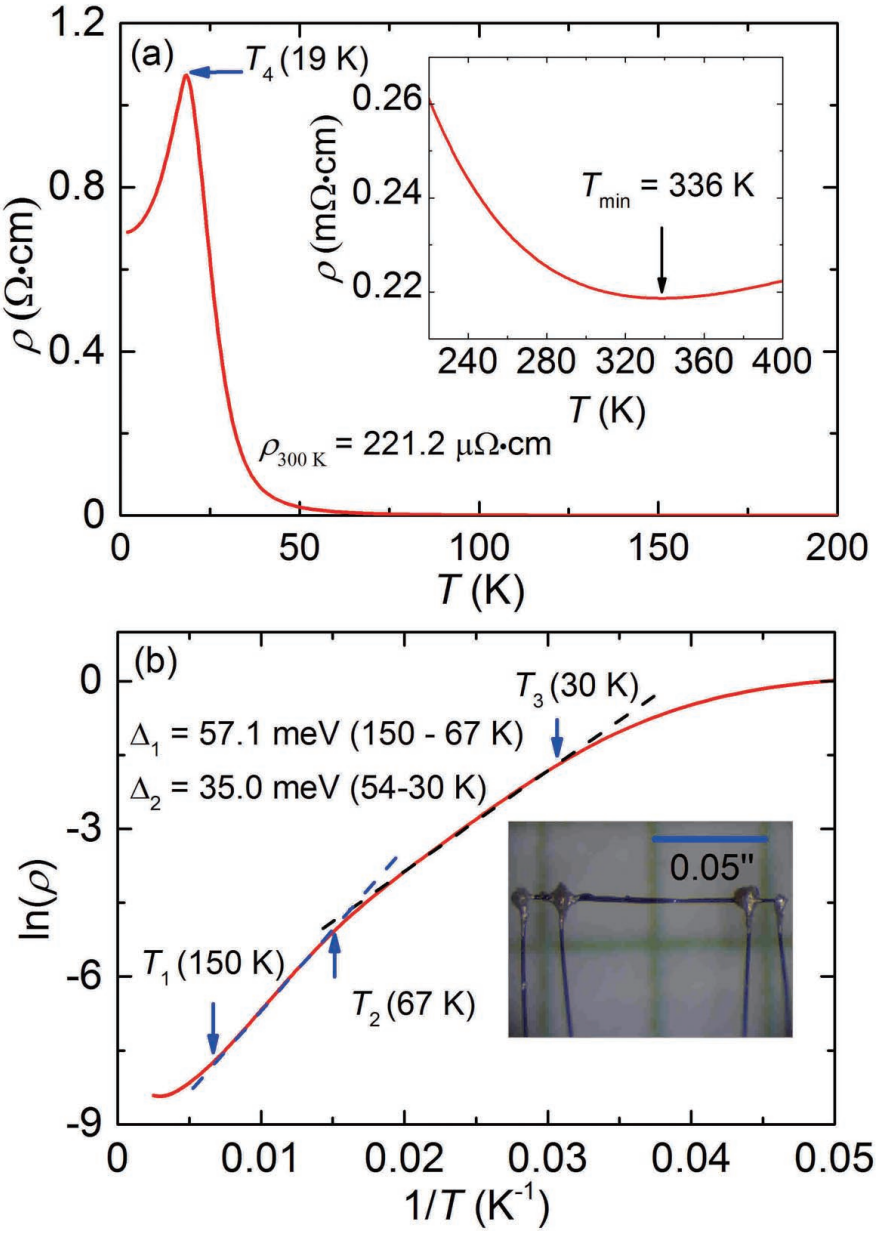

Figure VIII.2: (a) Electrical resistivity ρ vs. temperature T for FeSi with the current flowing along the [111] direction below 200 K. (b) ln(ρ) vs. 1/T. The insets of (a) and (b) show the resistivity at high temperatures and a picture of the sample with the four-wire electrical lead configuration, respectively.

investigations yielded no evidence of additional elements (see figures S1-S4 in the supplemental information).

Because of their bar-shape and high quality, the FeSi single crystals are very suitable for electron transport measurements along the [111] direction. Upon cooling from 400 K, metallic-like behavior can be observed down to 336 K, below which the resistivity increases with decreasing temperature, resulting in a minimum in $\rho(T)$ at T_{min} = 336 K (see the inset of Fig. VIII.2(a)). Similar features can also be found in other references with values of T_{min} mostly in the range 150-300 K) [5, 27–29]. Decreasing the temperature further results in a gradual enhancement of semiconducting behavior down to 152 K, which has been reported to be related to the opening of an energy gap [30–32].

Fig. VIII.2(b) shows a linear relation of ln(ρ) vs. (1/T) for FeSi in the temperature range 152 K (T_1) to 67 K (T_2), consistent with standard activated behavior with an energy gap Δ = 57.1 meV; this value of Δ is comparable to previously reported gap values of 50-60 meV [1, 3, 15, 18]. From 54-30 K, where the relation ln(ρ) vs. 1/T is also linear, the value of dln(ρ)/d(1/T) corresponds to an energy gap of 35 meV. Below 30 K (T_3), the $\rho(T)$ curve cannot be described by a standard activation model. Further decrease of the temperature below 19 K results in a crossover from semiconducting to metallic behavior (T_4) as shown in Fig. VIII.2(a). As the behavior observed in $\rho(T)$ below T_4 is quite different from that reported for FeSi in other references, we repeated the measurements on different FeSi single crystals which yielded consistent resistivity values at high temperates. However, a strong size dependence of the metallic conductivity can be observed at low temperates as shown in the Fig. VIII.3; As the average width/thickness (W) of the sample

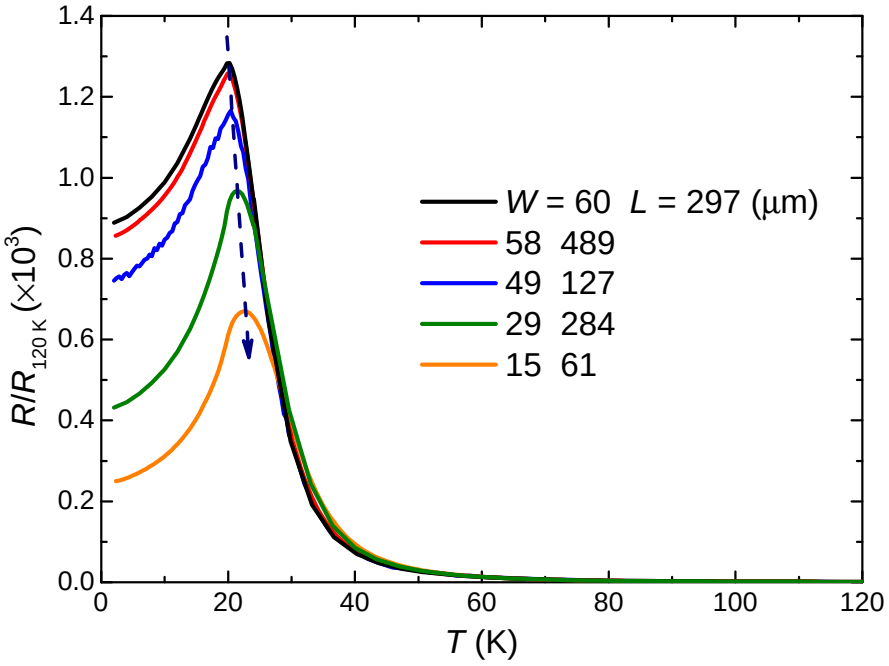

Figure VIII.3: Temperature dependence of the resistance (R) for FeSi single crystals with different size, normalized by the resistance at 120 K (R_{120}).The symbol W and L refer to the average width/thickness and effective length of the samples, respectively. The arrow indicates the increase of the semiconducting to metallic crossover temperature.

is reduced, the low temperature metallic conductivity increases dramatically and the semiconducting to metallic crossover temperature (indicated by the dashed arrow in Fig.3) gradually increases. In contrast, the electrical resistivity of the FeSi does not have a noticeable dependence on L, the effective length of the sample (the distance between the two voltage leads). As the surface area to volume ratio increases with the thinning of the samples, the results strongly suggest that the metallic conductivity originates from the FeSi surface.

In an effort to gain a better understanding of the temperature dependence of $\rho(T)$ of FeSi, especially the low temperature metallic behavior, we performed specific heat $C_p(T)$ measurements on the samples down to 1.8 K, the results of which are

shown in Fig. VIII.4. It should be mentioned that some of the early reports show additional features in $C_p(T)$ at $\sim$10 K or below 1 K which were attributed to Schottky like anomalies [5, 19]. However, in this study, no Schottky like features are found in $C_p(T)$. Thus, it is reasonable to describe the specific heat of the samples as the sum of electronic and lattice contributions at low temperatures; i.e., $C_p = \gamma T + \beta T^3$. No anomalies around T_2 = 67 K, T_3 = 30 K, and T_4 = 19 K can be observed, indicating the absence of any bulk phase transitions in FeSi at these temperatures. The estimated value of the Debye temperature θ_D of 457 K lies within the range 377-515 K previously reported [5, 33, 34]. On the other hand, the electronic specific heat coefficient γ is estimated to be 0.41 mJ·mol^{-1}·K^{-2}, which is only about 8-30$\%$ of previously reported values [5], suggesting that the samples studied in this work have a lower concentration of electron donor impurities, as the value of γ is proportional to the density of electronic states at the Fermi level. The metallic-like conduction below T_4 exhibited by the FeSi samples in this work is dramatically different from the semiconducting behavior observed in other FeSi samples which have higher concentrations of charge carriers. The seemingly contradictory phenomena suggest that the metallic conduction observed in this study is unlikely to be a bulk phenomenon, which is also supported by the absence of features indicative of phase transitions in the $C_p(T)$ data.

The temperature dependence of the magnetic susceptibility $\chi(T)$ for FeSi is shown in Fig. VIII.5. Above 100 K, the value of the magnetic susceptibility increases with increasing temperature, which is similar to the behavior of $\chi(T)$ for an antiferromagnet at temperatures below the Néel temperature. In the temperature range 20-100 K, $\chi(T)$

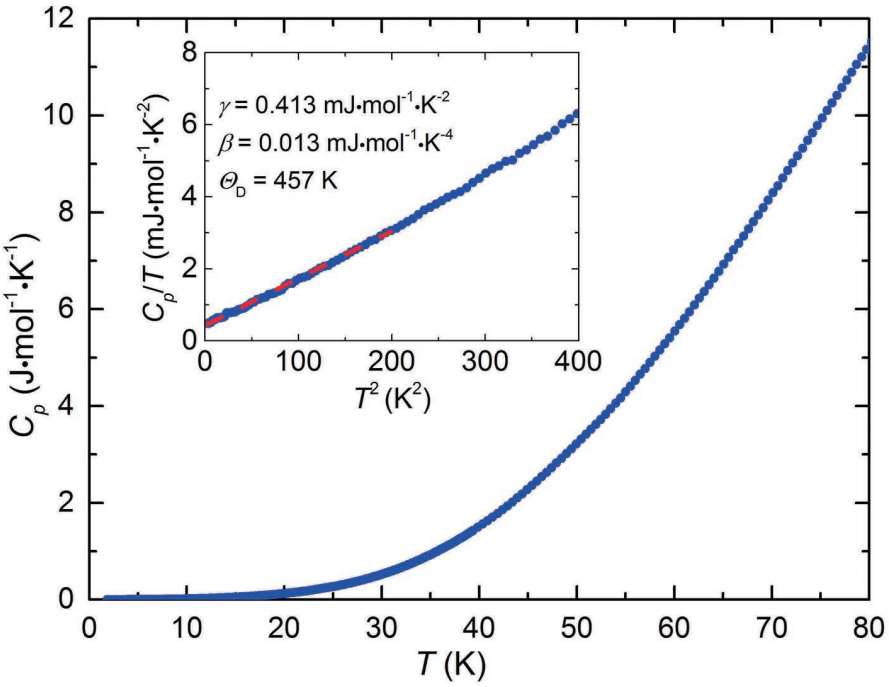

Figure VIII.4: Specific heat $C_p(T)$ of FeSi at low temperatures from 1.8 to 80 K. A plot of C_p/T vs T^2 below 20 K is shown in the inset. The dashed line in the inset is a fit of the expression $C_p/T = \gamma + \beta T^2$ to the data with the values of γ, β, and θ_D given in the inset of the figure.

is very small ($\sim$0.15 emu·mol^{-1}·T^{-1}), indicating that FeSi has a very weak response to external magnetic field and a non-magnetic ground state. Below 15 K, $\chi(T)$ of FeSi has a Curie-Weiss like upturn with decreasing temperature, which is apparently associated with magnetic impurities [1, 11]. In this study, however, the magnitude and the onset temperature of the $\chi(T)$ upturn is significantly smaller and lower, respectively, than previously reported values [15, 16, 35], indicating lower magnetic impurity concentration for the present samples. The knee observed in the $M(H)$ curve at around 2 T indicated by the arrow in the inset of Fig. VIII.5 is also consistent with a paramagnetic impurity scenario. Above 2 T, it seems that the magnetic field does not dramatically affect the magnetization of the samples, which also suggests the absence of magnetic order at low

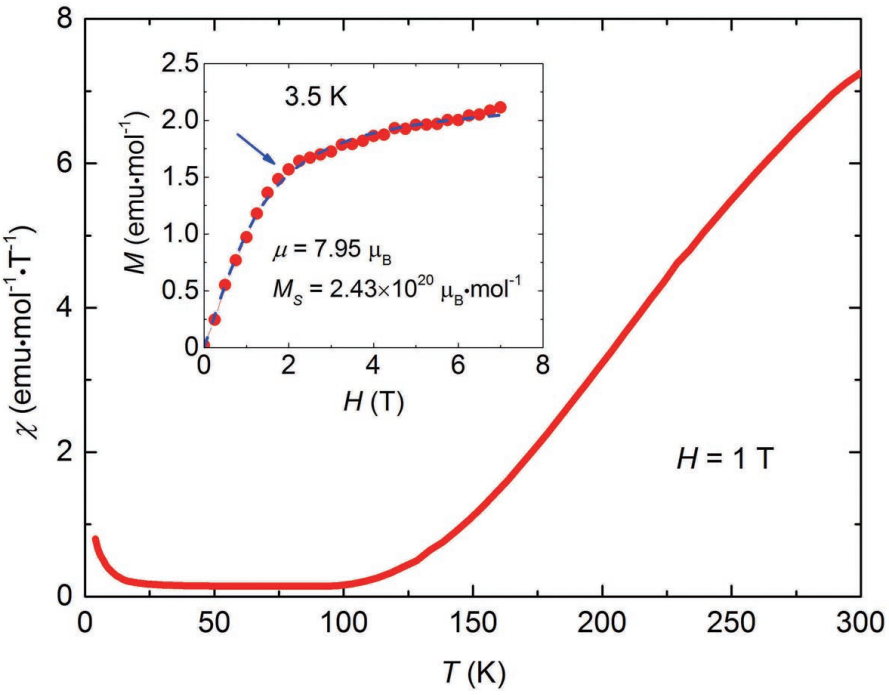

Figure VIII.5: Magnetic susceptibility χ vs. temperature T for FeSi single crystals. The corresponding magnetization curve at 3.5 K is shown in the inset. The dashed curve is a fit of the Langevin function to the $M(H)$ data.

temperatures. The results of the magnetic measurements reveal that the samples are of high quality and the features observed around T_2 and T_4 in the $\rho(T)$ curve are not related to any bulk magnetic transitions.

In this study, the magnetization of FeSi can be well described by the following Langevin function:

$$M = M_S[coth(\mu H/k_B T) - k_B T/\mu H] \tag{VIII.1}$$

in which μ is the magnetic moment of the impurity clusters and M_S is the saturation magnetization. The corresponding fitting of $M(H)$ at 3.5 K gives M_s = 2.433×10^{20} μ_B/mol and μ = 7.95 μ_B. If we assume that the magnetic moment per impurity atom is $3\mu_B$ as in pure iron, the concentration of Fe impurity atoms is only about 130 ppm per

Fe atom, which is comparable to or significantly lower than the impurity concentration previously estimated for single crystal specimens of FeSi [11, 19, 35]. The fitting results also show that, on average, only about 2-3 magnetic impurity atoms comprise each cluster, indicating atomic size magnetic clusters. The estimated value of the Wilson-Sommerfeld ratio of FeSi is $\sim$2.5, using the base magnetic susceptibility below 100 K and the electronic specific heat coefficient obtained in this study, which is slightly higher than the expected value of $\sim$2 for the Kondo model [36].

Figure VIII.6 shows $\rho(T)$ data for FeSi under external magnetic field. At high temperatures, the values of ρ are almost independent of the applied magnetic field; however, a negative magneto-resistivity (MR), where MR = ($\rho_{3\mathrm{T}}$ - $\rho_{0\mathrm{T}}$)/$\rho_{0\mathrm{T}}$, can be observed around 70 K, as indicated by the arrow in the inset of Fig. VIII.5, that becomes very significant below 30 K; these temperatures are very close to the temperatures T_2 = 67 K and T_3 = 30 K, respectively. It should be mentioned that previous studies of the MR are not consistent: A negative MR was reported by Paschen $et\ al.$ below 30 K and attributed to quantum interference effects [5]; however, a change of sign at around 70 K (close to T_2 = 67 K in this study) was reported later below which the MR is positive [14]. In this study, the negative MR reaches a minimum value at T_4. The peak in the absolute value of the MR in this study is about 20%, which is obviously higher than the peak in the absolute value of the MR reported in Refs. [5] and [14], revealing the sample dependence of the MR. While $\rho(T)$ is very sensitive to the applied field at low temperatures, the value of T_4 seems to be independent of H, which provides additional evidence that the emergence of metallic conductivity in $\rho(T)$ around T_4 is very robust

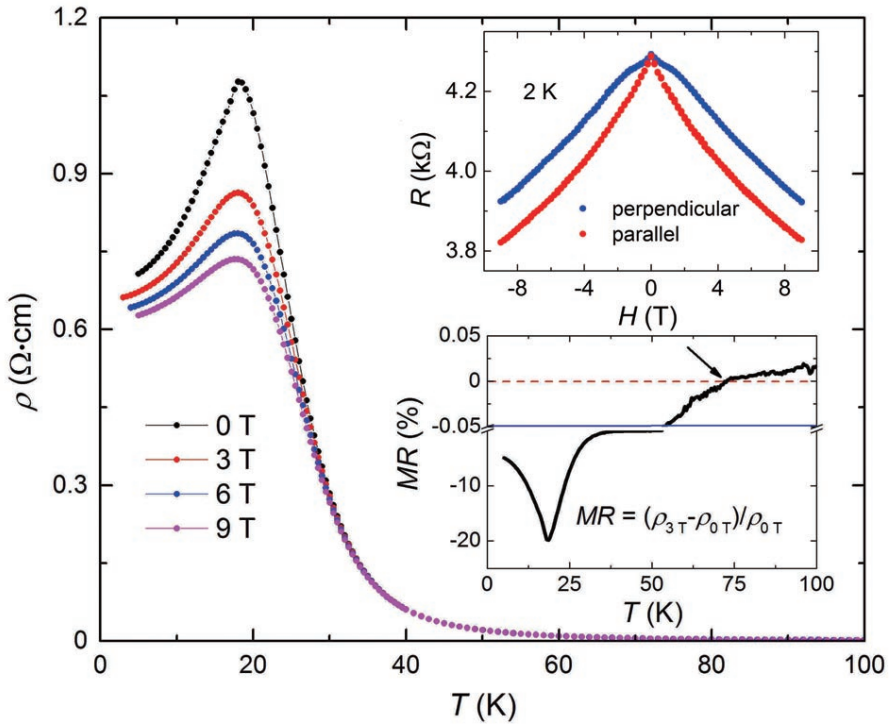

Figure VIII.6: Electrical resistivity ρ vs. temperature T in magnetic fields up to 9 T. The applied field is perpendicular to the current. Shown in the upper inset is ρ vs. H at 2 K with the applied fields perpendicular (blue) and parallel (red) to the current, respectively. Displayed in the lower inset is the temperature dependence of the magneto-resistance (MR). The definition of the MR is given in the lower inset.

with respect to the external magnetic field.

The evolution of ρ as a function of H with H perpendicular and parallel to the long axis of the FeSi crystal at 2 K is shown in the upper inset of Fig. 6. No noticeable hysteresis in the H dependence of the resistivity is observed, indicating no detectable free Fe impurities. The value of ρ is suppressed with increasing field, but the evolution of $\rho(H)$ deviates slightly from a linear relation. The angle between the directions of the applied field and the current (long axis of the sample) α has a small effect on the behavior of $\rho(H)$. This can be qualitatively understood by considering both bulk and surface electron conduction for FeSi. The negative MR can be observed at temperature

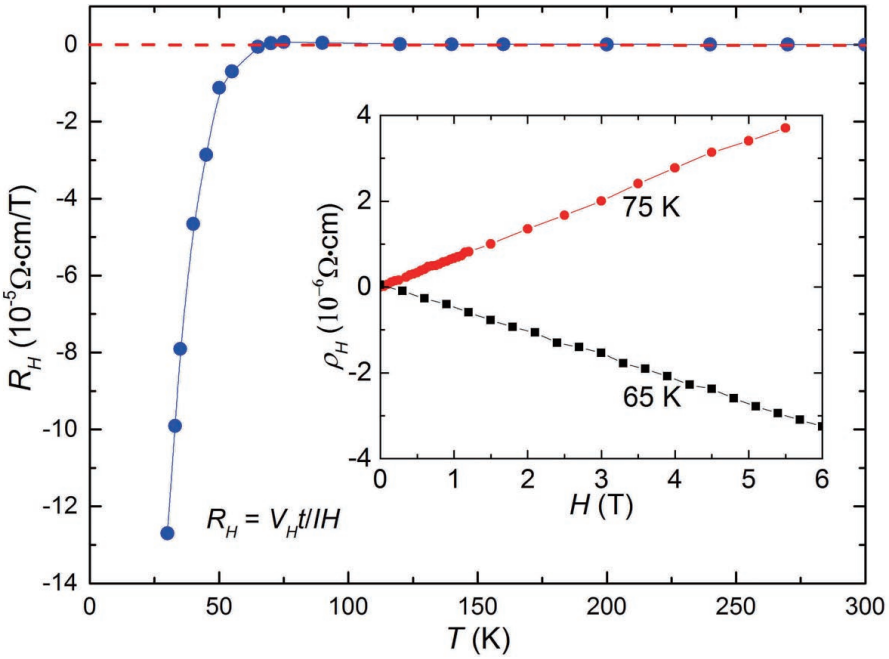

Figure VIII.7: Evolution of the Hall coefficient R_H with temperature T. The Hall resistivity ρ_H vs. H at 65 and 75 K is shown in the inset.

T_2 which is far above T_4, suggesting that the negative MR is a bulk phenomenon. If we assume that the response of the surface contribution to the resistivity to an external field is positive due to the additional scattering of free electrons by the Lorentz force, increasing α will increase the effective applied field on the sample surface and thus slightly enhance the MR.

The main results of the Hall effect measurements at temperatures down to 30 K are displayed in Fig. VIII.7. Unlike the results of previous reports [5], linear relations of the Hall resistivity vs. applied external field can be seen up to 9 T over a wide temperature range above 30 K (see the inset of Fig. VIII.7). At high temperatures, the Hall coefficient R_H is positive and increases slightly with decreasing temperature, indicating that the dominant charge carriers are holes. However, a change of sign in R_H is observed at $\sim$68

K, which is very close to T_2 = 67 K and to the temperature of the sign change of the MR. The phenomena observed in the $R_H(T)$, $MR(T)$, and $\rho(T)$ measurements are consistent with one another, indicating the resistivity is dominated by electron conduction and is sensitive to external field below T_2 = 67 K.

VIII.D Concluding Remarks

In summary, the following conclusions can be drawn from this study:

(1) The electron transport behavior of FeSi is very sensitive to sample quality. The high quality of the single crystal samples used in this study is supported by X-ray diffraction, dispersive X-ray spectroscopy, specific heat, and magnetization measurements.

(2) In the temperature range 150-67 K, the semiconducting energy gap is 57 meV. Below 67 K, a much smaller energy gap and a sign change of the magneto-resistance and Hall coefficient are observed, suggesting a change in dominant charge carriers.

(3) A further decrease of the temperature results in a sharp reversible crossover from a negative slope to a positive slope of $\rho(T)$ at $\sim$19 K. Corresponding magnetization and magneto-resistivity measurements suggest that there is no bulk magnetic order associated with this slope change in $\rho(T)$. No feature can be observed in specific heat measurements. Investigation of the dependence of the electrical resistivity on the geometrical factor reveals that the metallic conductivity increases dramatically in thinner samples. These results suggest that the metallic conductivity below T_4 is a surface phenomenon. The possibility that FeSi is a 3D topological insulator should be considered

for further research.

(4) The fact that T_4 shows no noticeable change with applied external field up to 9 T and the resistivity below T_4 is not strongly dependent on α imply that the metallic conducting state of FeSi is very robust with respect to external magnetic field.

(5) Since the surface conduction of FeSi is very robust under magnetic field and is significant only below 19 K, the negative magneto-resistivity of the sample should be associated with the bulk properties of the samples. The slight increase of MR with increasing α should be attributed to the surface state of FeSi.

The text and data presented in this chapter are reprints of material that appears in "Evidence for a conducting surface ground state in high-quality single crystalline FeSi" Yuankan Fang, Sheng Ran, Weiwei Xie, Shen Wang, Ying Shirley Meng, and M. B. Maple, *PNAS* submitted. The dissertation author is the primary investigator and author of this article.

Bibliography

[1] V. Jaccarino, G. K. Wertheim, J. H. Wernick, L. R. Walker, and S. Arajs, Phys Rev **160**, 476 (1967).

[2] Z. Schlesinger, Z. Fisk, H. T. Zhang, M. B. Maple, J. DiTusa, and G. Aeppli, Phys Rev Lett **71**, 1748 (1993).

[3] B. C. Sales, E. C. Jones, B. C. Chakoumakos, J. A. Fernandez-Baca, H. E. Harmon, J. W. Sharp, and E. H. Volckmann, Phys Rev B **50**, 8207 (1994).

[4] D. Mandrus, J. L. Sarrao, A. Migliori, J. D. Thompson, and Z. Fisk, Phys Rev B **51**, 4763 (1995).

[5] S. Paschen, E. Felder, M. A. Chernikov, L. Degiorgi, H. Schwer, H. R. Ott, D. P. Young, J. L. Sarrao, and Z. Fisk, Phys Rev B **56**, 12916 (1997).

[6] Y. Takahashi and T. Moriya, J Phys Soc Jpn **46**, 1451 (1979).

[7] Z. Fisk, J. L. Sarrao, J. D. Thompson, D. Mandrus, M. F. Hundley, A. Miglori, B. Bucher, Z. Schlesinger, G. Aeppli, E. Bucher, J. F. DiTusa, C. S. Oglesby, H. R. Ott, P. Canfield, and S. E. Brown, Physica B: Condensed Matter **206**, 798 (1995).

[8] C. M. Varma, Phys Rev B **50**, 9952 (1994).

[9] C. Fu and S. Doniach, Phys Rev B **51**, 17439 (1995).

[10] V. I. Anisimov, S. Y. Ezhov, I. S. Elfimov, I. V. Solovyev, and T. M. Rice, Phys Rev Lett **76**, 1735 (1996).

[11] G. K. Wertheim, V. Jaccarino, J. H. Wernick, J. A. Seitchik, H. J. Williams, and R. C. Sherwood, Phys Lett **18**, 89 (1965).

[12] M. Kohgi and Y. Ishikawa, Solid State Commun **37**, 833 (1981).

[13] T. Jarlborg, Phys Rev B **51**, 11106 (1995).

[14] P. Sun, B. Wei, D. Menzel, and F. Steglich, Phys Rev B **90**, 245146 (2014).

[15] A. E. Petrova, V. N. Krasnorussky, A. A. Shikov, W. M. Yuhasz, T. A. Lograsso, J. C. Lashley, and S. M. Stishov, Phys Rev B **82**, 155124 (2010).

[16] M. Mihalik, M. Timko, P. Samuely, N. Tomašovičova-Hudákova, P. Szabó, and A. A. Menovsky, J Magn Magn Mater **157**, 637 (1996).

[17] S. Bocellip, F. Marabelli, R. Spolenak, and E. Bauer, MRS Online Proceedings Library Archive **402** (1995).

[18] Z. . Schlesinger, Z. Fisk, H.-T. Zhang, M. Maple, J. DiTusa, and G. Aeppli, Phys Rev Lett **71**, 1748 (1993).

[19] M. B. Hunt, M. A. Chernikov, E. Felder, H. R. Ott, Z. Fisk, and P. Canfield, Phys Rev B **50**, 14933 (1994).

[20] C. S. Brian, D. Olivier, A. M. Michael, and A. F. May, Phys Rev B **83** (2011).

[21] T. Dietl, Nature Materials **9**, 965 (2010).

[22] B. C. Sales, A. F. May, M. A. McGuire, M. B. Stone, D. J. Singh, and D. Mandrus, Phys. Rev. B **86** (2012).

[23] J. F. DiTusa, K. Friemelt, E. Bucher, G. Aeppli, and A. P. Ramirez, Phys. Rev. B **58** (1998).

[24] Y. Fang, C. T. Wolowiec, D. Yazici, and M. B. Maple, Novel Superconducting Materials **1**, 79 (2015).

[25] G. M. Sheldrick, Acta Crystallographica Section A: Foundations of Crystallography **64**, 112 (2008).

[26] Y. Fang, D. Yazici, B. D. White, and M. B. Maple, Phys Rev B **91** (2015).

[27] P. Samuely, P. Szabó, M. Mihalik, N. Hudáková, and A. A. Menovsky, Physica B: Condensed Matter **218**, 185 (1996).

[28] R. Wolfe, J. H. Wernick, and S. E. Haszko, Phys Lett **19**, 449 (1965).

[29] B. Buschinger, C. Geibel, F. Steglich, D. Mandrus, D. Young, J. L. Sarrao, and Z. Fisk, Physica B: Condensed Matter **230**, 784 (1997).

[30] K. Ishizaka, T. Kiss, T. Shimojima, T. Yokoya, T. Togashi, S. Watanabe, C. Q. Zhang, C. T. Chen, Y. Onose, Y. Tokura, and S. Shin, Phys Rev B **72**, 233202 (2005).

[31] M. Arita, K. Shimada, Y. Takeda, M. Nakatake, H. Namatame, M. Taniguchi, H. Negishi, T. Oguchi, T. Saitoh, A. Fujimori, and T. Kanomata, Phys Rev B **77**, 205117 (2008).

[32] M. Klein, D. Zur, D. Menzel, J. Schoenes, K. Doll, J. Röder, and F. Reinert, Phys Rev Lett **101**, 046406 (2008).

[33] Y. Takahashi, T. Kanomata, R. Note, and T. Nakagawa, J Phys Soc Jpn **69**, 4018 (2000).

[34] K. Marklund, M. Larsson, S. Byström, and T. Lindqvist, Physica Scripta **9**, 47 (1974).

[35] K. Koyama, T. Goto, T. Kanomata, and R. Note, J Phys Soc Jpn **68**, 1693 (1999).

[36] K. G. Wilson, Rev. Mod. Phys. **47**, 773 (1975).